The effect of a nanocrystalline silver dressing, Acticoat™, on wound healing in full-thickness excisional wounds in a porcine model.

Carol Ann Hartmann

Dissertation submitted to the Faculty of Health Sciences
of the University of the Witwatersrand, Johannesburg
in fulfilment of the requirement for the degree of
Master of Science in Medicine

Johannesburg

2014

PLAGIARISM DECLARATION

I, Carol Hartmann (Student number: 397227), am a student registered for the degree of Master of Science in Medicine at the University of the Witwatersrand, Johannesburg, in the academic year 2014. I hereby declare the following:

_ I am aware that plagiarism (the use of someone else's work without their permission and/or without acknowledging the original source) is wrong.

_ I confirm that the work submitted for assessment for the above degree is my own unaided work except where I have explicitly indicated otherwise.

_ I have followed the required conventions in referencing the thoughts and ideas of others.

_ I understand that the University of the Witwatersrand may take disciplinary action against me if there is a belief that this is not my own unaided work or that I have failed to acknowledge the source of the ideas or words in my writing.

Signature: _____ Date: 18th August 2014

To my mother and father for their gift of learning
and to my husband who motivates and inspires me.

ACKNOWLEDGEMENTS

I sincerely thank the following people for their time, advice, support and assistance.

- **Professor Beverley Kramer**, for your guidance, support and encouragement not only in this research but in all aspects of my career.
- **Professor Heinz Rode** for providing the Acticoat™ and your guidance on the wounding protocol.
- **Dr Leith Meyer**, **Sr Mary-Ann Costello** and **the technical staff of the Central Animal Services** of the University of the Witwatersrand for your assistance with the care of the pigs and the animal surgeries and dressing changes.
- **Hasiena Ali**, **Monica Gomes** and **Alison Mortimer** for sharing your knowledge and experience while teaching me the biochemical and histological assays.
- **Margaret Badenhorst** for your help and perseverance with the total protein assays.
- **Pam Sharpe** for your assistance with confocal microscopy.
- **Carina Aitken** and **Dr Peter King** for sharing your knowledge of gram stains.
- **Glynis Veale** for your assistance with grants and funding.
- **Robert Ndou**, **Andrea Kolkenbeck-Ruh**, **Nicole Weber**, **Dr Tania Hartmann** and **Dr Daniel Surridge** for assisting me with the inter-observer errors.
- **Elena Libhaber** for your advice on the statistical analyses.
- **Eric Liebenberg** for your assistance with the images taken with the Olympus BX61VS microscope, XC10 Camera and Olympus Dot Slide software (Olympus Soft Image solutions).
- The **Faculty Research Committee** of the Faculty of Health Sciences and **Professor Beverley Kramer** for providing financial support for this research.

ABSTRACT

Nanocrystalline silver (NCS) dressings have antimicrobial and anti-inflammatory effects which aid healing, particularly in burns and chronic wounds. However, they are cytotoxic and may delay healing in acute wounds. Therefore, this study aimed to assess the effect of a NCS dressing on wound healing in full-thickness excisional wounds in a porcine model.

Healing of porcine skin was assessed on day 3, 6, 9 and 15 post-wounding. Five wounds dressed with NCS and five untreated wounds dressed with polyurethane film (the control) were assessed per day (n=40 wounds). The rate of healing was measured using digital photographs. The inflammatory response, restoration of the epithelium and blood vessel formation were evaluated using haematoxylin and eosin stained sections. Picrosirius red staining and confocal microscopy were used to assess collagen formation. Proliferation of keratinocytes was calculated using sections immunolabelled for Ki-67. Additionally, the quality of the re-epithelialised wounds was assessed using a Clinical Assessment Score.

There was no difference in the rate of healing between wounds treated with NCS and those dressed with polyurethane film. Inflammation was increased in NCS-treated wounds on day 3 post-wounding. However, compared to controls, on day 15 post-wounding the epithelium of NCS-treated wounds more closely resembled normal epithelium. Additionally, a greater number of mature blood vessels were seen in NCS-treated wounds. Differences were also observed in the deposition of collagen in NCS-treated wounds compared to controls.

These results suggest that NCS may be beneficial for scar formation. Further investigation is needed into the effect of NCS and its role in the treatment of wounds, including novel uses such as the prevention of scarring.

LIST OF TABLES

Table

LIST OF FIGURES

LIST OF ABBREVIATIONS

Cyr61	cysteine rich 61
ECM	extracellular matrix
EGF	epidermal growth factor
FGF	fibroblast growth factor
IFN	interferon
IL	interleukin
KGF	keratinocyte growth factor
MMP	matrix metalloproteinase
PDGF	platelet derived growth factor
ROS	reactive oxygen species
TIMP	tissue inhibitor or matrix metalloproteinase
TGF	transforming growth factor
TNF	tumour necrosis factor
VEGF	vascular endothelial growth factor

TABLE OF CONTENTS

1. INTRODUCTION AND LITERATURE REVIEW

Adult cutaneous wound healing is a complex sequence of molecular and cellular events, which culminates in the replacement of damaged tissue by a scar (Ho and Hantash, 2013). Therapeutic agents used to treat wounds aim to increase the rate of healing and maximize the production of functional scar tissue (Ho and Hantash, 2013). This aim is achieved by optimizing the molecular and cellular events of cutaneous healing and controlling local factors, such as infection, which can prolong inflammation and delay wound healing (Guo and DiPietro, 2010; Ho and Hantash, 2013). One such therapeutic agent, Acticoat^{TM} which contains nanocrystalline silver, has reported antimicrobial and anti-inflammatory properties (Atiyeh *et al*., 2007; Khundkar *et al*., 2010) which may aid wound healing. However, silver nanoparticles are cytotoxic to a number of cell types, including keratinocytes and fibroblasts (for examples see Asharani *et al*., 2009; Samberg *et al*., 2010). Additionally, there are conflicting reports on the ability of these dressings to improve the rate of wound healing (for examples see Olson *et al*., 2000; Innes *et al*., 2001). Therefore, further investigation is needed to determine the effect of nanocrystalline silver on cutaneous wound healing.

1.1 Normal cutaneous wound healing

In humans, cutaneous wound healing occurs primarily through the process of re-epithelialisation (Sullivan *et al*., 2001) with varying degrees of wound contraction. These events form part of the complex process of healing which can be divided into three phases. After skin injury, the initial or inflammatory phase of healing is characterized by haemostasis and the recruitment of inflammatory cells to the wound area (Ho and Hantash, 2013). These events merge with the second or proliferative phase of healing. During this phase damaged tissue is replaced with new epithelium (re-epithelialisation), blood vessels (neoangiogenesis) and extracellular matrix (ECM) components (Ho and Hantash, 2013). Through these

processes as well as wound contraction, in which the wound periphery advances towards the centre of the wound (Ehrlich and Hunt, 2012), the wound is closed. Finally, in the remodeling phase, the new ECM within the healed wound is transformed to create a mature, acellular scar (Ho and Hantash, 2013).

Therapeutic agents, such as nanocrystalline silver, impact on the complex cellular and molecular events of each of the above phases. Therefore, an understanding of these events is vital to appreciate the effects of the therapeutic agent on healing.

1.1.1 Early wound healing: the inflammatory phase

At the time of a cutaneous injury, endothelial damage and exposure of blood constituents to ECM proteins, such as collagen, initiate platelet aggregation and the coagulation cascade (Reinke and Sorg, 2012). Besides achieving haemostasis, the resulting fibrin clot provides a temporary ECM into which the cells involved in cutaneous wound healing can migrate. Furthermore, tissue damage and platelet aggregation cause the release of multiple cytokines which initiate the inflammatory response and mediate the proliferative phase of healing (Ho and Hantash, 2013).

Neutrophils are the first inflammatory cells in the wound and are recruited to the wound immediately after haemostasis is achieved (Broughton *et al*., 2006; Wilgus *et al*., 2013). They produce a number of antimicrobial substances and proteases. These include reactive oxygen species (ROS) and matrix metalloproteinases (MMPs), which aid the phagocytosis of microbes and damaged tissue (Broughton *et al*., 2006; Wilgus *et al.,* 2013). Additionally, neutrophils increase the inflammatory response by releasing pro-inflammatory cytokines

which recruit other inflammatory cells, such as macrophages, to the wound (Reinke and Sorg, 2012; Wilgus*t al*., 2013).

Approximately 72 hours after skin injury, macrophages replace neutrophils in the wound (Reinke and Sorg, 2012). Initially, macrophages perform an antimicrobial function, secrete pro-inflammatory cytokines which regulate the inflammatory response and produce MMPs and other proteases, which break down damaged tissue before it is removed by phagocytosis (Broughton *et al*., 2006; Sindrilaru and Scharffetter-Kochanek, 2013). As inflammation resolves, macrophages undergo a phenotypic change and become a primary source of cytokines and growth factors (Broughton *et al*., 2006; Sindrilaru and Scharffetter-Kochanek, 2013). These factors initiate the proliferative phase of cutaneous wound healing by stimulating keratinocyte, fibroblast and endothelial cell migration and proliferation (Baum and Arpey, 2005; Broughton *et al*., 2006).

1.1.2 Intermediate wound healing: the proliferative phase

The proliferative phase of cutaneous wound healing begins approximately three days after injury (Reinke and Sorg, 2012). It is mediated by macrophages, keratinocytes and fibroblasts through cell-ECM interactions and the release of cytokines and growth factors (Baum and Arpey, 2005; Broughton *et al*., 2006; Werner *et al*., 2007), a few of which are discussed below. During the proliferative phase, the inflammatory response decreases and keratinocyte, fibroblast and endothelial cell migration and proliferation increase (Ho and Hantash, 2013).

Re-epithelialisation is the process by which keratinocytes migrate, proliferate and terminally differentiate to cover the wound with a keratinized, stratified squamous epidermis (Li *et al*., 2007). After injury, interleukin (IL)-1, IL-6, IL-8, tumour necrosis factor (TNF)- α, platelet

derived growth factor (PDGF), epidermal growth factor (EGF), transforming growth factor (TGF)-β and keratinocyte growth factor (KGF; also known as fibroblast growth factor 7) as well as keratinocyte-ECM interactions induce basal and suprabasal keratinocytes adjacent to the wound edge to change into a migratory phenotype (Sivamani *et al*., 2007; Werner *et al*., 2007). These cells are able to detach from the basement membrane and adjacent cells and migrate into the wound along the temporary ECM components (Sivamani *et al*., 2007). A vital characteristic of migrating keratinocytes is the ability to secrete MMPs. MMP-2 and MMP-9 are particularly important for digestion of ECM components allowing keratinocytes to move through the fibrin clot (Ågren, 1999; Sivamani *et al*., 2007).

As keratinocytes migrate into the wound and form tongues of new epithelium, keratinocyte proliferation is stimulated by IL-1, IL-6, IL-8, TNF-α, PDGF, EGF and KGF (Sivamani *et al*., 2007; Werner *et al*., 2007). Initially, epithelial stem cells, found in the basal layer of the uninjured epidermis as well as epidermal appendages adjacent to the wound edge, proliferate (Sivamani *et al*., 2007; Reinke and Sorg, 2012). This provides a supply of keratinocytes which can migrate into the wound (Braiman-Wilksman *et al*., 2007). As re-epithelialisation progresses, keratinocyte proliferation also occurs within the new epithelium (Braiman-Wilksman *et al*., 2007).

In the final process of re-epithelialisation the keratinocytes terminally differentiate to form a keratinized, stratified squamous epithelium (Li *et al*., 2007). Terminal differentiation, stimulated by TGF-β (Werner and Smola, 2001), begins in the new epithelium at the wound edge and progresses along the new epithelium towards the centre of the wound (Braiman-Wilksman *et al*., 2007). However, it does not occur at the centre of the wound until epidermal continuity is restored (Odland and Ross, 1968; Braiman-Wilksman *et al*., 2007).

Oxygen and nutrients are vital for the function of fibroblasts, keratinocytes and the inflammatory cells within the cutaneous wound. Hypoxia and the acidic milieu created by anaerobic metabolism are potent stimuli for angiogenesis (Baum and Arpey, 2005). After skin injury, vascular endothelial growth factor (VEGF) and other angiogenic factors are released by macrophages, keratinocytes, fibroblasts and endothelial cells (Ho and Hantash, 2013). In response to VEGF, pericytes and endothelial cells from blood vessels adjacent to the wound loosen their cell junctions and detach from the basement membrane (Carmeliet and Jain, 2011). Endothelial cells secrete MMPs and migrate into the fibrin clot under the influence of VEGF, TGF-β, fibroblast growth factor (FGF) and the components of the ECM to which the cells are now exposed (Javerzat *et al.*, 2002; Pardali *et al.*, 2010; Carmeliet and Jain, 2011; Greaves *et al.*, 2013). The leading or tip cell determines the direction of migration in response to angiogenic factors while the stalk cells behind it proliferate and form a lumen (Carmeliet and Jain, 2011). Initially, the endothelial tubes are leaky and blood flows poorly through them (Carmeliet and Jain, 2011; DiPietro, 2013). Pericytes, stimulated by TGF-β, PDGF and angiopoetins, surround the endothelial tubes (Carmeliet and Jain, 2011). A new basement membrane is deposited and endothelial cell junctions are increased. This stabilises the vessels improving blood flow (Carmeliet and Jain, 2011). Endothelial tubes which have poor blood flow regress whereas those that have good blood flow and are surrounded by pericytes persist (Carmeliet and Jain, 2011). Thus a mature, functional vascular network is formed within the new ECM.

Restoration of damaged ECM begins during the proliferative phase and continues into the remodelling phase of cutaneous healing (Ho and Hantash, 2013). Under the influence of PDGF, TGF-β, IL-1, TNF-α FGF, EGF, interferon (IFN)-γ and ECM components such as cysteine rich 61 (cyr61), fibroblasts from the adjacent non-wounded dermis migrate into the

wound area, proliferate and secrete the components of a permanent ECM (Baum and Arpey, 2005; Broughton *et al*., 2006). Starting three to five days after injury, fibroblasts secrete collagens, proteoglycans and glycosaminoglycans, replacing the fibrin clot with a collagenous matrix (Baum and Arpey, 2005). TGF-β and fibroblast-ECM interactions are of particular importance as they control not only collagen synthesis, but also the secretion of MMPs by fibroblasts and differentiation of fibroblasts into myofibroblasts (Baum and Arpey, 2005; Broughton *et al*., 2006). Myofibroblasts can be found in the wound from day four or six after injury and are important in wound contraction, decreasing the size of the skin wound (Baum and Arpey, 2005). As with keratinocytes, MMPs play an important role in the migration of fibroblasts into the wound area. In addition, they are vital for the remodelling of the ECM from the temporary matrix of the fibrin clot into the collagenous matrix of a mature, functional scar (Baum and Arpey, 2005). Therefore, the secretion of MMPs and their inhibitors, tissue inhibitors of matrix metalloproteinases (TIMPs), are carefully regulated by TGF-β, IL1, cyr61, PDGF and EGF (Baum and Arpey, 2005).

1.1.3 Late wound healing: the remodeling phase

The collagen secretion that began three to five days after injury, in the proliferative phase of healing, continues at an increased rate for approximately three weeks (Baum and Arpey, 2005). Fibroblast-ECM interactions as well as TNF-α and IL-1 then mediate a decrease in collagen synthesis until the rate of collagen synthesis by fibroblasts and degradation by MMPs are equal. In this steady state remodelling occurs and may continue for 12 months (Baum and Arpey, 2005).

During the proliferative phase, fibroblasts lay down type III collagen and proteoglycans. In the remodelling phase, these ECM components are replaced by type I collagen which is

secreted by fibroblasts along lines of tension in the wound (Baum and Arpey, 2005; Broughton *et al.*, 2006). As remodelling progresses, the collagen fibres within the wound are aligned parallel to the wound surface (Ehrlich and Krummel, 1996). In addition, increased fibril cross-linking results in stronger collagen fibres with larger diameters (Baum and Arpey, 2005). Larger collagen fibres aid wound contraction and increase the tensile strength of the wound (Baum and Arpey, 2005; Ehrlich and Hunt, 2012). Wound contraction, mediated by myofibroblasts, occurs for approximately 14 days after skin injury and further decreases the size of the wound area. Concurrently, the number of blood vessels within the wound decreases and fibroblasts undergo apoptosis (Baum and Arpey, 2005). Thus, remodelling increases the tensile strength of the scar and results in the morphological characteristics of an acellular, 'mature' scar (Baum and Arpey, 2005).

This simplistic description of events in cutaneous wound healing belies the true complexity of the process. Growth factors may influence healing in different types of wounds in distinctive ways. Over-expression of TGF-β in partial-thickness wounds results in increased re-epithelialisation whereas in full-thickness wounds it delays healing (Tredget *et al*., 2005). In addition, the equilibrium of different growth factors and cytokines within a wound, the time at which they are expressed and ECM interactions all influence the effect of a particular factor (Sivamani *et al*., 2007; Wilgus 2012; Greaves *et al*., 2013). Furthermore, cleavage of factors by MMPs can result in factor activation or inactivation (Ho and Hantash, 2013; McCarty and Percival, 2013) or the formation of alternative isoforms with different functions (Carmeliet and Jain, 2011). Thus, the correct balance of growth factors, cytokines, MMPs and TIMPs are vital for the progression of healing. Indeed, an increased inflammatory response, excessive MMP activity and abnormalities in cytokine and growth factor expression are the hallmarks of chronic wounds (Widgerow, 2012).

1.2 Silver in wound healing

Traditionally, ionic silver (Ag^+), in the form of silver salts or silver sulfadiazine, has been used to treat wounds that are infected or at risk of infection (Khundkar *et al*., 2010). The rationale for using these dressings is the antimicrobial action of Ag^+ against gram negative and gram positive bacteria, including resistant strains, as well as fungal pathogens (Atiyeh *et al*., 2007). This broad spectrum of antimicrobial activity, which is concentration dependent, is attributed to the ability of Ag^+ to affect the bacterial cell wall, disrupt the respiratory chain and inhibit protein, RNA and DNA synthesis (Percival *et al*., 2005). While bacterial resistance to silver has been described, it is transient and infrequent (Percival *et al*., 2005). Therefore, silver is an attractive topical therapeutic and prophylactic antimicrobial agent, particularly in light of the emergence of multi-drug resistant bacteria (Khundkar *et al*., 2010).

However, there is evidence that Ag^+ is toxic to keratinocytes and fibroblasts *in vitro* (McCauley *et al*., 1989; Hidalgo and Domínguez, 1998; Lee and Moon, 2003; Fraser *et al*., 2004; Poon and Burd, 2004) and that wounds treated with Ag^+ heal more slowly compared to other dressings (Malik *et al*., 2010; Dokter *et al*., 2013; Hoeksema *et al*., 2013; Wasiak *et al*., 2013; Vloemans *et al*., 2014). An additional concern when using Ag^+ dressings is the increased pain and treatment cost due to frequent dressing changes (Tredget *et al*., 1998; Varas *et al*., 2005; Muangman *et al*., 2006; Cox *et al*., 2011). Ag^+ is delivered to the wound in a bolus form and is rapidly inactivated by chloride, proteins and other compounds within the wound (Atiyeh *et al*., 2007). Therefore, frequent dressing changes are needed to maintain the concentration of Ag^+ and thereby its antimicrobial effects (Atiyeh *et al*., 2007).

Technological advances have allowed the formulation of dressings which release Ag^+ into the wound in a sustained manner. Acticoat^{TM}, one of the slow-release silver dressings, consists of

two layers of polyethylene mesh coated with silver nanoparticles (<20nm diameter) surrounding a layer of absorbent rayon polyester gauze (Dunn and Edward-Jones, 2004; Atiyeh *et al*., 2007). As the silver is impregnated in the mesh, it is continuously released into the wound providing a sustained silver concentration over the time the dressing is used. Additionally, both ionic (Ag^{+}) and non -ionic (Ag^{0}) silver are released by Acticoat^{TM} (Atiyeh *et al*., 2007). Ag^{0} is deactivated less rapidly than Ag^{+} by chloride, proteins and other compounds in the wound (Atiyeh *et al*., 2007). Furthermore, Ag^{0} is ionized within the wound environment to provide an additional source of Ag^{+}, the active form of silver (Atiyeh *et al*., 2007). Thus, nanocrystalline silver dressings lead to a sustained concentration of active silver within the wound. This negates the need for frequent dressing changes thus improving patients perception of pain and decreasing treatment costs (Tredget *et al*., 1998; Varas *et al*., 2005; Muangman *et al*., 2006; Atiyeh *et al*., 2007; Cox *et al*., 2011).

Wounds treated with silver nanoparticles may heal faster that those treated with other forms of silver (Cuttle *et al*., 2007; Huang *et al*., 2007; Tian *et al*., 2007; Nadworny *et al*., 2008; Gravante and Montone, 2010; Wasiak *et al*., 2013). In addition, Acticoat^{TM} is a more effective antimicrobial agent than silver sulfadiazine (Wright *et al*., 1999; Yin *et al*., 1999; Uygur *et al*., 2009) as well as a number of other silver containing dressings (Thomas and McCubbin, 2003; Fong *et al*., 2005; Heggers *et al*., 2005; Edwards-Jones, 2006; Ip *et al*., 2006; Castellano *et al*., 2007). These differences are attributed to the sustained silver concentration released by Acticoat^{TM} (Thomas and McCubbin, 2003; Castellano *et al*., 2007), as well as the unique properties of the nanoparticles (Aityeh *et al*., 2007; Foldbjerg *et al*., 2009; Park *et al*., 2011; Beer *et al*., 2012). Therefore, the present review is restricted to *in vivo* or *in vitro* studies which investigate the effects of silver nanoparticles.

Due to their small size, silver nanoparticles are able to enter cells by endocytosis (AshaRani *et al*., 2009; Wei *et al*., 2010; Greulich *et al*., 20011b; Haase *et al*., 2011; Singh and Ramarao, 2012). Within the cytoplasm, the silver nanoparticles are found near or in the nucleus and mitochondria (AshaRani *et al*., 2009; Wei *et al*., 2010; Greulich *et al*., 2011b; Haase *et al*., 2011; Hackenberg *et al*., 2011; Singh and Ramarao, 2012; Bressan *et al*., 2013; Rigo *et al*., 2013). Silver nanoparticles affect mitochondrial structure and function which induces oxidative stress with the generation of ROS and decreases cell viability (Carlson *et al*., 2008; AshaRani *et al*., 2009; Teodoro *et al*., 2011; Singh and Ramarao, 2012; Bressan *et al*., 2013). While it is unclear if the generation of ROS and decreased cell viability always results in apoptosis and cell death (Arora *et al*., 2008; Hsin *et al*., 2008; Van den Plas *et al*., 2008; AshaRani *et al*., 2009; Foldbjerg *et al*., 2009; Singh and Ramarao, 2012; Rigo *et al*., 2013), it is clear that ROS damage DNA (Ahamed *et al*., 2008; Arora *et al*., 2008; AshaRani *et al*., 2009; Kalishwaralal *et al*., 2009; Hackenberg *et al*., 2011). This inhibits cell proliferation and causes arrest in the G2/M or S phase of the cell cycle (AshaRani *et al*., 2009; Park *et al*., 2010; Wei *et al*., 2010; Zanette *et al*., 2011; Beer *et al*., 2012).

The above effects are dependent on the length of exposure to and concentration of the silver nanoparticles (Arora *et al*., 2008; AshaRani *et al*., 2009; Greulich *et al*., 2009; Park *et al*., 2010; Wei *et al*., 2010; Greulich *et al*., 2011a; Greulich *et al*., 2011b; Hackenberg *et al*., 2011). Furthermore, smaller silver nanoparticles (Carlson *et al*., 2008; Wei *et al*., 2010; Park *et al*., 2011) and those that are not coated by stabilising agents, display increased toxicity (Samberg *et al*., 2010; de Lima *et al*., 2012). Culture of keratinocytes with unwashed- or washed- uncoated silver nanoparticles (20nm, 50nm and 80nm) at concentrations of 0.34μg/ml to 1.7μg/ml decreased cell viability compared to untreated controls and carbon coated silver nanoparticles (25nm and 35nm) (Samberg *et al*., 2010).

Additionally, silver nanoparticles have different effects on different cell types. Fibroblasts are more susceptible to the toxic effects of silver nanoparticles than keratinocytes (Van Den Plas *et al*., 2008; Liu *et al*., 2010) or macrophages (Park *et al*., 2011) and monocytes and T-cells respond differently to silver nanoparticles (Greulich *et al*., 2011a). Polyvinylpyrrolidone-coated (PVP) silver nanoparticles decreased cell viability when cultured with HaCaT cells (<48.8nm, >6.25µg/ml) (Zanette *et al*., 2011), endothelial cells (<5nm, >20µg/ml) (Kang *et al*., 2011), monocytes (<90nm, >25µg/ml) (Greulich *et al*., 2011a) and human mesenchymal stem cells (100nm, >3.5µg/ml) (Greulich *et al*., 2009). Furthermore, decreased cell viability is seen in human fibroblasts cultured with silver nanoparticles (5-15nm) at concentrations greater than 100µM[#] (Liu *et al*., 2010) in endothelial cells cultured with silver nanoparticles (50nm) at concentrations greater than 500nM (Gurunathan *et al*., 2009; Kalishwaralal *et al*., 2009) and in mouse macrophages cultured with silver nanoparticles (<90nm) at concentrations of 0.8 and 1.6ppm^ (Park *et al*., 2010).

Release of silver from Acticoat™ creates a sustained silver concentration of silver between 70µg/g and 100µg/g in human serum substitute* (Rigo *et al*., 2012). This concentration is substantially higher than those at which silver nanoparticles decrease cell viability *in vitro* (for examples see Arora *et al*., 2008; Carlson *et al*., 2008; Liu *et al*., 2010; Samberg *et al*., 2010; Park *et al*., 2011). Indeed, decreased viability is reported in keratinocytes, HaCaT cells and fibroblasts cultured with Acticoat™ (Fraser *et al*., 2004; Lam *et al*., 2004; Poon and Burd, 2004; Burd *et al*., 2007; Van Den Plas *et al*., 2008; Kempf *et al*., 2011). This is one reason Acticoat™ is not recommended for the treatment of acute, non-inflamed wounds (Widgerow, 2010).

1µM is approximately equal to 0.1µg/ml ^ 1ppm is approximately equal to 1µg/ml
* 1µg/g in human serum substitute is approximately equal to 1µg/ml

However, *in vitro* results may not be directly transferable to the clinical situation. Studies on wound fluid have shown that the quantity and type of proteins present in chronic wounds differ from acute wounds (Widgerow, 2011). As the silver released from Acticoat^{TM} forms complexes with chloride and proteins (Rigo *et al*., 2012), the wound environment may affect the concentration of silver within the wound. In addition, the complexity of the cell environment influences the activity of silver nanoparticles. Fewer keratinocytes and fibroblasts are viable when cultured with silver nanoparticles delivered in water or saline compared to culture media containing growth factors (Burd *et al*., 2007).

Furthermore, silver nanoparticles affect cell function as well as viability. Toxic concentrations of silver nanoparticles inhibit endothelial cell migration and tube formation (Gurunathan *et al*., 2009; Kalishwaralal *et al*., 2009) and human mesenchymal stem cell migration *in vitro* (Greulich *et al*., 2009). Additionally, toxic concentrations of silver nanoparticles stimulate secretion of IL-1, IL-6 and TNF-α by macrophages (Carlson *et al*., 2008; Park *et al*., 2010; Singh and Ramarao, 2012) and keratinocytes (Samberg *et al*., 2010) and decrease the secretion of IL-6, Il-8 and VEGF by human mesenchymal stem cells *in vitro* (Greulich *et al*., 2009; Hackenberg *et al*., 2011). However, lower non-toxic concentrations of silver nanoparticles can increase or decrease the function of different cell types.

Fibroblasts cultured with more than 25μM silver nanoparticles (5-15nm) produce less collagen and hydroxyproline and undergo a phenotypic change to myofibroblasts (Liu *et al*., 2010). The phenotypic change was confirmed *in vivo* in a mouse model of full-thickness excisional wounds treated with a dressing containing 0.04mg/cm^2 of silver nanoparticles, which showed increased α-SMA expression on day 7 post-wounding (Liu *et al*., 2010).

1μM is approximately equal to 0.1μg/ml 1ppm is approximately equal to 1μg/ml

Increased endothelial cell migration and tube formation, mediated via VEGF receptor signaling pathways, was reported when endothelial cells were cultured with PVP-coated silver nanoparticles (<5nm, concentration 5µg/ml to 20µg/ml) (Kang *et al*., 2011). These changes were associated with increased VEGF expression in endothelial cells (Kang *et al*., 2011). Similarly, increased VEGF expression has been described in mesenchymal stem cells cultured with non-toxic concentrations of silver nanoparticles (<80nm, ≤1µg/ml) (Hackenberg *et al*., 2011). Additionally, in a mouse matrigel model, thicker and more functional blood vessels were found in matrigel impregnated with 200µg (10mg/kg) of PVP coated silver nanoparticles (<5nm) than in matrigel which did not contain silver nanoparticles, ten days after the matrigel was injected into the mice (Kang *et al*., 2011).

Silver nanoparticles also affect the secretion of MMPs and TIMPs. Macrophages cultured with 0.8ppm and 1.6ppm of silver nanoparticles (<90nm) showed decreased expression of MMP-3, MMP-11 and MMP-19 RNA as well as TIMP-1 RNA (Park *et al*., 2010). Silver nanoparticles are also able to directly affect the function of MMPs. Acticoat™ and solutions of silver extracted from Acticoat™ decrease the activity of MMP -2, MMP -9 (Walker *et al*., 2007) and bacterial collegenase (Shi *et al*., 2010; Jovanovic *et al*., 2012) respectively. Silver ions also inhibit serine proteases (Chambers *et al*., 1974). The decrease in MMP-2 and MMP-9 levels and activity seen *in vitro* have been reproduced *in vivo* in porcine models of contact dermatitis (Nadworny *et al*., 2008; 2010) and contaminated wounds (Wright *et al*., 2002) treated with Acticoat™. However, as MMP-2 and MMP-9 are important in re-epithelialisation, their inhibition by Acticoat™ is another reason for recommending that the dressing is not used for the treatment of acute, non-inflamed wounds (Widgerow, 2010).

Changes in cytokine and growth factor secretion are also noted in cells cultured with silver nanoparticles. Macrophages cultured with non-toxic concentrations of silver nanoparticles secrete greater amounts of TNF-α (Carlson *et al*., 2008; Park *et al*., 2010; Park *et al*., 2011). Similarly, increased IL-1 and IL-6 secretion was observed in silver-nanoparticle treated macrophages (Carlson *et al*., 2008; Park *et al*., 2011) and human mesenchymal stem cells (Hackenberg *et al*., 2011). Increased IL-6 and IL-8 secretion was also noted when human blood monocytes were cultured with PVP coated silver nanoparticles at concentrations between 5µg/ml and 20µg/ml (Greulich *et al*., 2011a). In contrast, PVP coated silver nanoparticles did not affect the secretion of IL-2 or IL-4 by T-cells *in vitro* (Greulich *et al*., 2011a).

In contrast, decreased levels of TNF-α, IL-8 and TGF-β_1 and increased levels of EGF, KGF, KGF-2 and IL-4 are described in porcine and mouse models of contact dermatitis treated with Acticoat^{TM} or solutions of silver nanoparticles eluted from Acticoat^{TM} compared to inactive controls (Nadworny *et al*., 2008; 2010). Similarly, in a mouse burn wound model treated with Acticoat^{TM} compared to silver sulphadiazine or antibiotic dressings, decreased levels of IL-6 and increased levels of VEGF, IL-10 and IFN-γ were reported on all of the days investigated (Tian *et al*., 2007). However, TGF-β_1 levels were raised within the first 5 days after injury, but were significantly lower beyond the 5th day after injury in Acticoat^{TM}-treated wounds (Tian *et al*., 2007). These changes in cytokine and growth factor expression are associated with a decreased inflammatory response and an increase in macrophage and polymorphonuclear cell apoptosis (Wright *et al*., 2002; Bhol and Schechter, 2004; Bhol and Schechter, 2005; Tian *et al*., 2007; Nadworny *et al*., 2008; Nadworny *et al*., 2010). Due to the importance of the inflammatory response in regulating cutaneous wound healing (Broughton

et al., 2006), the ability of silver nanoparticles to modulate cytokine and growth factor production and the inflammatory response is significant.

Thus, silver nanoparticles may influence all phases of healing not only by direct effects on cell viability and function, but also through influencing cytokine, growth factor, MMP and TIMP expression and function. Due to these effects of silver nanoparticles as well as their anti-inflammatory action and potent antimicrobial activity *in vitro*, they are recommended for the treatment of wounds with high levels of inflammation, such as chronic and infected wounds and burns (Widgerow, 2010).

Indeed, studies show improvement in chronic wounds treated with silver dressings compared to Allevyn (a polyurethane foam dressing) (Jørgenson *et al*., 2005) or local best practice (Münter *et al*., 2006). Furthermore, improved rates of healing have been found when silver nanoparticle solutions, creams and dressings are compared to a variety of controls in rodent models of excisional wounds (Liu *et al*., 2010; Arican *et al*., 2012; Prestes *et al*., 2012), burns (Tian *et al*., 2007) and contact dermatitis (Bhol and Schechter, 2005). Similarly, improved healing is seen in silver nanoparticle-treated porcine donor sites compared to petrolatum gauze (Olson *et al*., 2000), porcine models of contaminated wounds (Wright *et al*., 2002) and porcine models of contact dermatitis (Nadworny *et al*., 2008; 2010). In addition, clinical studies have shown improved re-epithelialisation of split thickness skin graft donor sites when treated with Acticoat™ as compared to Allevyn (Argirova *et al*., 2007) as well as split thickness skin graft recipient sites when treated with Acticoat™ compared to a standard Xeroform dressing (Demling and DeSanti, 2002). Furthermore, a retrospective review found decreased healing times in full-thickness burns treated with Acticoat™ (Gravante and Montone, 2010).

However, decreased re-epithelialisation was noted in Aticoat^{TM}-treated split thickness skin graft donor sites compared to Allevyn (Innes *et al*., 2001) and mouse excisional wounds compared to Tegaderm (Burd *et al*., 2007). Similarly, decreased re-epithelialisation is seen in porcine models of deep partial-thickness burns treated with Acticoat^{TM} compared to hydrate gel/ gauze dressings (Wang *et al*., 2010). Acticoat^{TM} also inhibited re-epithelialisation of full-thickness wounds in a skin explant model (Fredriksson *et al*., 2009). Silver *et al* (2007) found no difference in healing between meshed autograft sites treated with Acticoat^{TM} or 5% sulfamylon. Similarly, no difference was found in the rate of healing of contact dermatitis in mice between silver nanoparticle creams and steroids or tacrolimus (Bhol and Schechter, 2004; 2005). Silver dressings, including Acticoat^{TM}, were also no more effective than 10% povidone-iodine in the treatment of MRSA infected excisional wounds in diabetic rats (Lee *et al*., 2013). Furthermore, systematic reviews report similar or worse healing times in silver-treated wounds compared to controls (Storm-Versloot *et al*., 2010; Aziz *et al*., 2012; O'Meara *et al*., 2013).

Interpretation of these contradictory results is difficult due to the multiple wound models used to investigate the effect of silver nanoparticles on healing. Apart from differences in healing between the various animal models (Ansell *et al*., 2012), differences exist in the manner in which different types of wounds heal. Partial-thickness wounds, such as burns, donor sites and contact dermatitis heal predominantly through re-epithelialisation, whereas in full-thickness wounds, such as excisional wounds, dermal constituents play an increased role in healing (Davidson, 1998). Furthermore, acute non-infected wounds heal differently to infected or chronic wounds (Davidson, 1998; Reinke and Sorg, 2013). Thus, results from studies investigating partial-thickness, infected or chronic wounds may not be applicable to

acute, full-thickness, non-infected wounds. In addition, few studies have described the effect of nanocrystalline silver on the acute wound bed (Atiyeh *et al*., 2007).

Therefore, the present study aimed to investigate the effect of a nanocrystalline silver dressing (Acticoat^{TM}) on wound healing in acute full-thickness excisional dermal wounds in a porcine model.

The domestic pig was chosen as the model for this study due to the known histological and physiological similarities between porcine and human skin (Sullivan, *et al*., 2001). Among many similarities, the arrangement of the epidermis and dermis, turnover time of epidermal cells, epidermal proteins and lipids, biochemical structure of collagen and the arrangement of vascular structures within the dermis are all comparable between humans and pigs (Mowafy and Cassens, 1975; Meyer *et al*., 1981; Meyer *et al*., 1982; Morris and Hopewell, 1990; Wollina *et al*., 1991; Vardaxis *et al*., 1997; Sullivan *et al*., 2001). Additionally, in both humans and pigs, wound healing occurs primarily through re-epithelialisation as compared to other common animal models, such as the mouse and rat which heal mainly through wound contraction (Sullivan *et al*., 2001).

As the phases of healing occur in a predictable manner in an acute wound, the events of each stage can be used to assess the progress of wound healing. Therefore, the following aspects were studied:

1. The rate of wound closure as evidenced by the percentage change in wound area
2. A clinical assessment of wound quality in the re-epithelialised wound
3. A histological assessment of epithelial restoration and blood vessel formation
4. The number of inflammatory cells in the wound
5. The number of proliferating keratinocytes and fibroblasts
6. An assessment of the percentage area and arrangement of collagen within the wound
7. A quantitative estimation of collagen content

2. MATERIALS AND METHODS

2.1 Experimental animals

Nine female "Large White" pigs (*Sus scrofa domesticus*), which weighed between 30 and 60kg, were used for the study. Each pig was housed in a separate pen at the Central Animal Services of the University of the Witwatersrand and was given free access to food and water. The pigs arrived in the unit at least five days before surgery, to allow them to acclimatise.

Ethical clearance for the study was obtained from the Animal Ethics Screening Committee of the University of the Witwatersrand (AESC number 2009/2604) (Appendix A).

2.2 Wound creation and specimen collection

Intramuscular Ketamine (11mg/kg) and Midazolam (0.3mg/kg) were used to sedate each pig before induction of general anaesthesia with 2-5% Isoflurane administered through a mask. The dorsum of the pig was shaved using animal clippers, washed with sterile water and draped with surgical drapes. A sterilised template was used to mark four paravertebral wounds of 5x20mm each, on each side of the midline. The short axis of the wound lay parallel to the vertebral column (Fig. 2.1). Full-thickness excisional wounds were created by using a scalpel blade to excise the skin of each marked area down to the fascial plane. In the first two pigs which underwent surgery, the wounds were spaced 20mm apart. Due to problems with adherence of the secondary dressing, the distance between wounds was increased to 40mm in subsequent experiments.

Wounds to the left and right of the midline were allocated as a pair for excision on either day 3, 6, 9 or 15 post-wounding. The allocation according to the day post-wounding varied between the pigs so that specimens from different regions of the dorsum of the pigs (e.g.

towards the head or tail) were collected on each of the excision days (Fig. 2.1). Day 3, 6, 9 and 15 post-wounding were chosen as the days for excision to allow for investigation of the effect of nanocrystalline silver in all of the phases of healing (Broughton *et al*., 2006).

Acticoat™ (Smith & Nephew Medical Limited) was provided by Professor Heinz Rode, Department of Paediatric Surgery, School of Adolescent and Child Health of the University of Cape Town. Opsite™ (Smith & Nephew Medical Limited) was obtained from the Central Animal Services of the University of the Witwatersrand. Opsite™, a polyurethane film dressing, was selected as the control dressing as it aids healing by providing a moist environment (Ahamed, 1982; Kaufman and Hirshowitz, 1983; Sullivan *et al*., 2001).

Before dressing the wounds, a calibrated scale was placed alongside each wound and standardised digital photographs were taken at right angles to the wound. The dorsum of the pig was then cleaned with sterile water. For each wound pair, the wound on the left of the midline was allocated to the experimental group and dressed with the experimental dressing (Acticoat™), which was cut to the size of the wound and moistened with sterile water as per the manufacturer's instructions. The wound on the right of the midline was allocated to the control group and dressed with the control dressing (Opsite™). All wounds received a secondary dressing of gauze, Opsite™, Elastoplast® and veterinary stocking in order to minimise the risk of infection and to prevent the experimental and control dressings being displaced when the pigs rolled on the floor or scratched their backs. The allocation to the experimental group (dressed with Acticoat™) or control group (dressed with Opsite™) and to a day for excision post-wounding was recorded by the researcher.

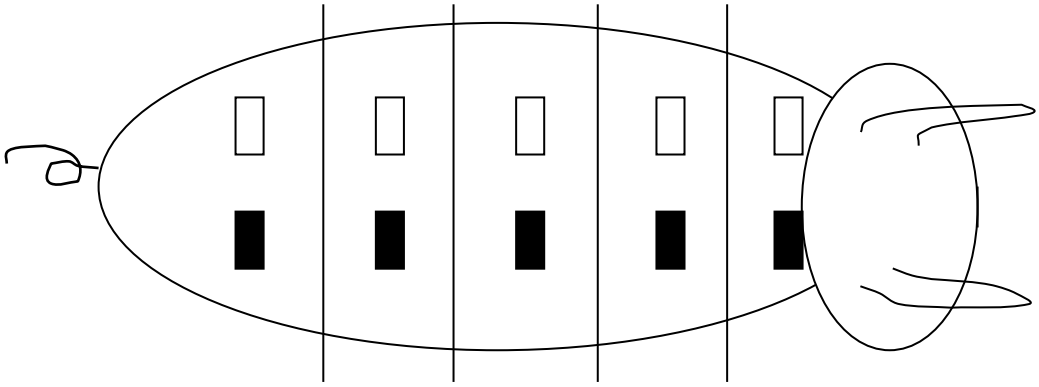

Pig number	**Weight (kg)**	**The day post-wounding on which the wound was excised**				
1	56.5	6*	9*	None	15*	3*
2	58.1	6*	9*	None	15*	3*
3	45.5	3	6	9	15*	15*
4	46.4	3	6	9	15	None
5	43.4	15*	3	6	9	None
6	40.2	15*	15*	3*	6*	9
7	35.8	9*	15*	3	6	15*
8	33.9	9*	15*	3	6	15*
9	38.75	15	9	15	15	15

Figure 2.1: Position of the wounds on the dorsum of the pig and allocation to the day for excision post-wounding.

□ = experimental wound ■ = control wound; *wound pair excluded from analysis

On day 3, 6, 9, 12 and 15 post-wounding, each pig was anaesthetised in the same way as on the day of wound creation. The dorsum of the pig was cleaned with sterile water, taking care not to remove adherent scabs or damage the new epithelium beneath scabs. Surgical drapes were placed on the dorsum of the pig. A calibrated scale was placed alongside each wound and digital photographs were again taken, as on the day of wound creation. The entire epidermis, dermis, hypodermis and underlying fascia of the site of the allocated experimental and control wounds were excised, together with a uniform perimeter of normal tissue. The resulting excisional site was sutured and excluded from further analysis. The excised tissue was fixed in 10% buffered formalin for 24 hours and then processed according to the protocols of the School of Anatomical Sciences (see Section 2.4). The remaining wounds were dressed with the experimental or control dressing as allocated, and the secondary dressing was applied as on the day of wound creation. If it was thought that hair would interfere with the adherence of the secondary dressing, the hair was shaved using animal clippers before the secondary dressing was applied.

Due to the pigs scratching their backs, the dressings on three experimental wounds for excision on day 3 post-wounding, three experimental wounds for excision on day 6 post-wounding, four experimental wounds for excision on day 9 post wounding and eleven experimental wounds for excision on day 15 post-wounding were displaced from the wound bed (Fig. 2.1). These wounds were excluded from the study and one wound pair, allocated for excision on the appropriate day, was added to each pig in subsequent experiments. Therefore, five experimental and five control wounds were analysed for each excision day (day 3, 6, 9 and 15) post-wounding (total number of wounds = 40).

2.3 Macroscopic assessment

2.3.1 Measurement of the change in wound area over time

The change in wound area over time for each of the 40 wounds was calculated using digital photographs taken at the time of wound creation and on days 3, 6, 9, 12 and 15 respectively post-wounding. The number of wounds measured for the change in area over time decreased on each day post-wounding as wounds were excised. Therefore, twenty experimental and twenty control wounds were measured for the change in wound area from day 0 to day 3 post-wounding, fifteen experimental and fifteen control wounds for the change in wound area from day 0 to day 6 post-wounding, ten experimental and ten control wounds for the change in wound area from day 0 to day 9 post-wounding and five experimental and five control wounds for the change in wound area from day 0 to day 12 and to day 15 post-wounding.

Using ImageJ® (version 1.46), a public domain, java based image analysis programme available at http://rsb.info.nih.gov/nih-image/, the appropriate scale was added and the area of each wound was calculated by tracing the perimeter of the un-epithelialised area of each wound. Adherent scab, if present, was included within the area of the wound. Each area was traced three times and the average area of the wound was calculated in mm^2 for each image (Branski *et al*., 2008; Pather, 2009). The average area of the wound was used to calculate the percentage change in the area of each wound from the time of wound creation to day 3, 6, 9, 12 or 15 post-wounding. The following formula (Pather, 2009) was used:

$$\text{Percentage change in area} = \frac{(\text{Area of wound on day 0} - \text{Area of wound on day x})}{\text{Area of wound on day 0}} \times 100$$

The percentage change in the area of each wound for the appropriate time period was used for further analysis.

2.3.2 Clinical assessment of wound quality

The "Clinical Assessment Score" was developed as a tool for the clinical and histological assessment of healed wounds in humans (Beausang *et al*., 1998). It has subsequently been utilised for the assessment of re-epithelialised wounds in porcine models of wound healing (Theunissen, 2001). The Score compares the re-epithelialised wound to the surrounding normal skin using five parameters, each of which is allocated a numerical value (Table 2.1). In addition, a visual analogue scale of 0 to 10 is used to indicate an overall assessment of each wound. The visual analogue score and numerical values are added together to give an overall score indicating the quality and clinical acceptability of each re-epithelialised wound (Beausang *et al*., 1998).

The researcher and two independent observers used the photographs of the five experimental and five control wounds on day 12 and 15 post-wounding to determine the Score for each re-epithelialised wound. As photographs were used to determine the Score, the fifth parameter (Texture) was excluded from the Score (Beausang *et al*., 1998).

Table 2.1: Clinical Assessment Score

Score	A: Colour	B	C: Contour	D: Distortion	E: Texture
1	Perfect match	Matte	Flush with surrounding skin	None	Normal
2	Slight mismatch	Shiny	Slightly proud/ indented	Mild	Just palpable
3	Obvious mismatch		Hypertrophic	Moderate	Firm
4	Gross mismatch		Keloid	Severe	Hard

Adapted from: Beausang *et al*., 1998.

2.4 Biochemical and histological assessment

All of the excised tissue from the five experimental and five control wounds for each excision day was divided into four pieces, each approximately 5mm in length. Each piece was fixed in 10% buffered formalin (Appendix B1) for 24 hours, dehydrated through a series of graded alcohols, cleared in chloroform and embedded in paraffin wax.

Serial 5µm thick sections, interspersed with five 15µm thick sections (for collagen estimation), were cut from the paraffin embedded tissue of the central portion of each wound and mounted on glass slides coated with Sta-on® tissue section adhesive (Leica, USA). Sections of 5µm thickness were selected from three spaced regions of each experimental and control wound for routine haematoxylin and eosin (H & E) staining (n=120 sections), immunocytochemical labelling with Ki-67 (n=120 sections) and staining with 0.1% picrosirius red (n=120 sections). A 15µm section adjacent to each picrosirius red stained 5µm section was allocated for the quantitative estimation of collagen content of the wound. In addition three spaced 5µm sections from each wound were used to determine if bacteria were present within the wound by use of a Gram stain (n=120 sections) (Bancroft and Gamble, 2002).

2.4.1 Histological analysis of haematoxylin and eosin stained sections

Following dewaxing in xylene and rehydration of the sections through a graded series of alcohols, routine H & E staining (Appendix B2) was carried out on the three spaced 5µm sections from each experimental wound (n= 5 for each day of excision) and control wound (n= 5 for each day of excision). This resulted in a total of 15 sections from experimental wounds and 15 sections from control wounds being analysed for each day of excision post-wounding (n=120 H&E stained sections).

A Zeiss Axioskop 2 microscope fitted with a Sony 3CCD camera (magnification 0.63x) was used to analyse each of the 120 H&E stained sections to assess the formation of blood vessels, the presence of inflammatory cells and the degree of wound closure and restoration of the epithelium, as outlined below.

Note that the figures illustrating H&E stained sections were taken using an Olympus BX61VS microscope and XC10 Camera using Olympus Dot Slide software (Olympus Soft Image solutions). As all figures were adjusted to fit the page, the scale bar in each image is representative of the true scale. The total magnification, included in the figure legend for ease of use, is indicative of the magnification of the image when it was taken and not the final magnification of the image. For composite images the total magnification is not included.

2.4.1.1 Wound closure and restoration of the epithelium

Wound closure was assessed histologically by determining the size of the gap between the edges of the epithelial tongue as well as the percentage by which the wound had closed (Jia *et al*., 2011). Three spaced sections were used from the experimental and control wounds excised on day 9 and day 15 post-wounding (n=15 sections from experimental wounds and 15 sections from control wounds for each day post-wounding). These measurements were not performed for wounds excised on day 3 or day 6 post-wounding as, in these latter wounds, the wound edges moved after excision thus obviating measurement of these wounds.

The restoration of the epithelium was evaluated by measuring the area and length of the epithelial tongue and the thickness of the epithelium at the edge of the wound and the tip of the epithelial tongue (Jia *et al*., 2011). These measurements were carried out on all 120 H&E stained sections.

Using the 10x objective, digital images were taken of the epithelial tongue on the left and right side of each wound. In addition, for measurement of the size of the epithelial gap, images were taken of the area between the tips of the epithelial tongues for wounds excised on day 9 and day 15 post-wounding. In cases where the region of interest could not be photographed in a single field of view, overlapping images were taken and reconstructed into a single image using Gnu Image Manipulation Program (GIMP version 2.8), a free image manipulation programme available online at http://www.gimp.org/downloads/. The size of the epithelial gap, the percentage by which the wound had closed, the area and the length of the epithelial tongue were measured in micrometres on these images using ImageJ® (version 1.46), after the addition of the appropriate scale.

The **percentage by which the wound had closed** was calculated using the following formula

$$\text{Percentage closure} = \frac{(\text{Width of the wound area} - \text{epithelial gap})}{\text{Width of the wound area}} \times 100$$

The **width of the wound area** was measured in experimental and control wounds excised on day 9 and day 15 post-wounding (n=60 sections) using the straight line tool in ImageJ®. To ensure that the measurement was not increased by measuring at an angle, vertical lines were drawn at the junction of the wounded and non-wounded dermis beneath the epithelium on the left and right sides of the section. The straight line distance between these reference lines was measured as the width of the wound area (Fig. 2.2) (Jia *et al*., 2011). For each section, each measurement was repeated three times and the mean width of the wound area was calculated. Similarly, the size of the **epithelial gap** between the tips of the epithelial tongues on the left and right side of the wound was measured three times and the mean calculated for each of the

three spaced sections from wounds excised on day 9 and 15 post-wounding (Fig. 2.2). The measurement was the straight line distance, parallel to the measurement of the width of the wound area, between vertical lines drawn through the most distal point of the epithelial tongues on the left and right sides of the section.

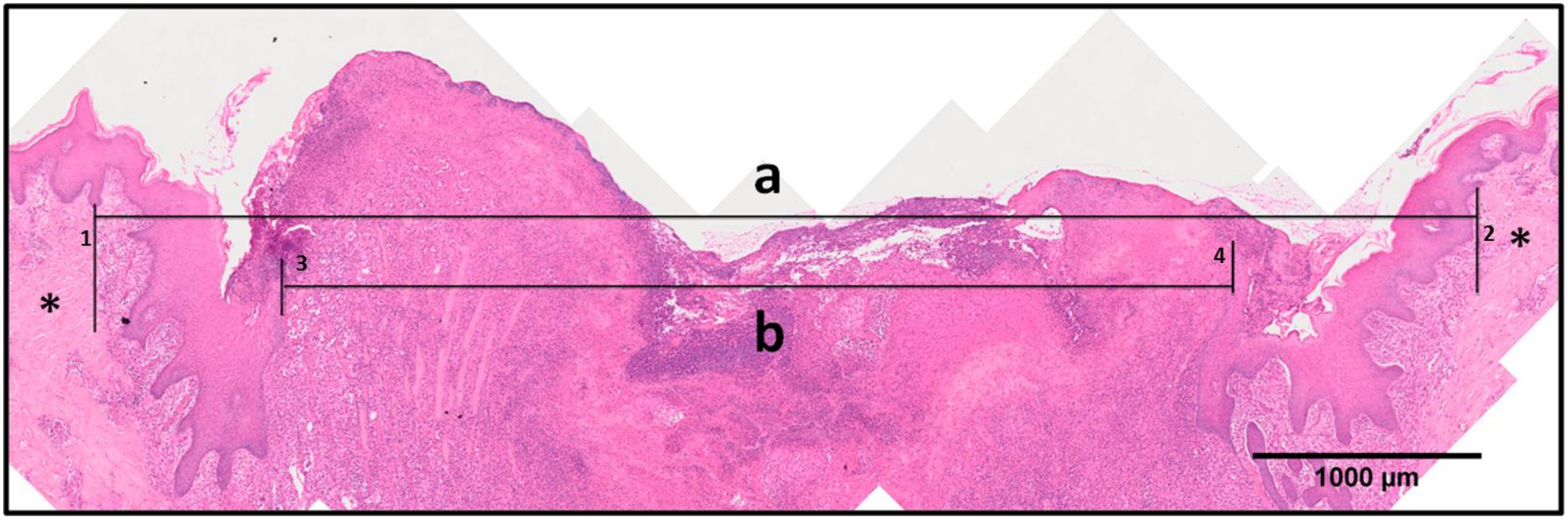

Figure 2.2. Representative photomicrograph of wounded skin illustrating the measurement of (a) the width of the wound area and (b) the size of the epithelial gap. The width of the wound area was measured between vertical lines placed at the junction of the wounded and non-wounded dermis on the left and right sides of the wound (lines 1 and 2). The epithelial gap was measured between vertical lines through the tips of the epithelial tongues (lines 3 and 4). *indicates normal collagen within the non-wounded dermis on each side of the wound. Note: Images have been merged to create a composite image. (H&E)

The **length of the epithelial tongue** along the basal layer of the epithelium from the wound edge to the tip of the epithelial tongue was also measured, using the freehand line tool in ImageJ® (Fig. 2.3). The wound edge was defined as the epithelium overlying the point of change from mature collagen of the normal dermis to a fibrin clot or immature collagen of the wound area. The tip of the epithelial tongue was defined as the most distal point of confluent epithelial cells on the epithelial tongue. The length of the epithelial tongue was measured along the basal layer of the epithelium and not, as is traditional, as the straight line distance perpendicular to the wound edge, from the wound edge to the tip of the epithelial tongue (Jia *et al*., 2011) as this parameter was utilised as a marker of epithelial restoration and not wound closure. The length along the basal layer of epithelium would indicate the migration and proliferation of epithelial cells in all directions, whereas measurement of the straight line distance might not account for epithelial cells which had not migrated in a straight line from the wound edge.

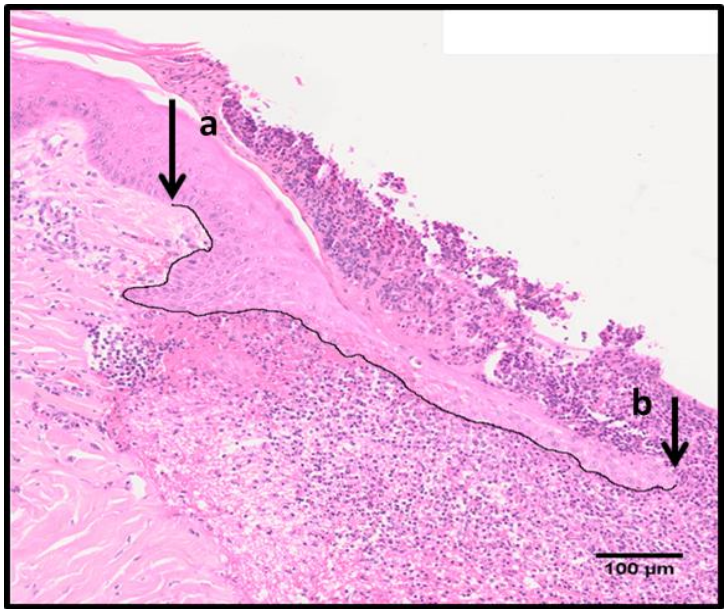

Figure 2.3. Representative photomicrograph of an epithelial tongue illustrating the measurement of the length of the epithelial tongue from the wound edge (indicated by arrow 'a') to the tip of the epithelial tongue (indicated by arrow b). Note: Images have been merged to create a composite image. (H&E)

Using the freehand tracing tool in ImageJ®, the perimeter of the epithelial tongue, as outlined in Figure 2.4, was traced and the **area of the epithelial tongue** calculated in μm^2. The presence and position of the stratum corneum on the skin sections was variable as the stratum corneum separated from the stratum granulosum during sectioning and staining of tissue. Therefore, the stratum corneum was excluded from the area of the regenerated epithelium as it could not be ascertained if its absence was due to technical constraints.

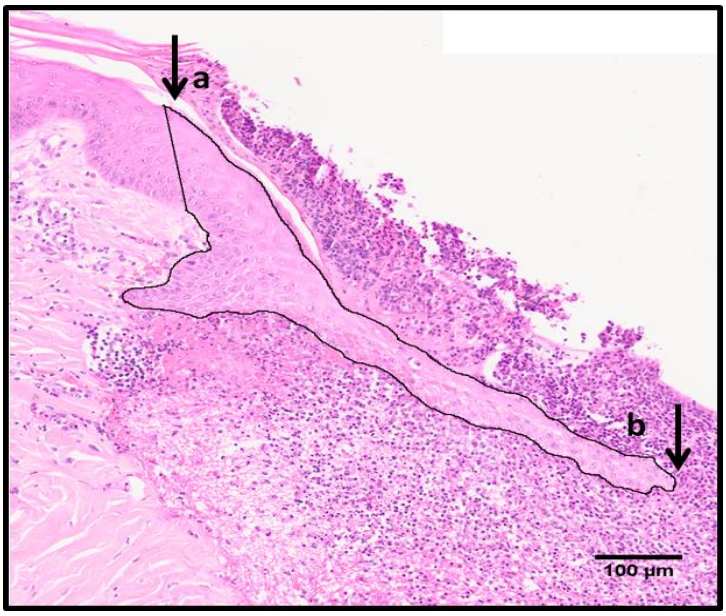

Figure 2.4. Representative photomicrograph of an epithelial tongue illustrating the measurement of the epithelial area (delineated by the black line). Arrow (a) indicates the wound edge and arrow (b) the tip of the epithelial tongue. Note: Images have been merged to create a composite image. (H&E)

For sections in which re-epithelialisation was complete, the area and length of the new epithelium, from wound edge to wound edge, was measured three times and a mean value calculated for each section. For sections in which re-epithelialisation was not complete, the area and length of the epithelial tongue on the left and right sides of the wound were measured three times and an average value calculated for each side of the wound. The average values from the left and right sides of the wound were then added to calculate a mean value for each section in which re-epithelialisation was not complete. The sum of the average

values was used to obtain the mean value for sections in which re-epithelialisation was not complete, as the mean value obtained from the sections in which re-epithelialisation was complete included both the left and right sides of the wound.

Once again, three spaced sections from each wound were utilised to acquire digital images of the epithelium at the wound edge and the tip of the epithelial tongue. These images, obtained using the 40x objective, were used to measure the **thickness of the epithelium** on both the left and right sides of each section (n=120 H&E stained sections). At later stages of healing, where no epithelial tongue was present due to complete re-epithelialisation, non-overlapping images were taken of the epithelium on the right and left of the midpoint of the regenerated epithelium. In cases where the region of interest could not be photographed in a single field of view, overlapping images were taken and reconstructed into a single image using GIMP.

Two precautions were taken to ensure that measurements of the thickness of the epithelium were not falsely increased due to the measurement being taken at an angle through the epidermis. Firstly, all 120 sections selected for analysis and stained with haematoxylin and eosin (H&E) were cut perpendicular to the epidermis as evidenced by the cells of the stratum basale being columnar or cuboidal in shape and containing round to oval nuclei (Therkildsen *et al*., 1998).

Secondly, all images were standardised before the measurements were taken. A line (R) was drawn parallel to the basement membrane of the wounded epithelium and the image rotated so that this line was in the horizontal plane with the dermis placed inferiorly. All measurements were taken at 90 degrees to this line. The measurements were taken from the basement membrane to the superficial edge of the stratum granulosum (Fig. 2.5). If the basement membrane was not visible, the transition point from the stratum basale to the dermis was used. If the superficial edge of the stratum granulosum was not visible, the deep edge of the stratum corneum was used. The stratum corneum was not included in the measurement due to its variable presence due to desquamation and technical constraints during processing of the sections.

After the addition of the appropriate scale using ImageJ® (version 1.46), the straight line tool was used to perform three measurements of the thickness of the epithelium on each image, namely: the maximum thickness of the epithelium, the minimum thickness of the epithelium and the thickness of the epithelium at the point midway between the maximum and minimum measurements (Fig. 2.5). All three measurements were repeated three times and a mean epithelial thickness calculated for each image. For each section, the mean epithelial thickness from the right and left sides of the section were averaged to calculate the mean thickness of the epithelium at the wound edge and the tip of the epithelial tongue respectively.

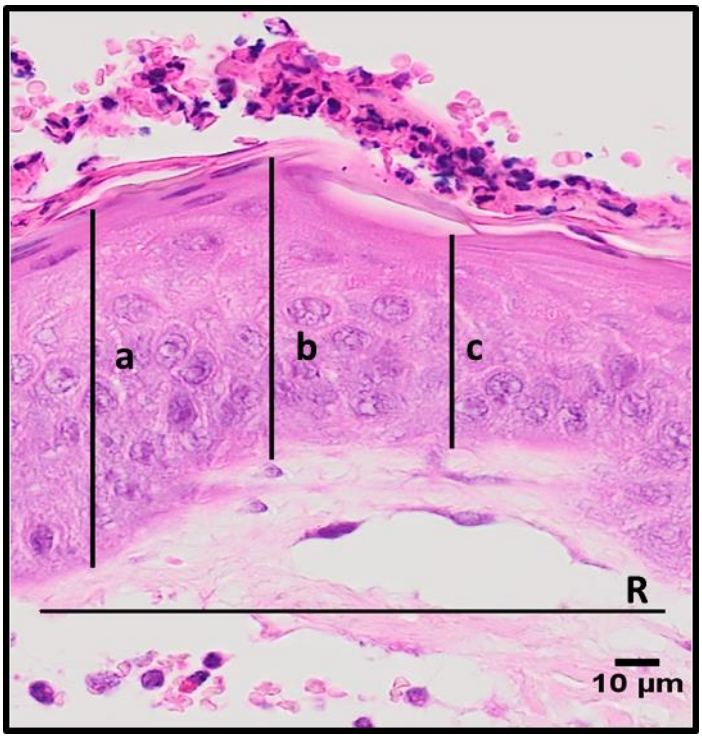

Figure 2.5. Representative photomicrograph of new epithelium at the wound edge illustrating the measurement of the epithelial thickness. (R) reference line, (a) maximum thickness, (b) thickness at the point midway between the maximum and minimum thickness measurements, (c) minimum thickness. (H&E, 20X magnification)

As epidermal appendages contribute to the re-epithelialisation of wounds, they may confound results when assessing the effect of treatment on re-epithelialisation (Broughton *et al*., 2006; Levey *et al*., 2007). Therefore, the presence or absence of epidermal appendages in the non-wounded dermis adjacent to the wound area on each side of the wound was recorded. Epidermal appendages were said to be present if they were visible in the field of view when the non-wounded dermis adjacent to the wound was viewed with the 40x objective.

2.4.1.2 Presence of inflammatory cells

Using the 40x objective, four non-overlapping, digital images were taken of the wound area for each H&E stained section (n=120 sections). The images were taken of the wound area adjacent to the non-wounded dermis in a manner which ensured that the wound area filled the field of view. Two images were taken on each side of the wound with the second image approximately 1mm deep to the first image (Fig. 2.6). In ImageJ® (version 1.46), the appropriate scale and a grid with squares of 1000 μm^2 were added to each image. The inflammatory cells, identified by their nuclei, were counted in every second square of the grid according to the principles outlined by Weibel and Gomez (1961). The total inflammatory cell count for each section, obtained by adding the counts from the four images, was determined three times and the mean inflammatory cell count was calculated for each section.

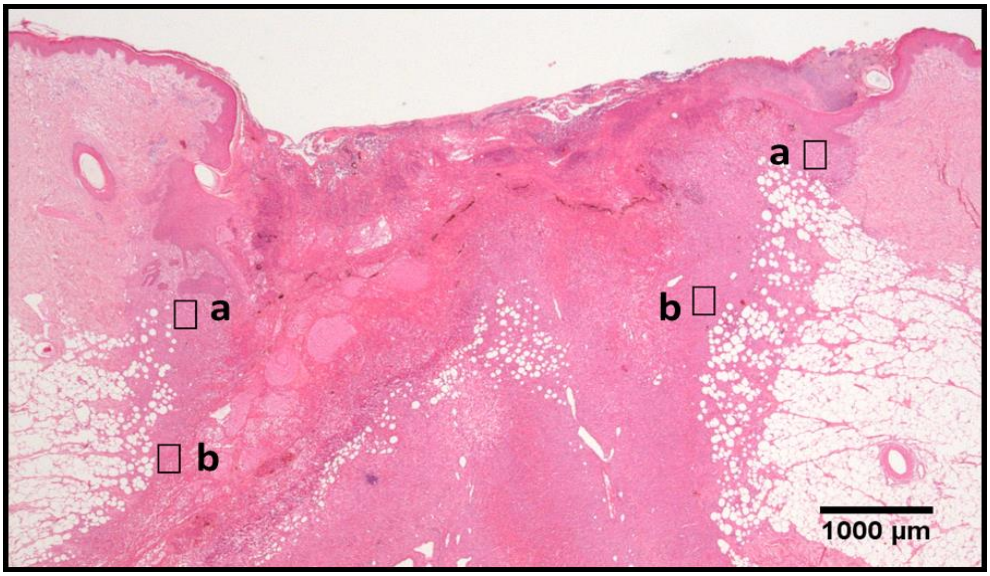

Figure 2.6. Representative photomicrograph of wounded skin illustrating the position of the first (a) and second (b) images used to assess the presence of inflammatory cells. (H&E, 5X magnification)

2.4.1.3 Formation of blood vessels

The wound area, to the left and right of the midline (Fig. 2.7), of each of the three spaced sections from each wound was scanned, using the 40x objective, to assess the formation of blood vessels. In order to distinguish blood vessels from aggregates of red blood cells within the fibrin clot, blood vessels were defined as a lumen with a distinct surrounding of endothelial cells. The number of blood vessels within the wound area was scored using a 4-point scale in which '0' indicated that no blood vessels were present and '3' indicated that many blood vessels were present. In addition, the type of blood vessels within the wound area were scored using a 3-point scale in which '0' indicated no blood vessels, '1' indicated that a single layer of endothelial cells surrounded the lumen of the vessel and '2' indicated that a second layer of tissue, indicative of either pericytes or a basement membrane, was visible within the vessel wall. The scores for the type and number of blood vessels from the left and right side of each section were averaged to give a mean score for each section.

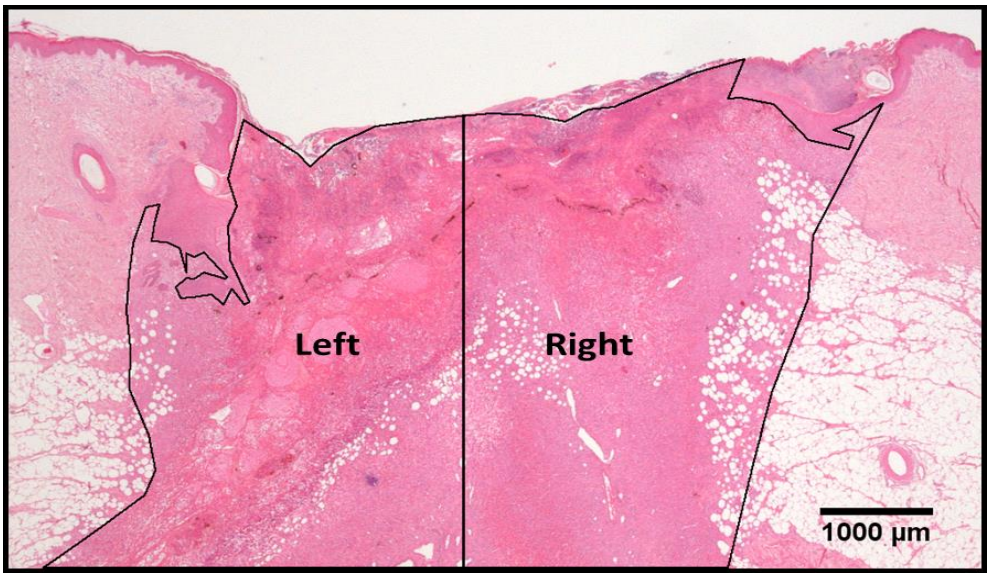

Figure 2.7. Representative photomicrograph of wounded skin illustrating the area of the wound used to assess the type and number of blood vessels. (H&E, 5X magnification)

2.4.2 Assessment of proliferation of keratinocytes and fibroblasts

Ki-67 is a nuclear protein associated with all stages of cell proliferation and absent during the resting stage of the cell cycle (Gerdes *et al*., 1984). It is therefore a reliable marker of cell proliferation, the use of which has been validated in porcine skin (Cuttle *et al*., 2006).

The percentage proliferating cells in the epidermis and dermis of each wound was assessed by immunocytochemical labelling for Ki-67 of one 5µm section from each wound mounted on a Superfrost® Plus slide (Thermo Scientific, Germany). Only one section from each wound was utilised as the sections mounted on glass slides using Sta-on® tissue section adhesive could not be used due to difficulties encountered with the antigen retrieval step of the immunocytochemical labelling protocol which are discussed below.

Prior to immunocytochemical labelling for Ki-67, the optimal protocol for immunocytochemical labelling for Ki-67, including the optimal concentration of polyclonal rabbit antibody to Ki-67 (Novocastra, United Kingdom), was determined using 5µm sections of human tonsil (as recommended by the manufacturer) mounted on glass slides using Sta-on® tissue section adhesive. Ethical clearance was obtained for the use of the human tonsil from the University of the Witwatersrand Human Research Ethics Committee (Medical) (M110801) (Appendix C).

In all further assays, human tonsil was used as a positive control. Negative controls were performed for each assay by omission of the primary and secondary antibody respectively, on a selection of 5µm sections which lay adjacent to the experimental and control sections which were labelled for Ki-67.

During the initial assays, sections of human tonsil mounted on glass slides using Sta-On® were incubated with ethylenediaminetetraacetic acid (EDTA) at a pH of 9.0 (Appendix C1) in a microwave (900W) for 10 minutes to retrieve the antigen (Ki-67) from the nucleus. In these experiments, polyclonal rabbit antibody to Ki-67 (Novocastra, United Kingdom) was used as the primary antibody and goat anti-rabbit antibody (Dako, Denmark) as the secondary antibody. Polyclonal rabbit antibody to Ki-67 was used as previous assays using monoclonal mouse antibody to Ki-67 (Sigma Aldrich, South Africa), used according to the manufacturer's instructions, had not produced staining of human tonsil. In the assays using polyclonal rabbit antibody to Ki-67, the avidin/biotin complex kit (ABC kit, Vector Laboratories, USA) was used to detect the secondary antibody and diaminobenzidine (DAB) was used as the chromagen. This protocol (Appendix C2) produced good labelling of proliferating cells in human tonsil (Fig. 2.8). However, when this protocol was used for immunocytochemical labelling of the selected sections of the skin mounted on glass slides using Sta-On®, the sections disintegrated. As the cause of disintegration of the sections was thought to be the high temperature and pH to which the sections were exposed during the antigen retrieval step, a number of antigen retrieval techniques were tried. These included incubation of the sections with citrate (pH 6.0 and 8.0) (Appendix C3), EDTA (pH 8.0) and 5% Tris urea solution (pH 9.5) (Appendix C4) in both a microwave (900W and 720W for 5, 7 and 10 minutes) and an incubator (5, 10 and 15 minutes at 60^{o}C and 95^{o}C). In addition, the above protocols were attempted using either the goat anti-rabbit antibody and ABC kit or the Peroxidase Detection System (Novocastra, United Kingdom). None of these protocols resulted in consistent immunocytochemical labelling of proliferating cells in sections of human tonsil or porcine skin. Neither did these protocols resolve the issue of disintegration of the sections mounted on glass slides using Sta-on® tissue section adhesive.

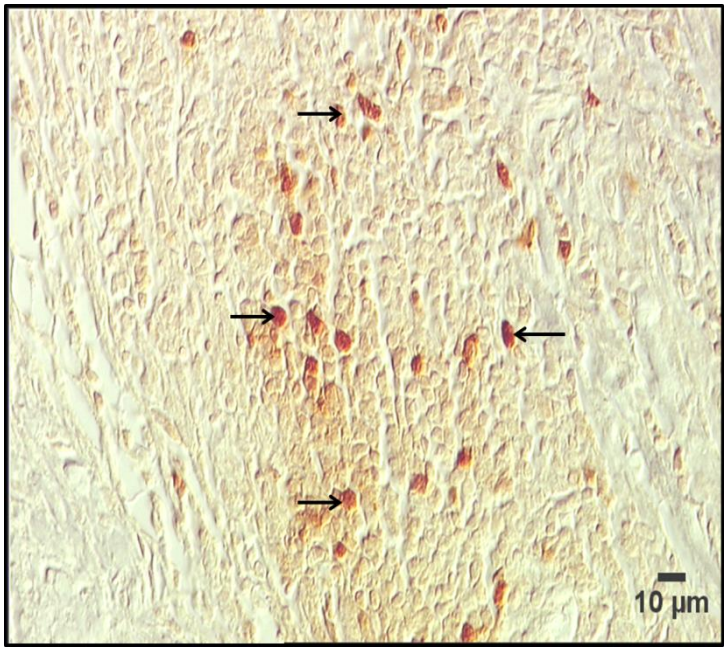

Figure 2.8. Representative photomicrograph of human tonsil immunolabelled with Ki-67 (initial protocol). Arrows indicate examples of nuclei positively labelled for the Ki67 antigen. (DIC microscopy, 25X magnification)

Ultimately, additional sections of experimental and control tissue were cut and mounted on Superfrost® Plus slides (Thermo Scientific, Germany). The increased adherence of the sections to the Superfrost® Plus slides allowed for the optimisation of the following protocol for immunocytochemical labelling of sections with Ki-67 antibody. This protocol produced good immunolabelling for Ki-67 in human tonsil (Fig. 2.9) as well as porcine skin. However, as minimal tissue remained, only one section could be obtained from each experimental and control wound for immunocytochemical labelling with Ki-67 antibody (n=5 sections from experimental wounds and 5 sections from control wounds for each day post wounding).

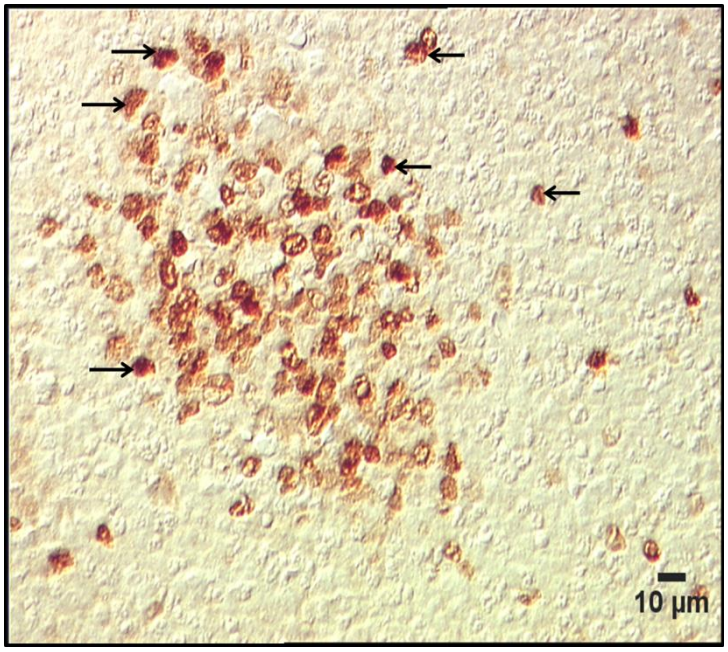

Figure 2.9. Representative photomicrograph of human tonsil immunolabelled with Ki-67 (final protocol). Arrows indicate examples of nuclei positively labelled for the Ki67 antigen. (DIC microscopy, 25X magnification)

Sections of the experimental and control wounds as well as the positive and negative control sections were dewaxed in xylene and rehydrated through a series of graded alcohols before being washed in running tap water for five minutes. To retrieve the antigen from within the cell nucleus, the sections were placed in a solution of EDTA (pH 9.0) in a microwave (900W) for ten minutes. After cooling for ten minutes at room temperature and being washed in running tap water for 5 minutes, the sections were incubated at room temperature for five minutes with 100 µl of peroxidase blocker, which forms part of the Peroxidase Detection System. The sections were washed for five minutes in two changes of a Tris Buffered Saline solution (TBS) (Appendix C5). Each section was then incubated at room temperature for 5 minutes with 100 µl of the protein blocking solution provided in the Peroxidise Detection System. After being washed in two changes of TBS for five minutes, each section was incubated overnight with 100µl of polyclonal rabbit antibody to Ki-67 diluted in TBS to a concentration of 1: 3000.

The following day, the sections were washed for five minutes in two changes of TBS before incubation at room temperature for 30 minutes with 100 µl of the secondary antibody provided in the Peroxidise Detection System. The sections were washed for five minutes in two changes of TBS and incubated for 30 minutes with 100µl of the strepavidin-HRP solution provided in the Peroxidase Detection System. Again, the sections were washed for five minutes in two changes of TBS. One hundred µl of DAB was diluted with 2000µl of the solution from the kit provided for this purpose. Each section was incubated with 100µl of DAB for five minutes. The excess DAB was removed from each section and the sections washed in running tap water for 5 minutes. The sections were then air-dried horizontally overnight before being passed through a graded series of alcohols and cleared in xylene Coverslips were mounted with entellan.

Using the 40x objective in conjunction with a Nomarski (differential interference contrast – DIC) lens, cells within the epidermis which were positively labelled for the Ki-67 antigen were counted in the epithelial tongue and in the non-wounded epidermis. One 253.67µm x 190.25µm field of view of the non-wounded epidermis at the wound edge was utilised for this count (Fig. 2.10). The proliferating cells were identified as being within the epidermis due to their position above the basement membrane. As co-localisation of the Ki-67 antibody with keratinocyte- or melanocyte-specific antibodies was not carried out, it was not possible to determine if the proliferating cells within the epidermis were keratinocytes or melanocytes. However, as keratinocytes are more numerous than melanocytes within the epidermis and the proliferation of melanocytes is slower than keratinocytes (Ross and Pawlina, 2003), the majority of the proliferating cells within the epidermis were taken to be keratinocytes. The number of proliferating keratinocytes within the epidermis on the left and right of the section

were counted three times and the values averaged to give a mean count of the proliferating keratinocytes for each section.

While the above protocol produced optimal labelling of human tonsil (Fig 2.9) and porcine skin for Ki-67 antigen, the antigen retrieval step still resulted in disruption of the dermis. Therefore, analysis of the number of fibroblasts positively labelled for Ki-67 antigen in the dermis was not investigated further.

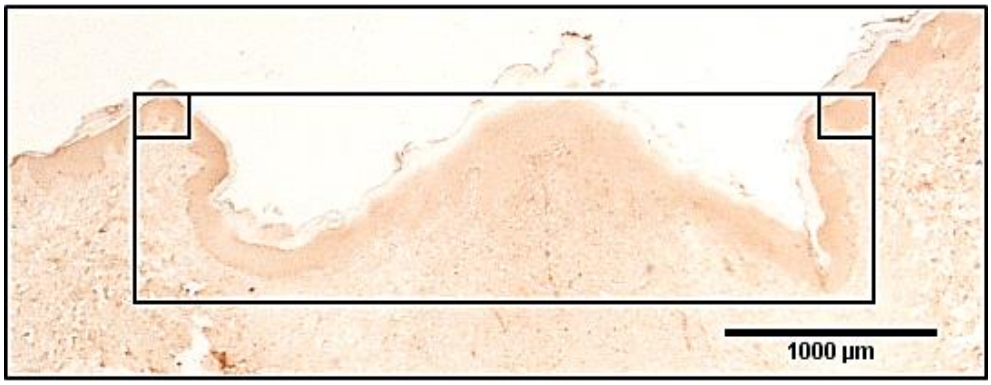

Figure 2.10. Representative photomicrograph of wounded skin illustrating the area in which proliferating keratinocytes in the non-wounded epidermis (small boxes) and epithelial tongue (large box) were counted.
(Immunocytochemical labelling for Ki-67, brightfield microscopy, 5X magnification)

2.4.3 Assessment of collagen

From each of the three spaced regions of each experimental wound (n=5 wounds per day post-wounding) and control wound (n=5 wounds per day post-wounding), a 5µm section which lay adjacent to a 15µm section was utilised. These 5µm sections were dewaxed in xylene and rehydrated through a graded series of alcohols. The sections were then stained with a 0.1% solution of Sirus red in saturated picric acid (Appendix D1) (n=120 picrosirius red stained sections).

The 25x objective (glycerine/ water) of a Zeiss confocal laser scanning microscope (LSM 710), utilising Zen 2010 software and fitted with an Axiocam MRm camera (magnification 1.0x), was used to acquire four 566.5µm x 566.5µm images of the wound area on each of the picrosirius red stained sections. Two images, indicated by the boxes labelled 'a' in Fig 2.11, were taken adjacent to the non-wounded dermis on the left and right sides of the section. The third and fourth images, indicated by the boxes labelled 'b' in Fig 2.11, were at least 1mm deep to image 'a'.

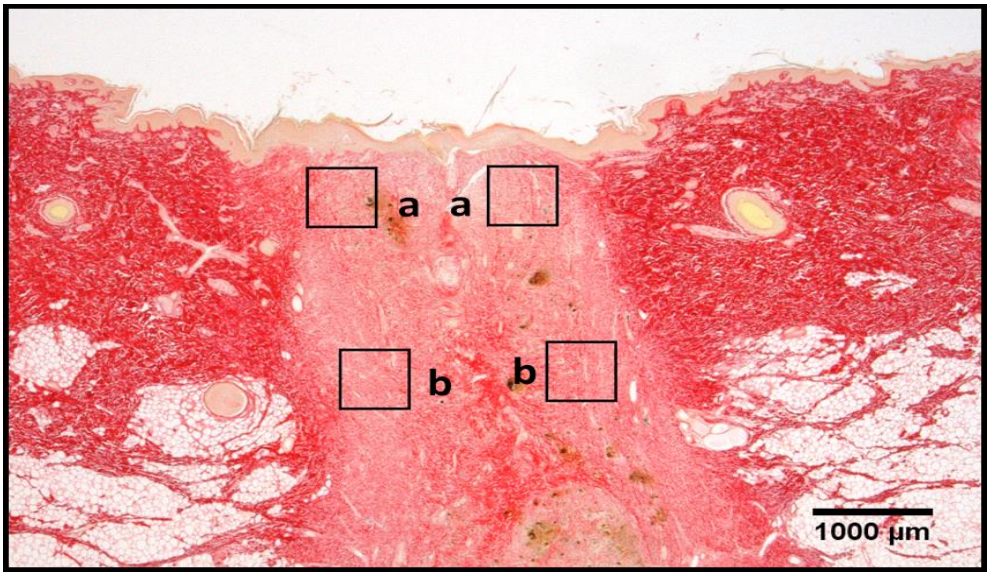

Figure 2.11. Representative photomicrograph of wounded skin illustrating the position of the first (a) and second (b) images on the left and right sides of the wound area for the assessment of collagen. (Picrosirius red, brightfield microscopy, 5X magnification)

Confocal microscopy has previously been used to view collagen in tissues stained by the picrosirius red method, including pig skin (Dolber and Spach, 1993; Vardaxis *et al.*, 1997). However, when images of non-wounded collagen were acquired using the standard excitation (488nm) and emission (514nm) wavelengths described by Dolber and Spach (1993), poor quality images were obtained. Therefore, the same area of non-wounded collagen was imaged using the different rhodamine and fluorescein channels provided with the LSM 710 and the Zen 2010 software, in order to determine which wavelengths produced the best quality images. Ultimately, using excitation and emission wavelengths of 561nm and 606nm respectively (rhodamine channel) produced the best fluorescent images (laser: 2%, pinhole: 36.8µm, zoom: 0.6, digital gain: 830, digital offset: 2). As areas of the field of view which are not in focus do not fluoresce optimally, the collagen in these areas cannot be seen clearly. Therefore a second channel utilising the photomultiplier tube (PMT) was added to obtain a brightfield microscopy image of the same area shown in the fluorescent image. The fluorescent and brightfield images were combined to produce a single tif image. This ensured that all collagen within the field of view was visible within the image (Fig. 2.12A). For each of the four fields of view on each section, the combined tif image was used for image analysis.

2.4.3.1 Percentage area of collagen

Using ImageJ® (version 1.47), thirty images of non-wounded collagen, obtained using the above confocal settings, were colour thresholded in the hue, saturation and brightness (HSB) colour space by adjusting the saturation levels so that all collagen was included in the thresholded image (Fig. 2.12B). As the upper saturation level did not change, only the lower saturation level for each image was recorded and the mean value calculated. The lower saturation level to use in thresholding the images of the experimental and control wounds was

then determined as the mean value minus two standard deviations (value = 105) as this would include the majority of collagen in the images.

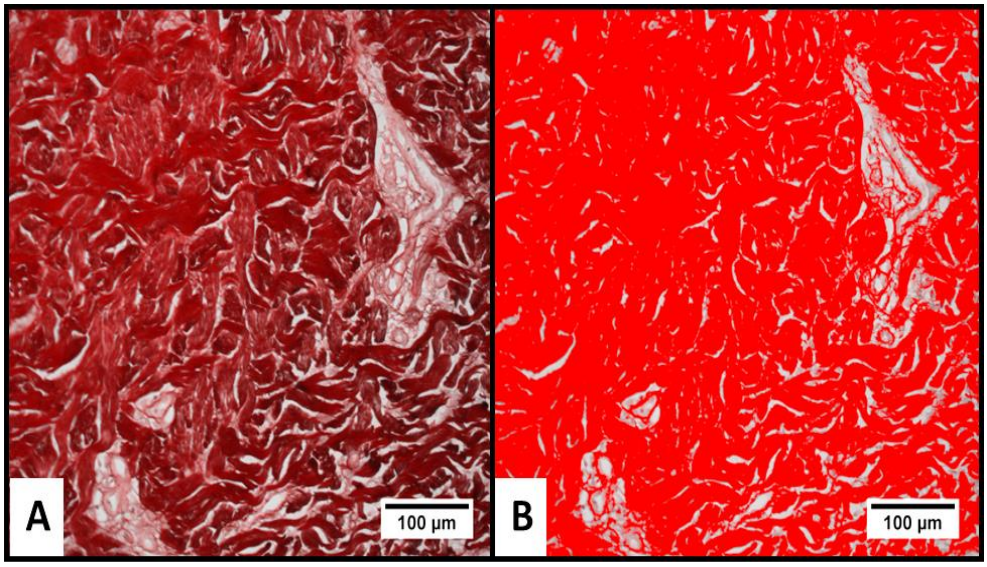

Figure 2.12. Representative photomicrograph of non-wounded collagen before (A) and after (B) thresholding. (Picrosirius red, confocal microscopy, 25X magnification)

After the addition of the appropriate scale and colour thresholding as described above, the area of the image which contained collagen, was calculated in μm^2 for each image from the experimental and control wounds. The percentage of the wound area which contained collagen was then calculated by dividing the area which contained collagen by the total area of the image. For images in which the wound area did not fill the field of view, the image was cropped so that the area analysed was filled by the wound. For each section, the percentage of the wound area which contained collagen was measured three times. The percentage values for the images from the same section were averaged to give a mean percentage for each section.

2.4.3.2 Qualitative assessment of collagen

The density of collagen, collagen bundle size and organisation of collagen fibres were scored using scales based on those described by Singer and McClain (2006). The density of collagen and collagen bundle size were scored using a 5- point scale in which '0' indicated the least dense or no collagen and '4' indicated the most dense or largest bundle size. The organisation of collagen was scored using a 4- point scale in which '0' indicated no collagen, '1' disorganised collagen in the entire image, '2' areas of organised collagen in the image and '3' organised collagen in the entire image.

2.4.3.3 Quantitative estimation of collagen

The 15µm sections, which lay adjacent to each picrosirius red stained 5µm section, were allocated for the quantitative estimation of the collagen content of each wound according to the dye-binding method described by Lopez-De Leon and Rojkind (1985) and modified by Castelo-Branco *et al* (1994). In this method, the absorbance values of solutions of picrosirius red and Fast Green, obtained by elution from a stained section, are determined by spectrophotometry and used to calculate the collagenous and non-collagenous protein content of the section. This calculation is dependent on colour equivalence values which relate the absorbance values of picrosirius red and Fast Green to the concentration of collagen and non-collagenous proteins respectively.

In order to determine the colour equivalence values of collagen and non-collagenous proteins in this study, absorbance values obtained by the dye-binding method were plotted against biochemical estimations of hydroxyproline and total protein in normal pig skin (James *et al*., 1990).

Permission was obtained from the Animal Ethics Screening Committee of the University of the Witwatersrand to harvest normal pig skin, 20mm x 20mm in size, from the abdomen and dorsum of seven pigs euthanased for reasons not associated with this study. Half of the skin from each region was frozen at -80^{o}C and used for hydroxyproline and total protein determination (Woessner, 1961; Bradford, 1976; Reddy and Enwemeka, 1996). The remaining skin was fixed in 10% buffered formalin for 24 hours, dehydrated through a series of graded alcohols, cleared in chloroform and embedded in paraffin wax. Six 15µm thick sections cut from each block of paraffin embedded tissue were processed according to the dye-binding method, to give absorbance values at 540nm and 620nm.

Biochemical determination of the concentrations of hydroxyproline and total protein

To determine the hydroxyproline content of the tissue, 0.02g of normal pig skin was frozen in liquid nitrogen, crushed with a mortar and pestle and mixed with 50µl of 0.9% normal saline. Freezing the tissue in liquid nitrogen before crushing the tissue was chosen as the method to create the solution as previous attempts at homogenising the pig skin using an ultra-turrax homogeniser (IKA, Germany) were unsuccessful due to the small amount of liquid.

Fifty µl of 10M sodium hydroxide was added to the above solution. The resulting solution was vortexed before being autoclaved at 120^{o}C for 20 minutes. One hundred µl of Chloramine T reagent (Appendix D2) was added to 100µl of the hydrolysis solution in an eppendorf tube and the resulting solution was incubated at room temperature for 25 minutes after which 500µl of freshly prepared Ehrlich's reagent solution (Appendix D3) was added. After incubation for 20 minutes at 60^{o}C, 150µl of the solution was transferred to a 96 well plate and the absorbance read at 540nm using a spectrophotometer. The hydroxyproline content of the tissue was then determined from a standard curve obtained by using serial

dilutions of 1mg hydroxyproline in 1ml of assay buffer solution (Appendix D4). This was repeated three times for each piece of normal pig skin (n=10).

To determine the total protein content of the tissue, 0.2g of normal pig skin was homogenised in 5 ml of homogenising buffer (Appendix D6) using the ultra-turrax homogeniser. The total protein content of the tissue was then determined using the Bradford protein assay (Bradford, 1976). Standard dilutions of bovine serum albumin (50µg/ml to 1000µg/ml) (Sigma-Aldrich, USA) were prepared. Five microlitres of each standard solution and the homogenised solution were transferred to wells on a 96 well plate and 250µl of Bradford reagent (Sigma-Aldrich, USA) was added. The resulting solutions were mixed on a rotary shaker for 30 seconds before being incubated at room temperature for 10 minutes. The absorbance of the solutions was read at 595nm on a Multiskan FC spectrophotometer (Thermo Fisher Scientific, USA). The total protein content of the tissue was calculated from the standard curve. The assay was repeated three times for each piece of normal pig skin (n=10).

Dye-binding method for quantitative estimation of collagen

Each 15µm section of normal skin was placed in a small, glass cell culture plate and incubated sequentially for five minutes with 2ml of xylene, xylene: ethanol (v:v), ethanol, ethanol: distilled water (v:v) and distilled water. Each section was then incubated with 2ml 0.01% Fast Green in saturated picric acid for 15 minutes in the dark at room temperature. The excess fluid was withdrawn with a pipette and each section rinsed in distilled water until the water was colourless. Each section was then incubated with 2ml of a solution of saturated picric acid containing 0.1% Sirius Red and 0.04% Fast Green for 30 minutes in the dark at room temperature on a rotary shaker. The excess fluid was withdrawn and each section rinsed in distilled water until the water was colourless. One millilitre of 0.1N sodium hydroxide in

absolute methanol (v:v) was added to each section and the colour eluted from the section by gently shaking the section in the solution for a few seconds. For each section, 150µl of the fluid containing the eluted dye was placed into three wells of a 96 well plate and the absorbance of the fluid was read immediately on an Anthos 2010 spectrophotometer at 540nm and 620nm, the maximal absorbance of Sirius Red and Fast Green respectively.

Fast Green also has absorbance at 540nm which is reported in the literature to be 7.8% of the absorbance at 630nm (Castelo-Branco *et al*., 1994). To determine the percentage absorbance attributable to Fast Green at 540nm, the absorbances of serial dilutions of a 0.04% Fast Green solution were read on the Anthos 2010 spectrophotometer (Biochrom Ltd, United Kingdom) at 540nm and 620nm (n=10). While there was a good correlation (r=0.99) between the absorbance readings at 540nm and 620nm, the relationship varied according to the concentration of the solution (Appendix D7). Therefore, the absorbance of Fast Green at 540nm could not be expressed as a single percentage of the absorbance of Fast Green at 620nm.

In addition, no constant relationship could be found between the hydroxyproline and total protein values obtained for normal pig skin using the biochemical assays and the absorbance values obtained by the dye-binding method (Appendix D8). Therefore, the colour equivalences for collagen and total protein could not be calculated and the dye-binging method was not applied to the 15µm sections of experimental or control wounds.

2.4.4 Presence of bacteria

Due to differences in the inflammatory cell infiltrate found in experimental and control wounds on day 3, 9 and 15 post-wounding, three spaced 5µm sections from each of these wounds (n=90) were dewaxed in xylene, rehydrated through a graded series of alcohols and stained using the Gram method for paraffin sections (Appendix E) (Bancroft and Gamble, 2002). The Gram stain is used to demonstrate gram positive and gram negative bacteria (Bancroft and Gamble, 2002). Sections of lung tissue from individuals with pneumonia, obtained from the School of Pathology of the University of the Witwatersrand, were utilised as control sections. Use of these sections was authorised by the Chair of the Human Research Ethics Committee (HREC) of the University of the Witwatersrand.

The granulation tissue of each stained section was viewed using the 100x objective of the Zeiss Axioskop 2 microscope and the presence or absence of bacteria within the fibrin clot or granulation tissue of wounds was noted.

2.5 Statistical analysis

Microsoft Excel® and Statistica (version 12) were used for all statistical analyses.

2.5.1 Observer errors

For quantitative variables, the relevant measurement, as described in section 2.5.1 to 2.5.3, was repeated on 10% of the sample by the primary observer as well as a second observer. Lin's Concordance correlation was used to calculate the intra- and inter-observer error (Lin, 1989). A co-efficient of 0.9 or greater was accepted as evidence of an acceptably low level of observer error (Allan, 1982).

For categorical variables, the relevant measurement, as described in section 2.5.1 to 2.5.3, was repeated on the entire sample by both the primary and second observer and Cohen's kappa co-efficient was used to calculate the intra- and inter-observer error (Cohen, 1960). A co-efficient of 0.8 or greater was accepted as evidence of acceptably low levels of observer error for categorical variables (Blackman and Koval, 2000).

The coefficients of the Lin's concordance correlation and Cohen's kappa test obtained in the current study are presented in Appendix F.

2.5.2 Calculation of mean values

As described in section 2.5.1 to 2.5.3, mean values for each quantitative variable were obtained for each section. The mean values for the three spaced sections from the same wound were averaged to calculate a mean value for each experimental wound (n= 5 per day post-wounding) and control wound (n= 5 per day post-wounding). Similarly, mean scores for

each experimental wound and control wound were calculated for the categorical variables, using the mean scores from the three spaced sections from the same wound.

2.5.3 Descriptive statistics

The distribution of the data was assessed using a Shapiro-Wilks test. A p-value greater than 0.05 indicated that the data was normally distributed. Results of the Shapiro-Wilks test are presented in Appendix G.

Despite the majority of the data being normally distributed (Appendix G), the median and minimum and maximum values were chosen to describe the data due to the small sample size and the tendency of the median to remain unaffected by outliers (Whitley and Ball, 2002).

2.5.4 Tests for statistical significance

Due to the small sample size, the Mann-Whitney U test was used to establish if statistical differences were present ($p < 0.05$) between experimental and control wounds on day 3, 6, 9 and 15 post-wounding, for both quantitative and categorical variables.

As the presence of epidermal appendages, the age of the pig and the region in which the wound is positioned can affect the rate of healing, the differences between these variables on day 3, 6, 9 and 15 post-wounding were assessed. A Kruskall-Wallis one-way-analysis of variance by ranks was used to assess if a significant difference ($p < 0.05$) existed in the presence of epidermal appendages or the weight of the pigs. Contingency tables were used to identify differences in the region in which the wound was positioned as well as which pigs were utilised for each day post-wounding. However, due to the number of categories within

these latter variables as well as the small sample size, neither the Fischer exact test nor Pearson's Chi- squared test was suitable to determine if differences were significant.

To assess the effect of weight, region, pig and treatment group on healing between days 3, 6, 9 and 15 post-wounding a main effects analysis of variance (ANOVA) was utilised. Levene's test was used to assess the assumption that the variances were homogenous. However, the assumptions that the residuals were normally distributed and that the variances were homogenous were not met, despite log transformation of the data. Therefore, this analysis could not be pursued.

3. RESULTS

3.1 Macroscopic assessment

Throughout the study, no pig showed signs of adverse effects due to the nanocrystalline silver or systemic signs attributable to wound infection.

Although inspection of the experimental and control wounds on day 3 post-wounding revealed erythema surrounding the edges of both wound types, this was noted to be greater in the experimental wounds (Fig. 3.1). In addition, by day 3 post-wounding, the area of the experimental wounds had increased by a median value of 47%, which was significantly greater than the 7% median increase in the area of the control wounds (Table 3.1).

On day 6 post-wounding the increase in the area of the experimental wounds from the day of wound creation remained significantly greater than that of the control wounds (Table 3.1). However, the erythema surrounding the control wounds on day 6 post-wounding appeared to be greater than that surrounding the experimental wounds (Fig. 3.1). In addition, greater volumes of exudate were noted in control wounds on day 3, day 6 and day 9 post-wounding (Fig. 3.1). Signs of re-epithelialisation were not visible at the wound margins in either wound type on day 3 or day 6 post-wounding.

In both experimental and control wounds on day 9 post-wounding, areas of re-epithelialisation were observed at the wound margins with the central portion of the wound being filled with granulation tissue (Fig. 3.1). However, the area of the control wounds decreased significantly by a median value of 63% compared to only 31.5% in the experimental wounds (Table 3.1; Fig. 3.1).

By day 12 post-wounding there was no longer a significant difference between the change in the area of experimental and control wounds (Table 3.1). However, of the five experimental and five control wounds remaining on day 12 post-wounding, only two control wounds were considered to have re-epithelialised (Fig. 3.2 C & E). These wounds were given Clinical Assessment Scores of 11.5 and 10.5 on day 12 post-wounding and 10.9 and 11 respectively on day 15 post-wounding (Fig. 3.2 D & F).

On day 15 post-wounding, the only additional wound which was considered to have re-epithelialised was one experimental wound (Fig. 3.2 B). This wound was given a Clinical Assessment Score of 10.6. All wounds obtained similar scores for each of the variables as well as similar values for the visual analogue scales (Table 3.2).

Of the three control and four experimental wounds which were considered to be incompletely re-epithelialised by day 15 post-wounding, two control wounds and all four experimental wounds were covered by adherent scabs. The remaining control wound did not have any clinical sign of infection and the wound area had decreased by 80% in comparison to the day of wound creation. In all experimental wounds, the scabs were noted to be black due to discolouration from the nanocrystalline silver (Fig. 3.1). However, discolouration of the skin and hair seen in experimental wounds from day 6 to day 15 post-wounding (Fig. 3.1) was superficial and could be removed with normal saline. No grey discolouration, suggestive of argyria, was noted in the normal skin surrounding the wounds or in the scars of re-epithelialised wounds. Neither were silver deposits seen in the non-wounded dermis or epidermis of the sections of experimental wounds assessed histologically.

3.2 Histological assessment

There was no significant difference in the presence of epidermal appendages between experimental and control wounds on any day post-wounding (Table 3.3- 3.6).

While few significant differences were found in the measured variables between experimental and control wounds on any day post-wounding, differences were observed between the granulation tissue and new epithelium of experimental and control wounds (Table 3.3- 3.6). By day 15 post-wounding, it was apparent that the rete ridges and thickness of the new epithelium of the experimental wounds more closely resembled the epithelium of normal skin than did that in the new epithelium of control wounds. In addition, blood vessels within the granulation tissue of experimental wounds appeared more mature, with an additional layer of tissue seen within the vessel wall more frequently, when compared to control wounds.

3.2.1 Histological assessment of wounds on day 3 post-wounding

On day 3 post-wounding, newly formed epithelium was seen to extend from the wound edge into the wound area in both experimental and control wounds (Fig. 3.3). While no significant differences were found between experimental and control wounds for the measures of epithelial restoration (Table 3.3), the higher ranges found in the experimental wounds were supported by observation. When compared to control wounds, the length and thickness of the epithelial tongue in experimental wounds was greater and more variable (Fig. 3.4). In addition, experimental wounds tended to have two cell layers in the tip of the epithelial tongue compared to the single layer of cells found in control wounds (Fig. 3.5). In contrast to the above findings, preliminary results for the number of proliferating keratinocytes within the epidermis indicated that control wounds had a significantly greater number of

proliferating keratinocytes than experimental wounds (Table 3.3; Fig. 3.6). Proliferating keratinocytes were observed within the basal layer of cells of the epithelial tongue more frequently in control wounds than in experimental wounds. No proliferating keratinocytes were visible amongst suprabasal keratinocytes.

At the wound edge, all layers of the epidermis, including the stratum corneum, were present in both experimental and control wounds (Fig. 3.4). However, neither differentiated layers of the epidermis nor basement membrane were visible at the tip of the epithelial tongue in either wound type (Fig. 3.5).

In both experimental and control wounds, isolated fibroblasts, aggregates of red blood cells and numerous inflammatory cells were visible throughout the fibrin clot which was adherent to the wound edge within the dermis and hypodermis (Fig. 3.7). In the control wounds the fibrin clot appeared larger and more organized than in the experimental wounds (Fig. 3.7). Quantification of the number of inflammatory cells within the wound confirmed that significantly more inflammatory cells were present within the wound area of experimental wounds than in control wounds (Table 3.3). However, on sections that were gram stained, no bacteria were seen within the fibrin clot of experimental or control wounds (Fig. 3.8).

Neither blood vessels nor collagen were visible within the wound area of either type of wound (Fig. 3.7; Fig. 3.9), as is reiterated in the scores of zero obtained for the size, density and organization of collagen bundles as well as the type and number of blood vessels (Table 3.3). While the percentage area of collagen on picrosirius red stained sections, is not significantly different between experimental and control wounds, the variability within the

experimental group is substantial (Table 3.3). This may be attributed to silver particles within the wound area of experimental wounds (Fig. 3.10).

3.2.2 Histological assessment of wounds on day 6 post-wounding

No significant differences were found between the experimental and control wounds for any measure used to assess epithelial restoration on day 6 post-wounding (Table 3.4). However, on observation, a greater number of larger developing rete ridges as well as longer and thicker epithelial tongues were noted in control wounds when compared to experimental wounds (Figs. 3.11 and 3.12). In contrast, at the tip of the epithelial tongue three or four layers of cells were found more frequently in experimental wounds whereas control wounds, comparable to the findings on day 3 post-wounding, tended to have one or two layers of cells (Table 3.4; Fig. 3.13). Similarly to day 3 post-wounding, the layers of the epidermis, including the stratum basale and stratum corneum, were not visible at the tip of the epithelial tongue in either experimental or control wounds (Fig. 3.13).

As on day 3 post-wounding, proliferating keratinocytes were found more often within the basal layer of the epithelial tongue of control wounds than in experimental wounds. Additionally, proliferating keratinocytes in experimental wounds were noted to occur as single cells while in control wounds they were more often arranged in groups (Fig. 3.14). This arrangement of cells was not related to the plane of the tissue.

In contrast to day 3 post-wounding, granulation tissue filled the wound area in the majority of experimental and control wounds on day 6 post-wounding (Fig. 3.11). Numerous fibroblasts as well as variable numbers of adipocytes, inflammatory cells and blood vessels were seen within the granulation tissue of both experimental and control wounds on day 6 post-

wounding (Fig. 3.15). Scores for the number and type of blood vessels indicate that both experimental and control wounds contained an intermediate number of blood vessels with a single layer of cells in the wall of the vessel (Table 3.4; Fig. 3.15). Similar to day 3 post-wounding, silver particles were visible within the dermis of experimental wounds on day 6 post-wounding.

On day 6 post-wounding, most experimental and control wounds contained small collagen bundles, arranged close to the non-wounded dermis, which were neither densely packed nor well organised (Table 3.4; Fig. 3.16). However the amount of collagen visible in both wound types was very variable with some wounds displaying large, densely packed bundles of collagen while others contained no collagen. In general, denser collagen and larger collagen bundles were observed in a greater number of control wounds as compared to experimental wounds.

3.2.3 Histological assessment of wounds on day 9 post-wounding

On day 9 post-wounding, both experimental and control wounds were approximately 70% healed (Table 3.5). In regions of the wound which were not completely re-epithelialised, the layers of the epidermis, including the stratum corneum and stratum basale, were visible in the new epithelium a variable distance from the wound edge but not at the tip of the epithelial tongue. This was similar to day 6 post-wounding (Figs. 3.17 and 3.18). In contrast, in the regions of the wound which were completely re-epithelialised, the distinct layers of the epidermis, including the stratum corneum, were noted throughout the new epithelium of both experimental and control wounds (Figs. 3.19 and 3.20). However, when compared to the epithelium of normal porcine skin, the stratum granulosum and stratum corneum of the new epithelium in both wound types contained a greater number of nuclei (Fig. 3.20).

Additionally, the thickness of the new epithelium of experimental wounds more closely resembled normal skin whereas that of control wounds was more variable being either thinner or thicker than the epithelium of normal skin (Figs. 3.19 and 3.20). This observation was also noted in regions of the wound which had not completely re-epithelialised. These latter observations are reflected in the higher range values for the area of the new epithelium and length of the epithelial tongue seen in experimental wounds (Table 3.5). However, in both wound types on day 9 post-wounding, the number and size of developing rete ridges as well as the number of cell layers at the tip of the epithelial tongue (Figs. 3.17 and 3.19) were highly variable.

Similarly to day 6 post-wounding, proliferating keratinocytes in control wounds were grouped and were seen more frequently within the basal layer of the new epithelium. In the experimental wounds the proliferating keratinocytes were more common within the basal layer of the non-wounded epidermis and as single cells (Fig. 3.21).

By day 9 post-wounding, granulation tissue filled the wound area of all experimental and control wounds (Figs. 3.22 and 3.23). The amount and density of granulation tissue was similar in both wound types. While numerous adipocytes and fibroblasts were visible in both wound types, they were less densely arranged than on day 6 post-wounding (Fig. 3.24). An intermediate number of blood vessels were still present in both experimental and control wounds. However, a second layer of tissue was visible within the vessel wall in a greater number of blood vessels in both wound types than on day 6 post-wounding (Table 3.5; Fig. 3.24).

Inflammatory cells appeared to be more numerous in regions of both wound types which had not completely re-epithelialised. In experimental wounds additional aggregations of inflammatory cells were seen around silver deposits at the level of the lower dermis (Fig. 3.23). These inflammatory cells formed nodules which also contained giant cells as well as cells with large, pale-staining, basophilic nuclei and prominent nucleoli, and were suggestive of granulomas (Fig. 3.25). No bacteria were visible within the granulomas on gram staining of the experimental sections (Fig.3.26).

On day 9 post-wounding, a great deal of variability was still seen in the area, density, size and organisation of the collagen within and between experimental and control wounds. However, in contrast to day 6 post-wounding, denser, larger collagen bundles which were arranged parallel to the wound surface, (Fig. 3.27) were seen towards the centre of experimental and control wounds on day 9 post-wounding, i.e. further from the non-wounded dermis. It is noteworthy that experimental wounds showed significantly greater organisation of collagen than control wounds on day 9 post-wounding (Table 3.5).

3.2.4 Histological assessment of wounds on day 15 post-wounding

By day 15 post-wounding, only one control wound had not completely healed (Table 3.6). In the region of this control wound which had not completely re-epithelialised, the epithelium and granulation tissue resembled that from similar regions in control wounds on day 9 post-wounding. In contrast, in regions of the control wounds which had completely re-epithelialised, the thickness of the new epithelium was less variable on day 15 (Fig. 3.28) than on day 9 post-wounding (Figs. 3.22 and 3.23) whereas in experimental wounds the thickness of the new epithelium seemed similar on both days. However, the new epithelium at the centre of experimental wounds (i.e. at the tip of the epithelial tongue) was significantly

thicker than control wounds on day 15 post-wounding (Table 3.6, Figs. 3.28 and 3.29). In addition, rete ridges were more numerous and larger in experimental wounds than in the control wounds (Figs. 3.28 and 3.29). Therefore the new epithelium of experimental wounds more closely resembled normal skin than did the new epithelium of control wounds.

All layers of the epidermis were present throughout the new epithelium in both the experimental and control wounds and the stratum granulosum contained fewer nuclei and was seen more clearly than on day 9 post-wounding (Fig. 3.29).

By day 15 post-wounding, arrangement of proliferating keratinocytes within experimental wounds more closely resembled that of control wounds. The proliferating keratinocytes were arranged in groups and were seen throughout the basal layer of the new epithelium (Fig. 3.30).

In both experimental and control wounds on day 15 post-wounding, the granulation tissue contained fewer fibroblasts, adipocytes and blood vessels than on day 9 post-wounding (Fig. 3.28). However, on day 15 post-wounding, control wounds appeared to have a greater number of blood vessels within the wound area than experimental wounds (Fig. 3.31). In contrast, the blood vessels in experimental wounds had a second layer of tissue within the vessel wall more frequently than did those in control wounds. However, the blood vessels in both wound types had a second layer of tissue in the vessel more frequently on day 15 post-wounding than on day 9 post-wounding (Table 3.6, Fig. 3.31).

The granulomas seen on day 9 post-wounding which surrounded silver deposits in experimental wounds were larger and more numerous on day 15 post-wounding (Figs. 3.28

and 3.32). Again, no bacteria were visible within the granulomas on gram staining of the experimental sections (Fig. 3.33). In contrast only scattered inflammatory cells were seen in the granulation tissue of control wounds (Fig. 3.31).

As on day 9 post-wounding, the collagen within the wound area of both wound types was arranged parallel to the epidermis. However, from day 9 to day 15 post-wounding, the percentage area of collagen within the control wounds increased, whereas it remained constant in the experimental wounds (Table 3.6). Similarly, for control wounds, the density, size and organisation of the collagen bundles increased from day 9 to day 15 post-wounding (Fig. 3.34). Surprisingly, in experimental wounds the density, size and organisation of collagen bundles decreased from day 9 to day 15 post-wounding (Table 3.6). This decrease combined with the increase in size of the collagen bundles in control wounds resulted in the size of the collagen bundles in experimental wounds being significantly smaller than in control wounds (Table 3.6).

3.2.5 Assessment of healing from day 3 to day 15 post-wounding

The differences observed between experimental and control wounds on day 3, 6, 9 and 15 post-wounding were apparent when healing was studied across all of the days post-wounding.

The rate of increase in the area (Fig. 3.35) and length of the epithelial tongue (Fig. 3.36) from day 3 to 6 post-wounding was similar in both experimental and control wounds. However, between day 6 and 9 post-wounding experimental wounds continued to increase at a constant rate whereas the rate of increase in control wounds slowed (Figs. 3.35 and 3.36). This is evident in the differences observed in the epithelial tongues of experimental and control wounds on day 9 post-wounding (Figs. 3.22 and 3.23).

Similar to the longer rate of increase in the area and length of the epithelial tongue in experimental wounds, a higher rate of increase in the thickness of the epithelium at the tip of the epithelial tongue was noted from day 9 to day 15 post-wounding in experimental wounds when compared to control wounds (Fig. 3.37). This was apparent in the significantly greater thickness of the epithelium within the centre of experimental wounds on day 15 post-wounding when compared to control wounds (Table 3.6). In addition, the preliminary results for the number of proliferating keratinocytes revealed a greater increase in the number of proliferating keratinocytes in control wounds when compared to experimental wounds, before day 9 post-wounding (Fig. 3.38). From day 9 to day 15 post-wounding there was a rapid increase in the number of proliferating keratinocytes in experimental wounds at a time when the numbers of proliferating keratinocytes within control wounds remained constant (Fig 3.38).

From day 6 post-wounding, the score for the number of blood vessels decreased in experimental wounds whereas it continued to increase in control wounds (Fig. 3.39). In contrast, the score for the type of blood vessels increased from day 9 to day 15 post-wounding, suggesting that experimental wounds contained fewer, more mature blood vessels than control wounds on day 15 post-wounding (Fig. 3.40).

The percentage area of collagen (Fig. 3.41) and the scores for the density (Fig. 3.42) and size of collagen bundles (Fig. 3.43) increased at a similar rate in both experimental and control wounds to day 9 post-wounding. However, the score for the organisation of collagen in experimental wounds had a greater increase between day 6 and 9 post-wounding than control wounds (Fig. 3.44). From day 9 post-wounding, the percentage area of collagen and scores for size, density and organisation of collagen bundles in experimental wounds decreased

whereas in control wounds these parameters continued to increase, although the rate slowed (Fig. 3.41- 3.44). These findings reiterate the significantly greater organisation of collagen found in experimental wounds on day 9 post-wounding compared to control wounds as well as the significantly greater size in collagen bundles found in control wounds compared to experimental wounds on day 15 post-wounding (Tables 3.5 and 3.6).

These findings should be interpreted with caution as different pigs and regions on the dorsum of the pig were utilised for assessing healing on day 3, 6, 9 and 15 post-wounding (Table 3.7 and 3.8). While the Kruskall-Wallis one-way-analysis of variance by ranks showed no difference in the weight of the pigs ($p=0.54$) or the presence of epidermal appendages ($p=0.57$) between the days post-wounding, the assumptions of the ANOVA were not valid and therefore the contribution of these factors to differences in the healing of experimental and control wounds between different days post-wounding could not be determined.

In summary, the following differences were found between experimental and control wounds.

- Although experimental wounds decreased in area significantly more slowly than control wounds, from day 12 post-wounding there was no significant difference in the percentage change in area between experimental and control wounds.

- Experimental wounds contained a significantly greater number of inflammatory cells on day 3 post-wounding compared to control wounds. In addition, within experimental wounds on day 9 and 15 post-wounding, granulomas were seen surrounding silver deposits.

- While the results are preliminary, a significantly greater number of proliferating keratinocytes were found in control wounds than in experimental wounds on day 3 post-wounding.

- On day 15 post-wounding, the thickness and number of rete ridges within the new epithelium of experimental wounds more closely resembled normal skin than did the new epithelium in control wounds. The new epithelium within the centre of experimental wounds was significantly thicker than in control wounds.

- On day 15 post-wounding, fewer blood vessels were observed in experimental wounds as compared to control wounds. In addition, a greater number of more mature blood vessels were seen within experimental wounds than in control wounds.

- While the amount of collagen within both wound types was similar on day 15 post-wounding, the size of the collagen bundles within control wounds was significantly greater than in experimental wounds.

Thus, despite a greater inflammatory response in experimental wounds, no difference was found in the rate of healing of experimental and control wounds on day 15 post-wounding. In addition, in experimental wounds the blood vessels were more mature and the new epithelium more closely resembled normal skin when compared to control wounds on day 15 post-wounding. Furthermore, smaller collagen bundles and decreases in the organisation, density and percentage area of collagen were observed in experimental wounds from day 9 to day 15 post- wounding compared to control wounds.

Table 3.1: Percentage change in wound area for experimental and control wounds

	Experimental wound Median (Minimum: Maximum)	**Control wound** Median (Minimum: Maximum)	p (Mann Whitney U test)
Wound area on day 0 post-wounding (mm)	94.00 (31.00: 123.00)	96.50 (41.00: 147.00)	0.66
Day 0 to day 3 post-wounding	-47.00 (-202.00: 13.00)	-7.00 (-80.00: 35.00)	0.001
Day 0 to day 6 post-wounding	-25.00 (-94.00: 19.00)	0.00 (-110.00: 33.00)	0.04
Day 0 to day 9 post-wounding	31.50 (-36.00: 91.00)	63.00 (25.00: 92.00)	0.04
Day 0 to day 12 post-wounding	83.00 (46.00: 98.97)	97.00 (77.00: 100.00)	0.310
Day 0 to day 15 post-wounding	83.00 (73.00: 100.00)	98.29 (80.00: 100.00)	0.31

Note: negative values indicate an increase in wound area

Table 3.2: The Clinical Assessment Scores of the re-epithelialised wounds on day 12 and day 15 post-wounding.

Wound	**Day**	**Observer**	**A**	**B**	**C**	**D**	**VAS**	**Total**
Control 1	12	1	3	2	1	2	3.5	11.5
		2	2	1	2	3	3	11
		3	2	2	2	2	4	12
Control 2	12	1	3	1	2	1	3.5	10.5
		2	4	1	2	2	3	12
		3	3	1	2	2	5	13
Control 1	15	1	3	1	1	2	3.9	10.9
		2	3	1	2	2	2.4	10.4
		3	2	1	2	1	3	9
Control 2	15	1	3	2	1	1	4	11
		2	4	2	1	1	2	10
		3	3	2	1	1	4	11
Experimental	15	1	4	1	1	1	3.6	10.6
		2	4	1	1	1	2.3	9.3
		3	2	1	2	1	3	9

A: Colour, B: matte/ shiny, C: Contour; D: Distortion
VAS: Visual analogue scale: 10 indicates a poor scar, 0 indicates a good scar.

Table 3.3: Median values for histological measurements on day 3 post-wounding

	Experimental wound Median (Minimum: Maximum)	**Control wound** Median (Minimum: Maximum)	p (Mann Whitney U test)
Area of the epithelial tongue (μm^2)	82324.72 (58001.89:128672.80)	61420.48 (40090.70:88520.06)	0.14
Length of the epithelial tongue (µm)	1565.04 (1283.34: 2215.80)	1347.27 (1070.54: 1470.41)	0.09
Thickness of the epithelium at the wound edge (µm)	96.28 (87.38:117.84)	92.22 (50.27: 99.23)	0.30
Thickness of the epithelium at the tip of the epithelial tongue (µm)	52.93 (42.85: 71.56)	38.31 (32.60: 55.80)	0.09
Score for epidermal appendages	0.83 (0.33: 0.83)	0.83 (0.33: 0.83)	0.92
Number of proliferating keratinocytes	4.67 (1.33: 7.00)	9.33 (7.00: 26.00)	0.02
Number of inflammatory cells	314.78 (232.78: 373.22)	120 (54.56: 147.00)	0.01
Score for blood vessel type	0 (0: 0)	0 (0: 0)	0.92
Score for blood vessel number	0 (0: 0)	0 (0: 0)	0.92
Percentage area of collagen (μm^2)	2.65 (0.84: 5.23)	0.53 (0.17: 1.96)	0.06
Score for collagen density	0 (0: 0)	0 (0: 0)	0.92
Score for collagen bundle size	0 (0: 0)	0 (0: 0)	0.92
Score for collagen organisation	0 (0: 0)	0 (0: 0)	0.92

Table 3.4: Median values for histological measurements on day 6 post-wounding

	Experimental wound Median (Minimum: Maximum)	**Control wound** Median (Minimum: Maximum)	p (Mann Whitney U test)
Area of the epithelial tongue (μm^2)	424848.10 (204293.80: 530267.50)	495958.60 (363205.70: 673859.70)	0.53
Length of the epithelial tongue (µm)	5061.80 (3047.00: 6002.10)	5881.10 (4209.00: 8693.30)	0.30
Thickness of the epithelium at the wound edge (µm)	147.57 (92.78:192.39)	129.29 (103.57:159.85)	0.53
Thickness of the epithelium at the tip of the epithelial tongue (µm)	72.89 (61.39:110.63)	58.57 (53.18: 65.60)	0.09
Score for epidermal appendages	0.67 (0.33: 0.83)	0.67 (0.50: 0.83)	1.00
Number of proliferating keratinocytes	8.00 (0.00: 13.33)	25.67 (8.33: 100.33)	0.09
Number of inflammatory cells	39.44 (26.78: 174.44)	96.67 (29.89: 142.89)	0.83
Score for blood vessel type	1.00 (1.00: 1.00)	1.00 (1.00: 1.33)	0.35
Score for blood vessel number	1.83 (1.00: 2.00)	1.83 (1.33: 2.67)	0.46
Percentage area of collagen (μm^2)	12.22 (6.10: 22.85)	18.61 (3.45: 43.20)	0.68
Score for collagen density	0.58 (0.17: 1.67)	0.92 (0.08: 2.00)	0.83
Score for collagen bundle size	1.25 (0.92: 1.67)	1.50 (1.00: 2.00)	0.30
Score for collagen organisation	0.92 (0.58: 1.25)	1.0 (0.25: 1.83)	0.60

Table 3.5: Median values for histological measurements on day 9 post-wounding

	Experimental wound Median (Minimum: Maximum)	**Control wound** Median (Minimum: Maximum)	p (Mann Whitney U test)
Size of the epithelial gap (µm)	1431.55 (868.66: 1575.74)	1159.18 (0.00: 2615.38)	0.53
Percentage by which the wound has closed	70.43 (64.39: 81.39)	69.58 (53.58: 100.00)	1.0
Width of the wound area (µm)	4095.105 (3484.32: 4663.460)	3048.418 (2660.75: 5365.21)	0.14
Area of the epithelial tongue or new epithelium (μm^2)	989659.20 (618998.60: 1181906.00)	640817.60 (393321.60: 790971.80)	0.09
Length of the epithelial tongue (µm)	8691.20 (6034.60: 9223.00)	7016.20 (3887.50: 8070.50)	0.14
Thickness of the epithelium at the wound edge (µm)	158.61 (130.19: 174.30)	204.90 (151.30: 251.26)	0.14
Thickness of the epithelium at the tip of the epithelial tongue (µm)	86.31 (73.12: 96.02)	91.83 (36.95: 135.43)	1.00
Score for epidermal appendages	0.67 (0.17: 1.00)	0.67 (0.67: 1.00)	0.83
Number of proliferating keratinocytes	8.33 (0.00: 39.00)	31.33 (8.33: 65.33)	0.17
Number of inflammatory cells	19.89 (13.44: 27.67)	36.78 (17.11: 44.33)	0.09
Score for blood vessel type	1.33 (1.17: 2.00)	1.50 (1.17: 1.83)	0.75
Score for blood vessel number	1.50 (1.50: 2.33)	2.00 (1.17: 2.33)	0.46
Percentage area of collagen (μm^2)	45.67 (41.68: 60.86)	43.55 (24.93: 59.55)	0.40
Score for collagen density	2.17 (1.83: 2.75)	2.17 (1.50: 2.33)	0.40
Score for collagen bundle size	2.33 (2.00: 2.33)	2.08 (1.92: 2.25)	0.21
Score for collagen organisation	1.75 (1.50: 2.17)	1.42 (1.00: 1.67)	0.04

Table 3.6: Median values for histological measurements on day 15 post-wounding

	Experimental wound Median (Minimum: Maximum)	**Control wound** Median (Minimum: Maximum)	p (Mann Whitney U test)
Size of the epithelial gap (μm)	0 (0: 0)	0 (0: 819.95)	0.68
Percentage by which the wound has closed	100 (100: 100)	100 (78.91: 100)	0.68
Width of the wound area (μm)	2112.36 (1279.21: 2387.66)	1717.733 (1205.75: 3048.87)	0.83
Area of the epithelial tongue (μm^2)	377299.40 (218576.10: 589713.40)	191806.90 (146321.30: 303423.10)	0.09
Length of the epithelial tongue (μm)	3931.90 (2457.30: 4392.40)	2860.90 (2262.40: 4752.20)	0.53
Thickness of the epithelium at the wound edge (μm)	141.93 (73.81: 221.80)	119.41 (107.03: 166.20)	0.40
Thickness of the epithelium at the tip of the epithelial tongue (μm)	146.83 (125.65: 200.47)	83.32 (79.01: 140.51)	0.04
Score for epidermal appendages	0.50 (0.33: 0.83)	0.83 (0.50: 1.00)	0.14
Number of proliferating keratinocytes	39.67 (6.33: 78.00)	31.00 (1.33: 74.00)	0.68
Number of inflammatory cells	8.67 (3.89: 18.33)	14.67 (12.00: 35.11)	0.14
Score for blood vessel type	1.83 (1.83: 2.00)	1.67 (1.33: 1.83)	0.06
Score for blood vessel number	1.00 (1.00: 1.17)	1.17 (1.00: 1.50)	0.40
Percentage area of collagen (μm^2)	46.39 (24.25: 61.08)	54.47 (39.20: 65.71)	0.30
Score for collagen density	1.83 (1.25: 2.42)	2.25 (1.92: 2.58)	0.14
Score for collagen bundle size	2.00 (2.00: 2.25)	2.42 (2.17: 2.50)	0.03
Score for collagen organisation	1.42 (1.17: 1.83)	1.67 (1.17: 1.83)	0.75

Table 3.7: Contingency table indicating the regions on the dorsum of the pigs utilized on each day post-wounding

Day post-wounding	**Towards the head**	**Middle**	**Towards the tail**	**Total* (experimental and control wounds)**
3	0	4	6	10
6	4	2	4	10
9	4	4	2	10
15	6	2	2	10

*Total number of experimental and control wounds

Table 3.8: Contingency table indicating the pigs utilized on each day post-wounding

Day post-wounding	**Pig 1**	**Pig 2**	**Pig 3**	**Pig 4**	**Pig 5**	**Pig 6**	**Pig 7**	**Pig 8**	**Pig 9**	**Total***
3	0	0	2	2	2	0	2	2	0	10
6	0	0	2	2	2	0	2	2	0	10
9	0	0	2	2	2	2	0	0	2	10
15	0	0	0	2	0	0	0	0	8	10

*Total number of experimental and control wounds

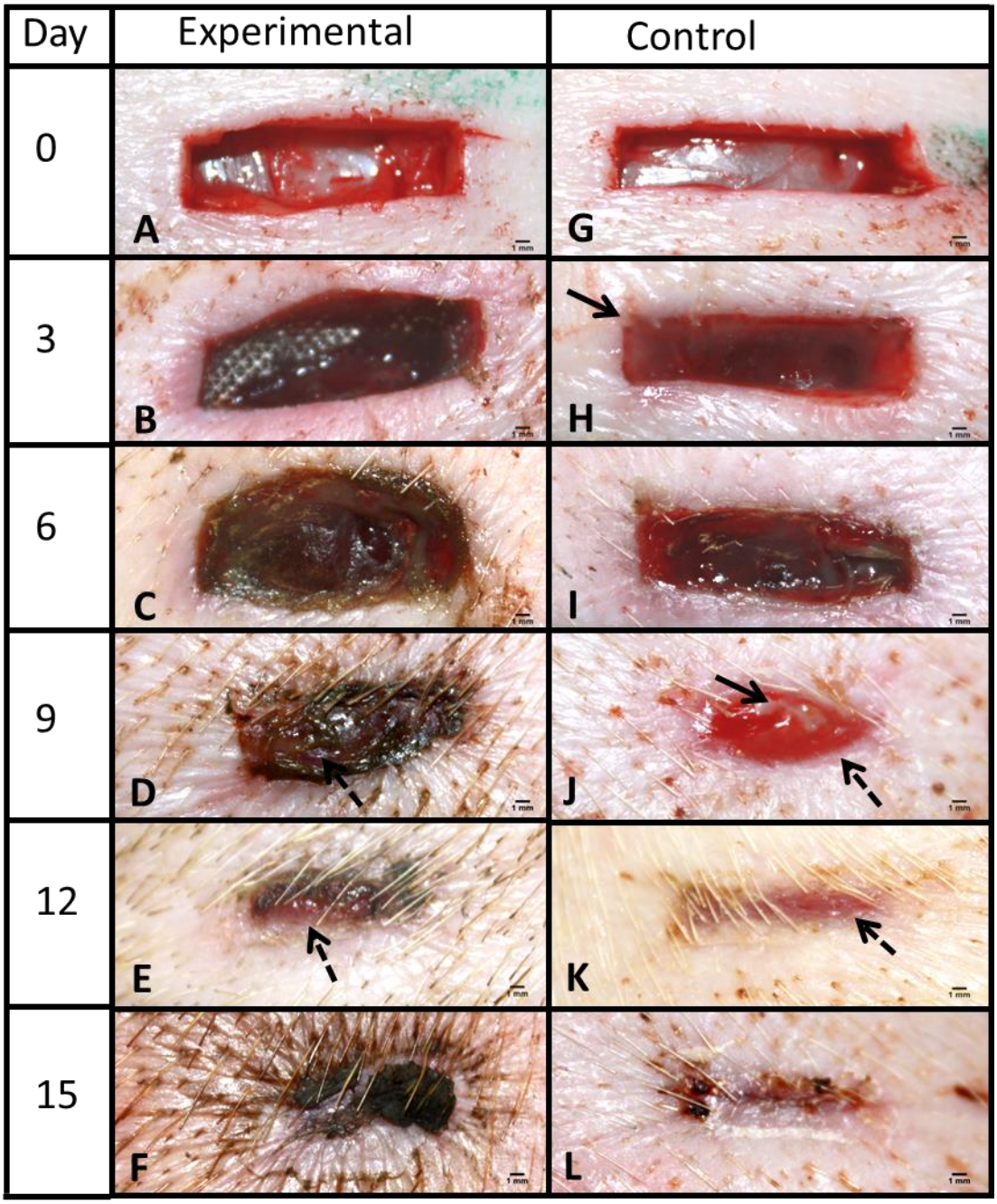

Figure 3.1 Representative photographs of experimental (A-F) and control wounds (G-L) on the day of wound creation (A, G) and on day 3 (B, H), day 6 (C, I), day 9 (D, J), day 12 (E, K) and day 15 (F, L) post-wounding. Note the erythema surrounding the experimental wound on day 3 (B) and the control wound on day 6 (I). The solid arrows indicate small amounts of exudate visible on the control wounds on day 6 (I) and day 9 (J). The dotted arrows indicate areas of new epithelium. Black scabs, discoloured by the silver, are present on experimental wounds on day 12 (E) and day 15 (F). Discolouration of the hair in experimental wounds is particularly noticeable on day 15 (F).

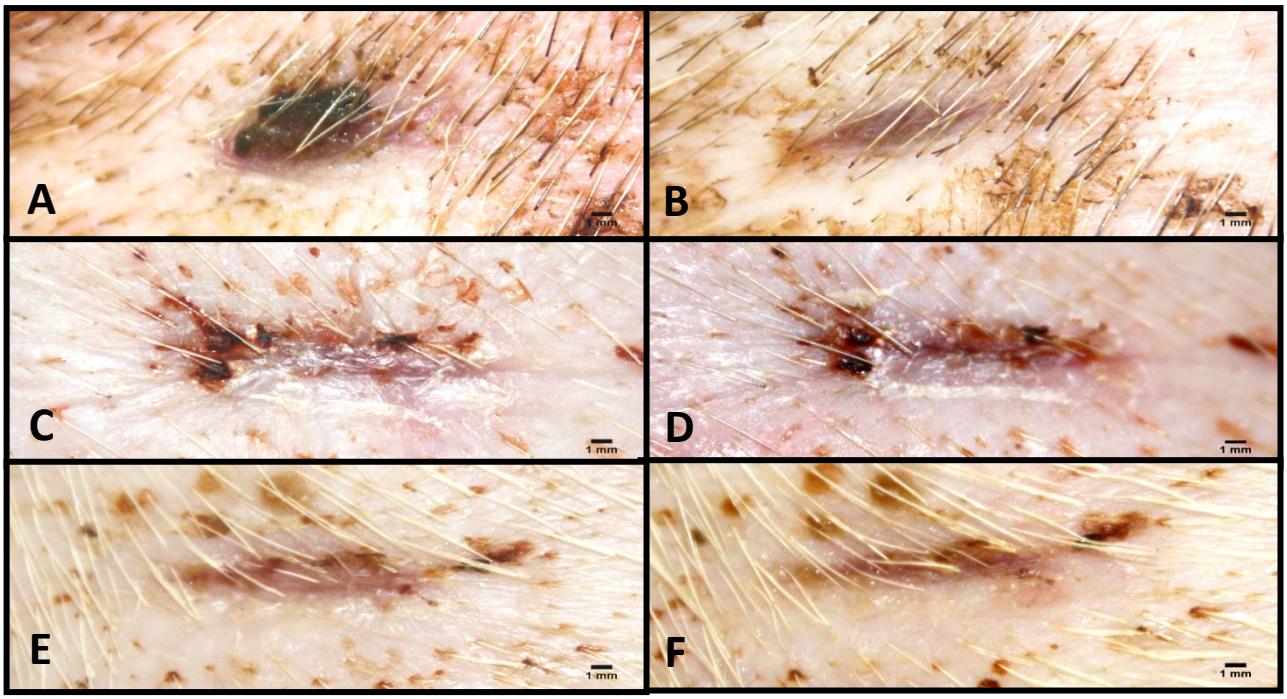

Figure 3.2 Photographs of experimental (A, B) and control (C-F) wounds utilised for the Clinical Assessment Score on day 12 (A, C, E) and day 15 (B, D, F) post-wounding. Note B-F are re-epithelialised and A is not.

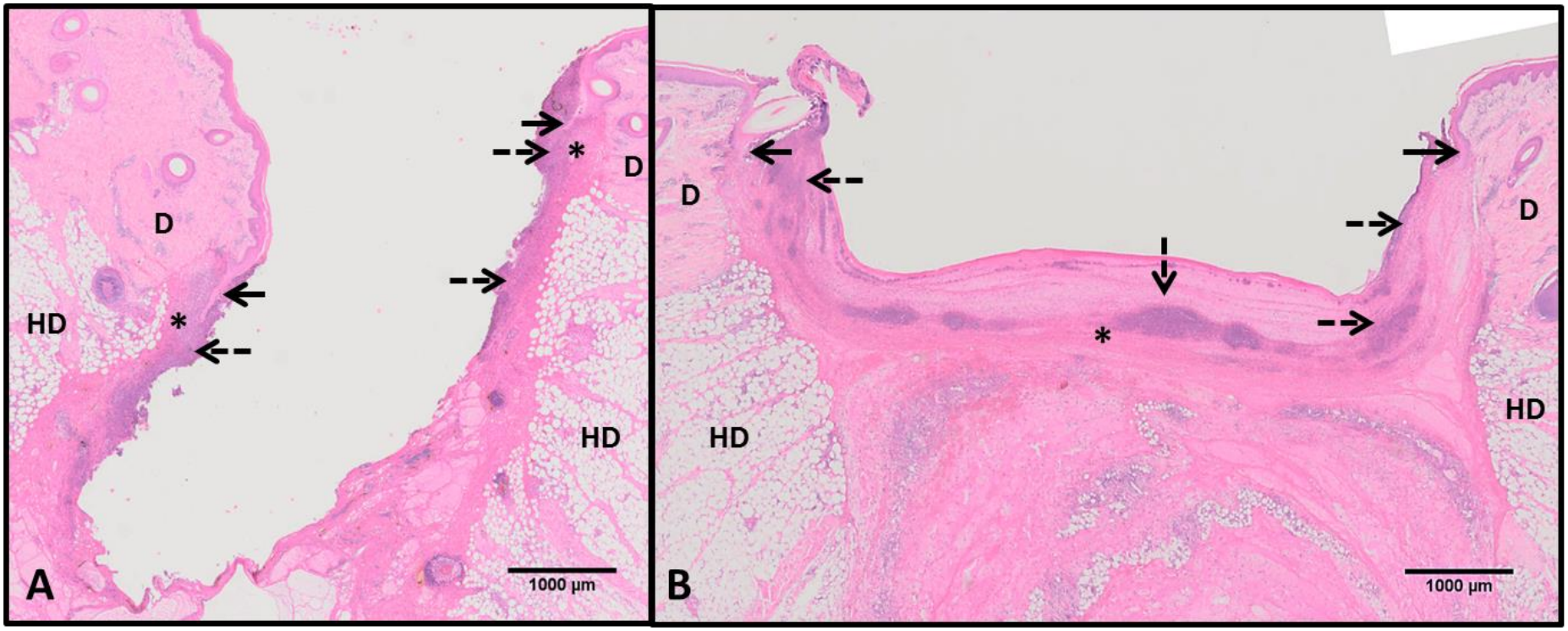

Figure 3.3 Representative photomicrographs of experimental (A) and control (B) wounds on day 3 post-wounding illustrating the new epithelium (solid arrow) extending into the wound area and the fibrin clot (*) adjacent to the dermis (D) and hypodermis (HD). Note the longer epithelium tongue (solid arrows) on the left of the experimental wound (A) when compared to the control wound (B). However, the epithelial tongue on the right of the experimental wound (A) is shorter than the left, illustrating the variability in experimental wounds. The amount of fibrin clot (*) is greater in control wounds (B). Areas of inflammatory infiltrate within experimental (A) and control (B) wounds are also visible (dashed arrows). Note: images have been merged to create a composite image. (H&E)

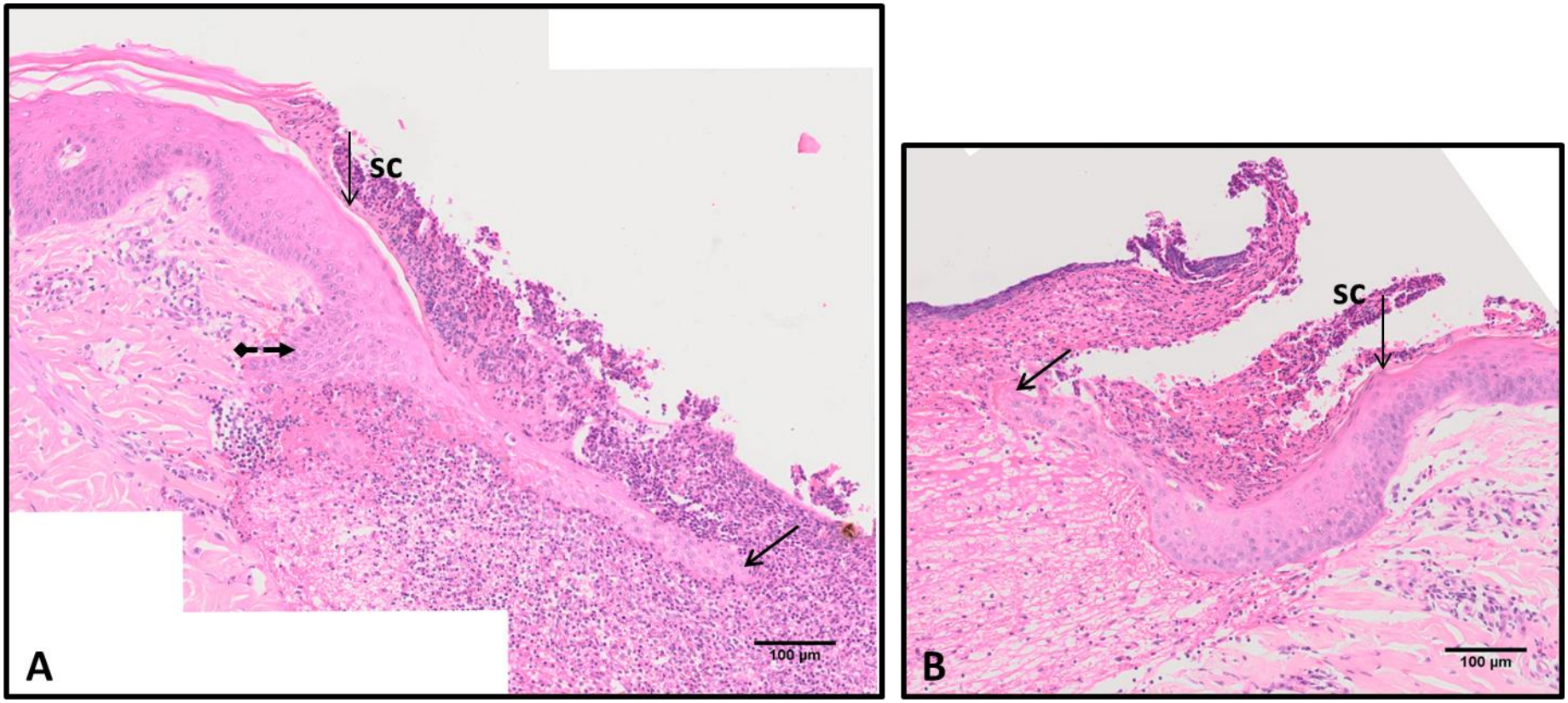

Figure 3.4 Representative photomicrographs of epithelial tongues in experimental (A) and control (B) wounds on day 3 post-wounding illustrating the longer and thicker epithelial tongue seen in experimental wounds. The tips of each epithelial tongue are indicated by the solid arrows. Note that the epithelial tongue in the experimental wound (A) contains a rete ridge (dashed arrow). All layers of the epidermis, including the stratum corneum (sc) are visible at the wound edge in both experimental (A) and control wounds (B). The greater inflammatory response in the experimental wound (A) is also visible. Note: images have been merged to create a composite image. (H&E)

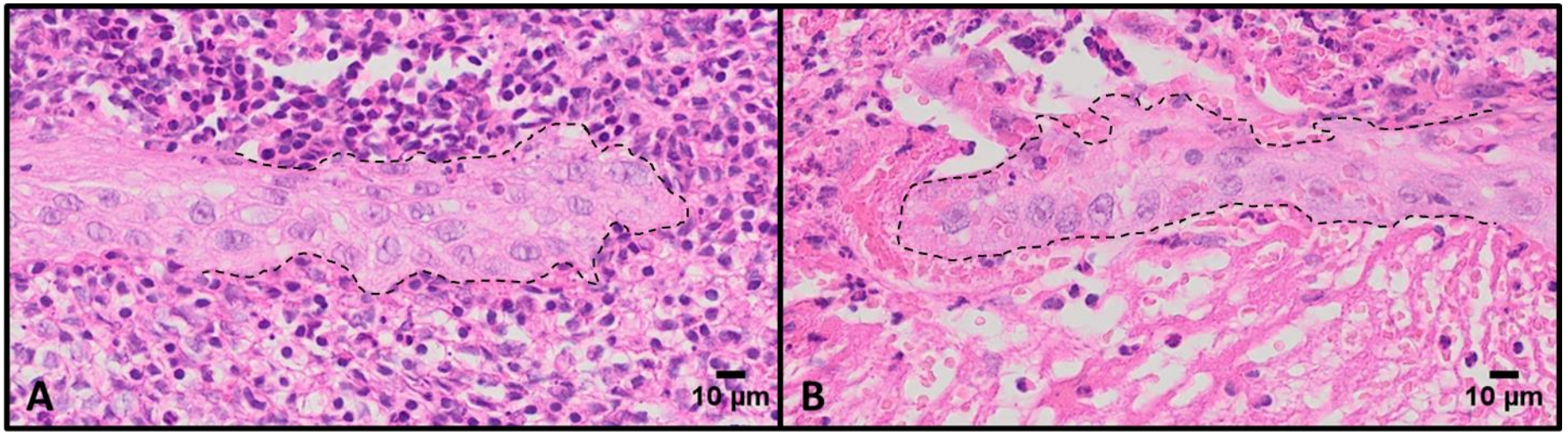

Figure 3.5 Representative photomicrographs of the tips of epithelial tongues in experimental (A) and control (B) wounds on day 3 post-wounding. This illustrates the greater number of cell layers in the tip of the epithelial tongue of experimental wounds (A) and the lack of differentiation of the epithelium in both wound types. (H&E, 20X magnification)

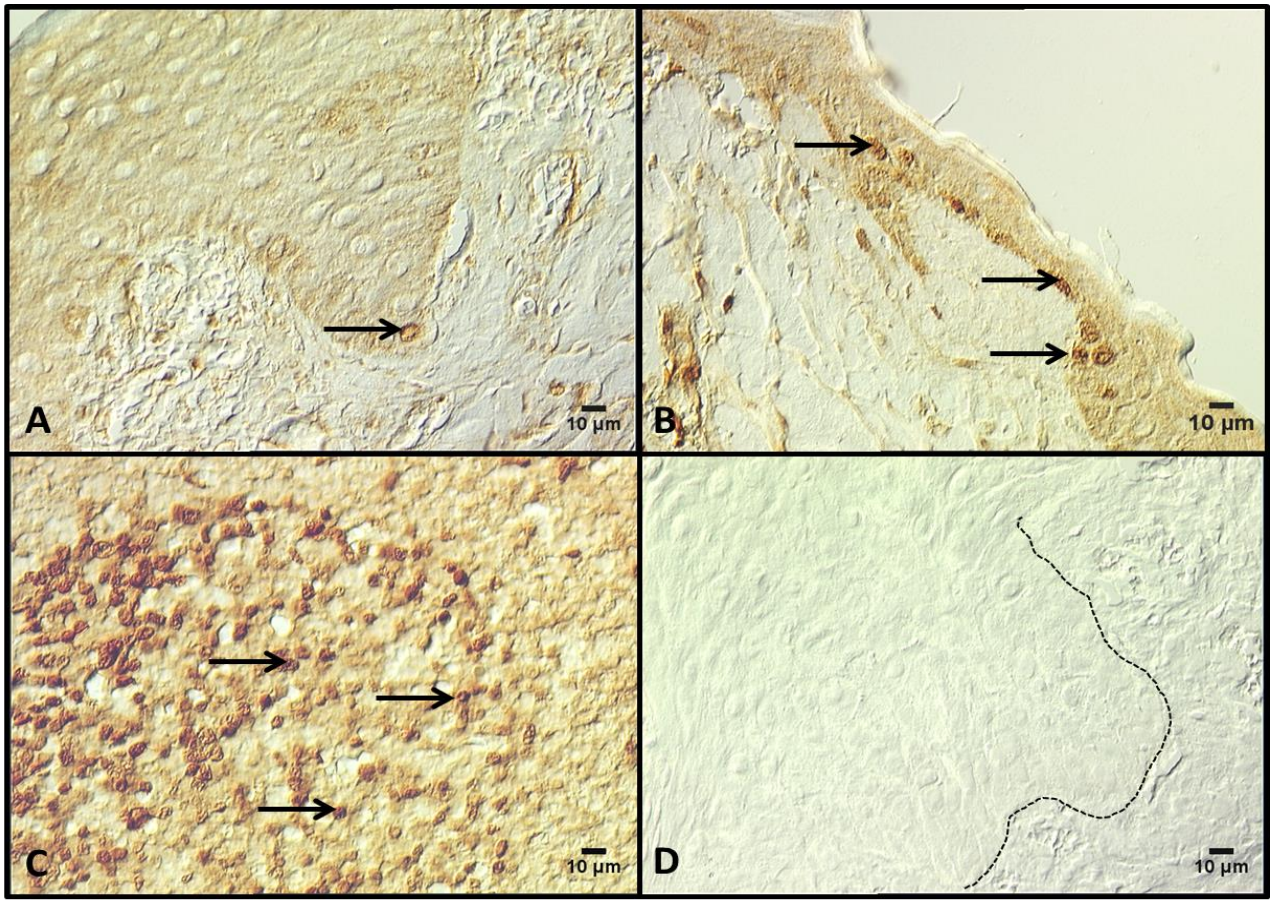

Figure 3.6 Representative photomicrographs of proliferating keratinocytes in the epithelium of experimental (A) and control (B) wounds on day 3 post-wounding. The positive control (C: human tonsil) and negative control (D: an adjacent section to A) are also shown. Arrows indicate examples of the nuclei of proliferating cells immunolabelled for Ki-67. Note the single cell within a rete ridge of non-wounded epithelium in the experimental wound (A) compared to the greater number of cells which are situated within the basal layer of the epithelial tongue in the control wound (B). The dotted line in D indicates the position of the epidermal-dermal junction. (Immunocytochemical labelling for Ki-67, DIC microscopy, 25X magnification)

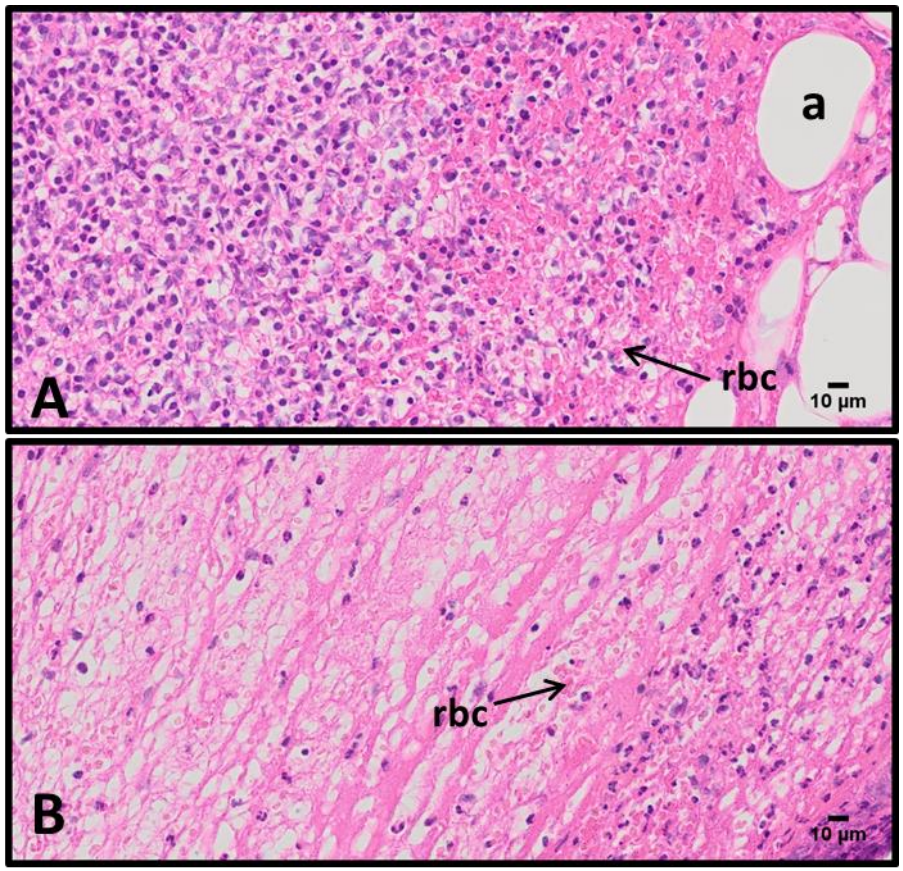

Figure 3.7 Representative photomicrographs of a fibrin clot in experimental (A) and control (B) wounds on day 3 post-wounding illustrating the greater inflammatory response in the experimental wound (A). 'a' indicates an adipocyte. rbc indicates red blood cells within the fibrin clot. Note the lack of blood vessels or collagen in both wound types. (H&E, 20X magnification)

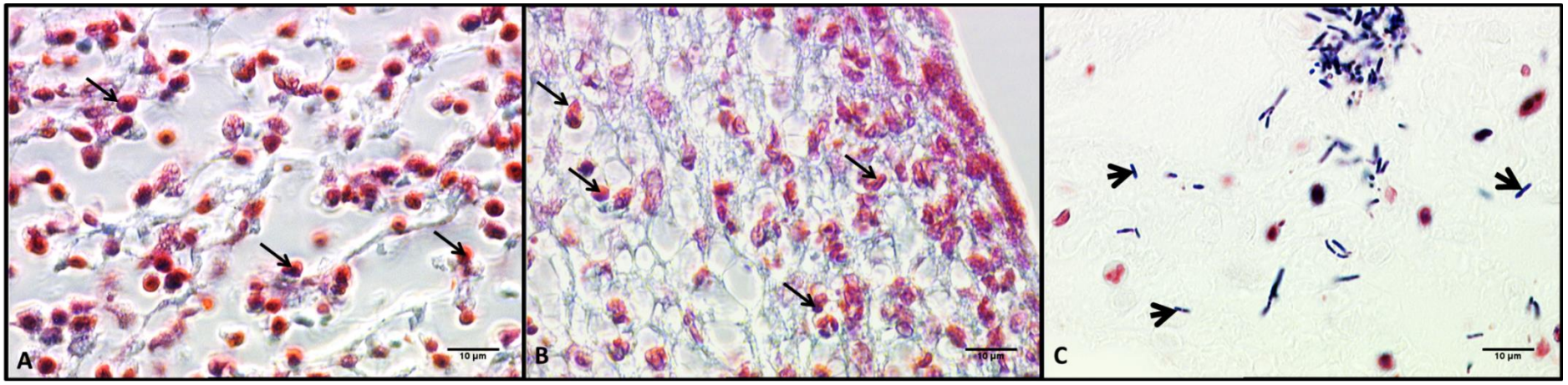

Figure 3.8 Representative photomicrographs of fibrin clot in experimental (A) and control (B) wounds on day 3 post-wounding, illustrating the absence of bacteria. Long arrows in A and B indicate examples of inflammatory cell nuclei. C is the positive control in which gram positive bacilli can be seen (short arrows). (Gram stain, 63X magnification)

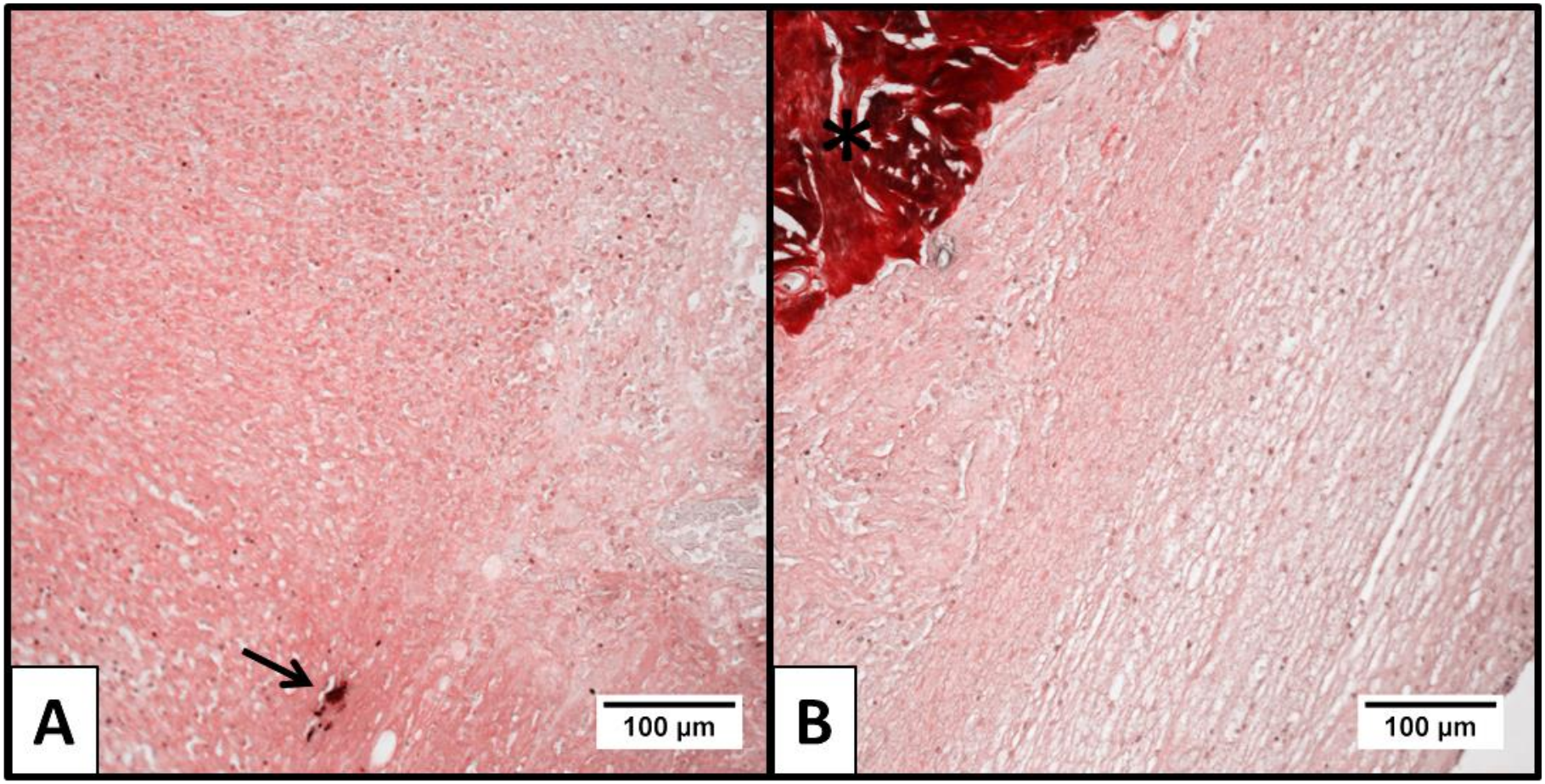

Figure 3.9 Representative photomicrographs of the wound area of experimental (A) and control (B) wounds on day 3 post-wounding illustrating the lack of collagen within the wound area. * indicates an area of normal collagen in the control wound (B). Note the silver particle (arrow) in the experimental wound (A). (Picrosirius red stain, confocal microscopy, 25X magnification)

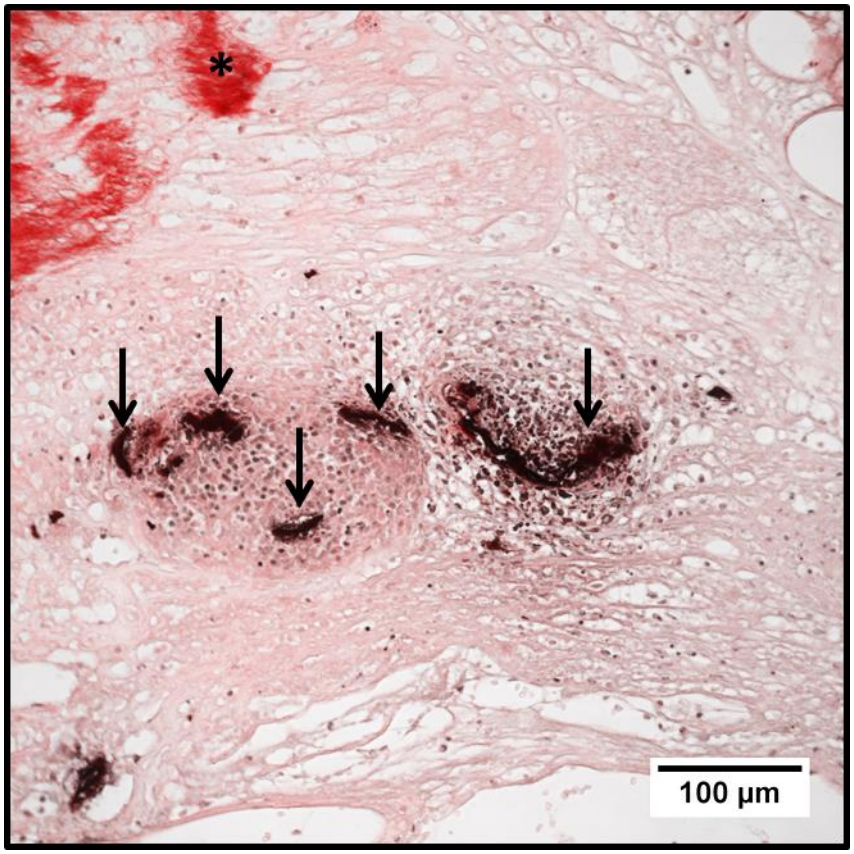

Figure 3.10 Representative photomicrograph showing deposits of silver (solid arrows) within the wound area of an experimental wound on day 3 post-wounding. * indicates an area of normal collagen. (Picrosirius red stain, confocal microscopy, 25X magnification)

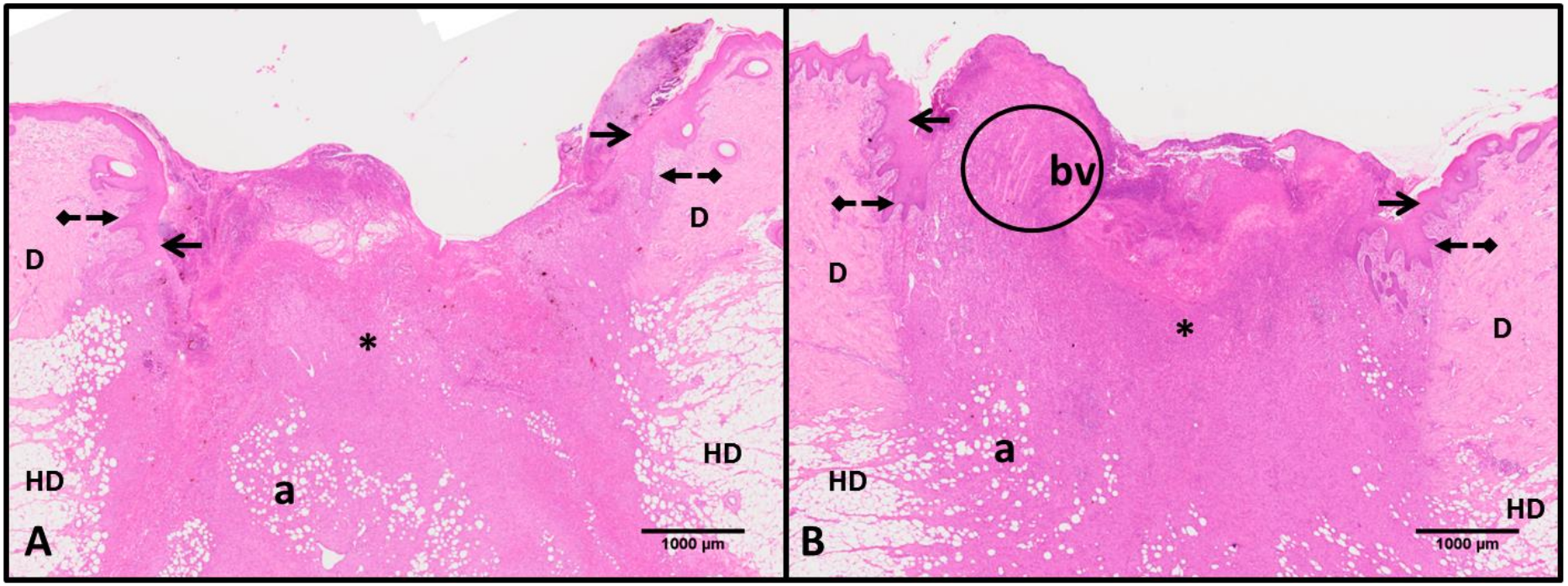

Figure 3.11 Representative photomicrographs of experimental (A) and control (B) wounds on day 6 post-wounding illustrating the longer and thicker epithelial tongues (solid arrows) in the control wound. Note the larger rete ridges (dashed arrows) of the new epithelium (solid arrows) within the control wound (B). * indicates the granulation tissue which fills the wound area of both wound types and in which adipocytes (a) can be seen. bv indicates new blood vessels within the control wound (B). D: non-wounded dermis, HD: hypodermis. Note: images have been merged to create a composite image. (H&E)

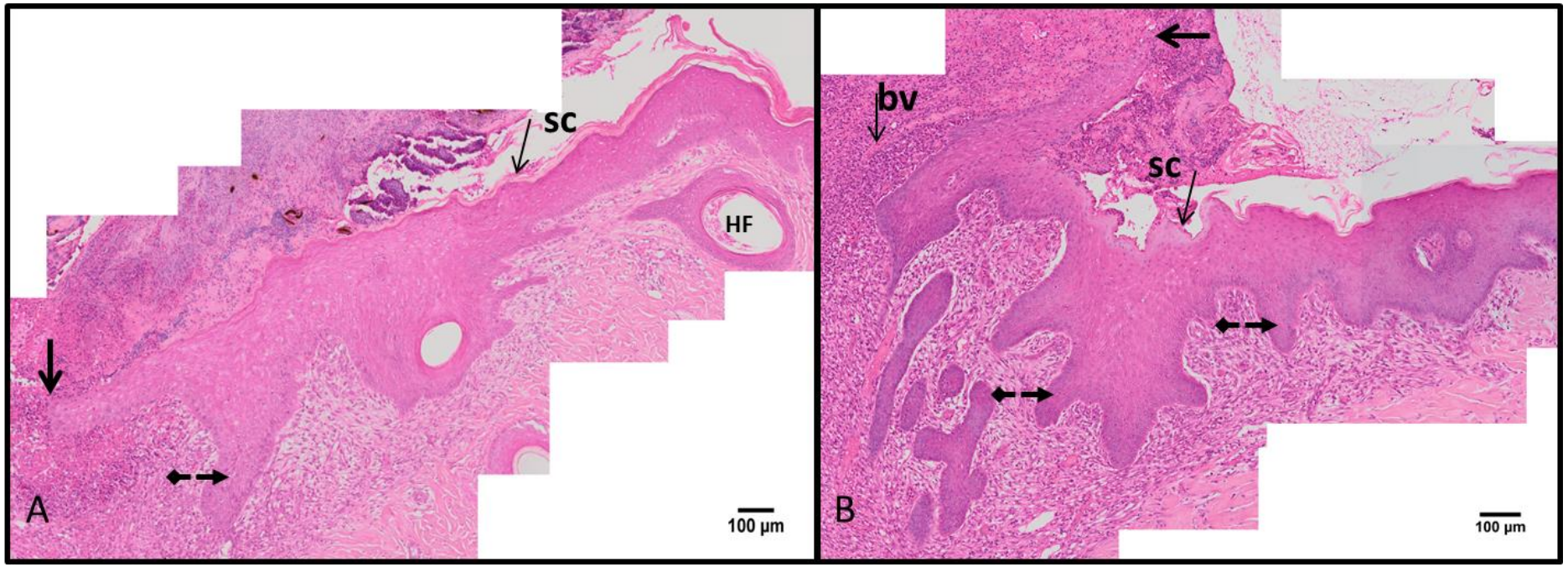

Figure 3.12 Representative photomicrographs of epithelial tongues in experimental (A) and control (B) wounds on day 6 post-wounding. The tips of each epithelial tongue are indicated by the thick, solid arrows. While rete ridges (dashed arrows) are seen in both wound types, the epithelial tongue of the control wound (B) is longer and thicker than that of the experimental wound (A) and also contains a greater number of rete ridges. The stratum corneum (sc) can be seen extending down the epithelial tongues of both wound types. In addition, a blood vessel (bv) can be seen in the control wound (B). Note: images have been merged to create a composite image. (H&E).

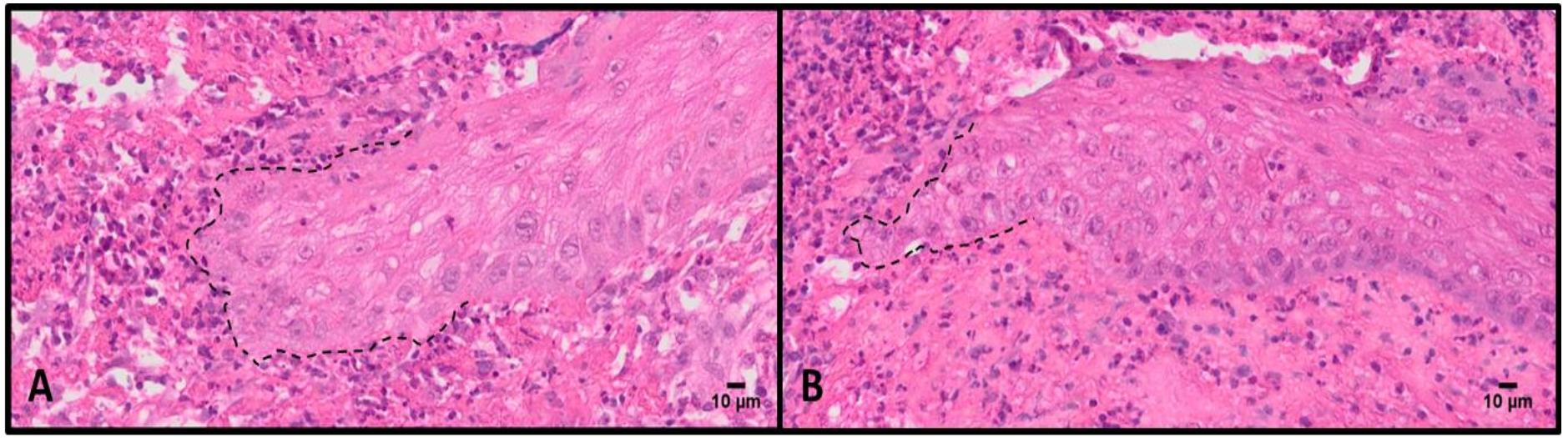

Figure 3.13 Representative photomicrographs of tips of epithelial tongues (outlined by the dotted lines) in experimental (A) and control (B) wounds on day 6 post-wounding illustrating the greater number of cell layers in the experimental wound (A). (H&E, 20X magnification)

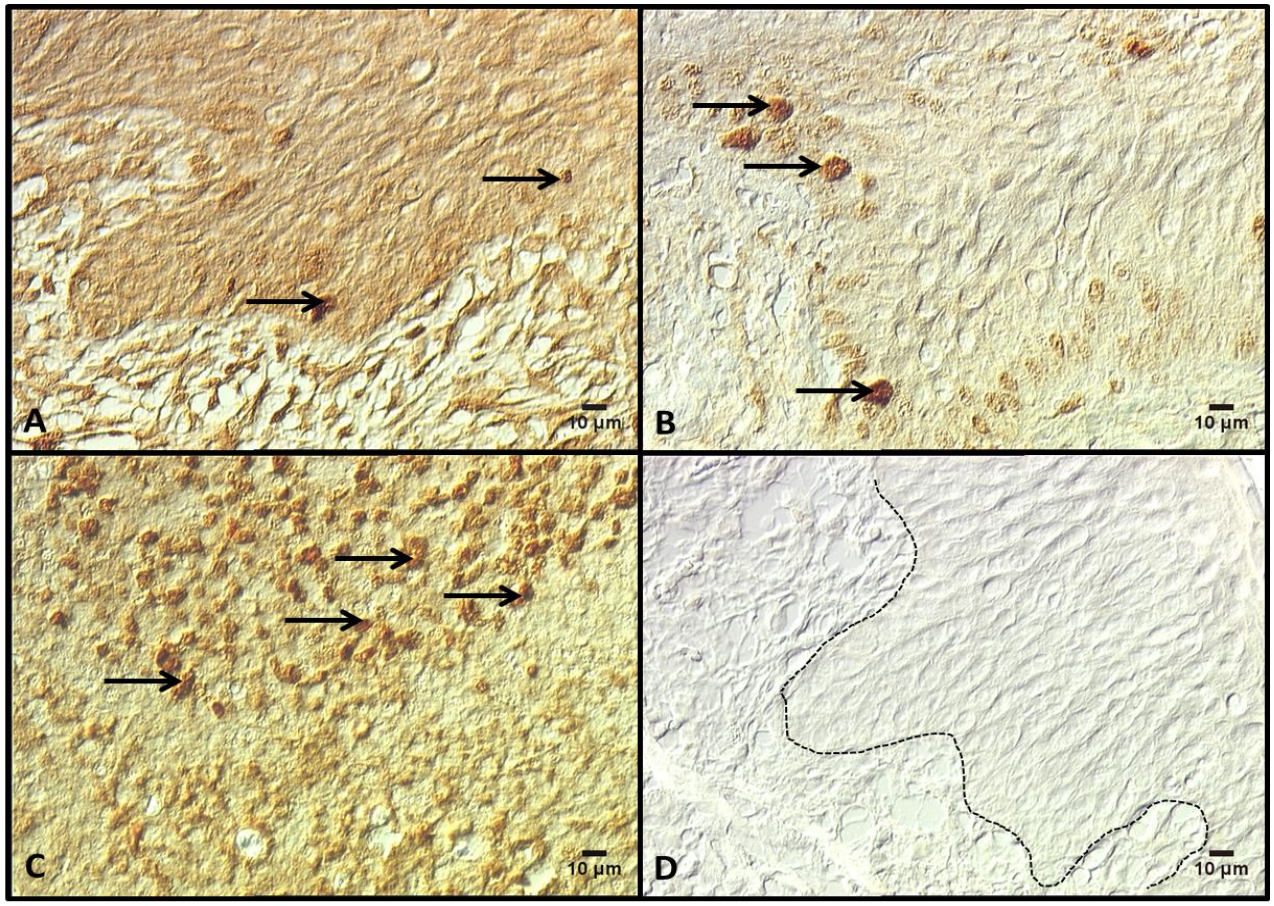

Figure 3.14 Representative photomicrographs of proliferating keratinocytes in the epithelium of experimental (A) and control (B) wounds on day 6 post-wounding. The positive control (C: human tonsil) and negative control (D: an adjacent section to B) are also shown. Arrows indicate examples of the nuclei of proliferating cells immunolabelled for Ki-67. Note the cluster of Ki-67 labelled cells within the control wound (B) compared to the single cells within the experimental wound (A). The dotted line in D indicates the position of the epidermal-dermal junction. (Immunocytochemical labelling for Ki-67, DIC microscopy, 25X magnification)

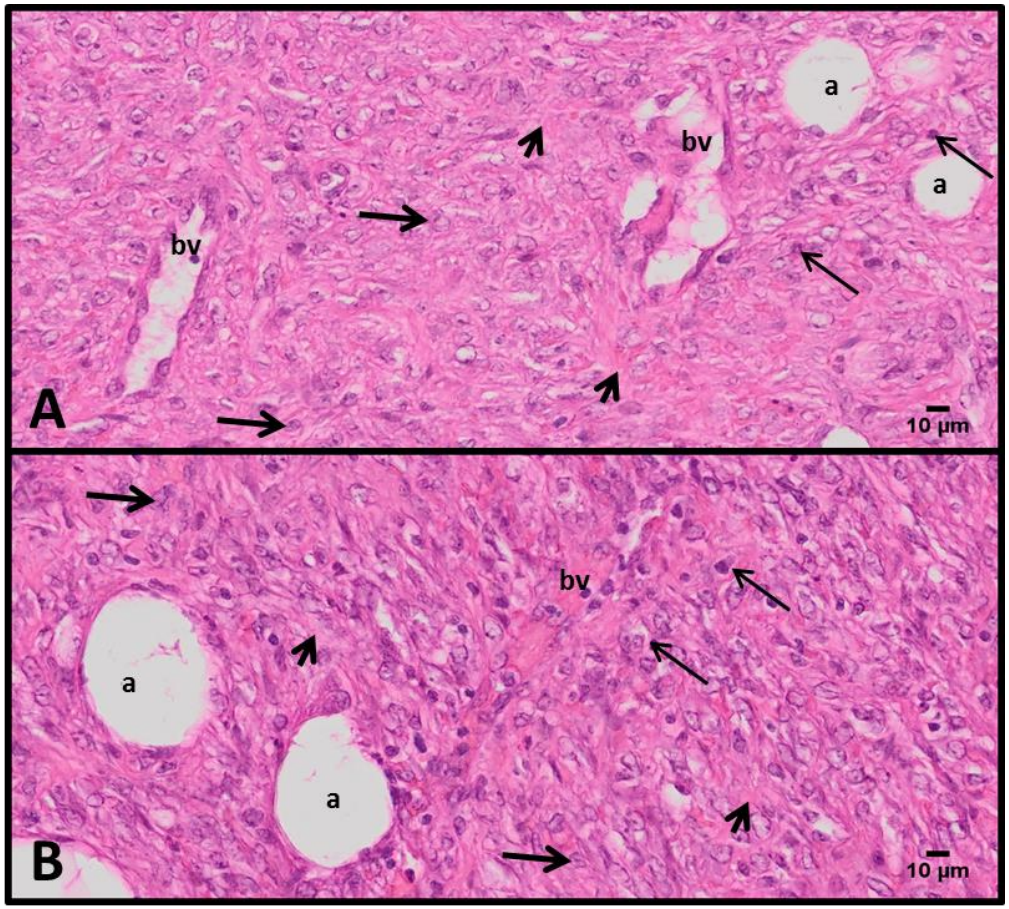

Figure 3.15 Representative photomicrographs of granulation tissue in experimental (A) and control (B) wounds on day 6 post-wounding illustrating blood vessels (bv) with a single layer of cells in the vessel wall and areas of new collagen deposition (short arrows) in both wound types. 'a' indicates adipocytes. The thin arrows indicate the nuclei of scattered inflammatory cells while the long, thick arrows illustrate fibroblast nuclei. (H&E, 20X magnification)

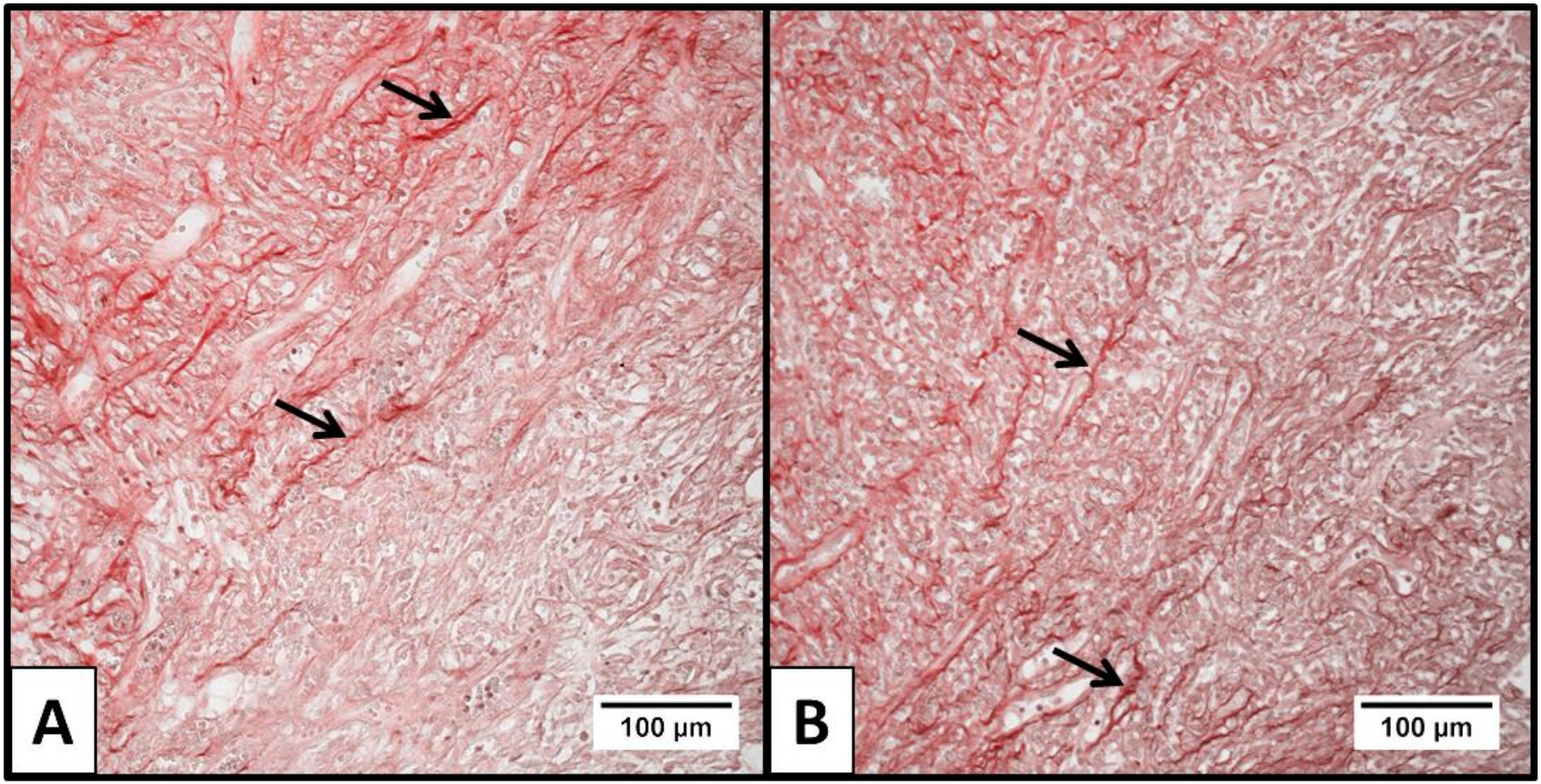

Figure 3.16 Representative photomicrographs of collagen within the wound area of experimental (A) and control (B) wounds on day 6 post-wounding illustrating small collagen bundles (arrows) which are not densely arranged nor organised. (Picrosirius red stain, confocal microscopy, 25X magnification).

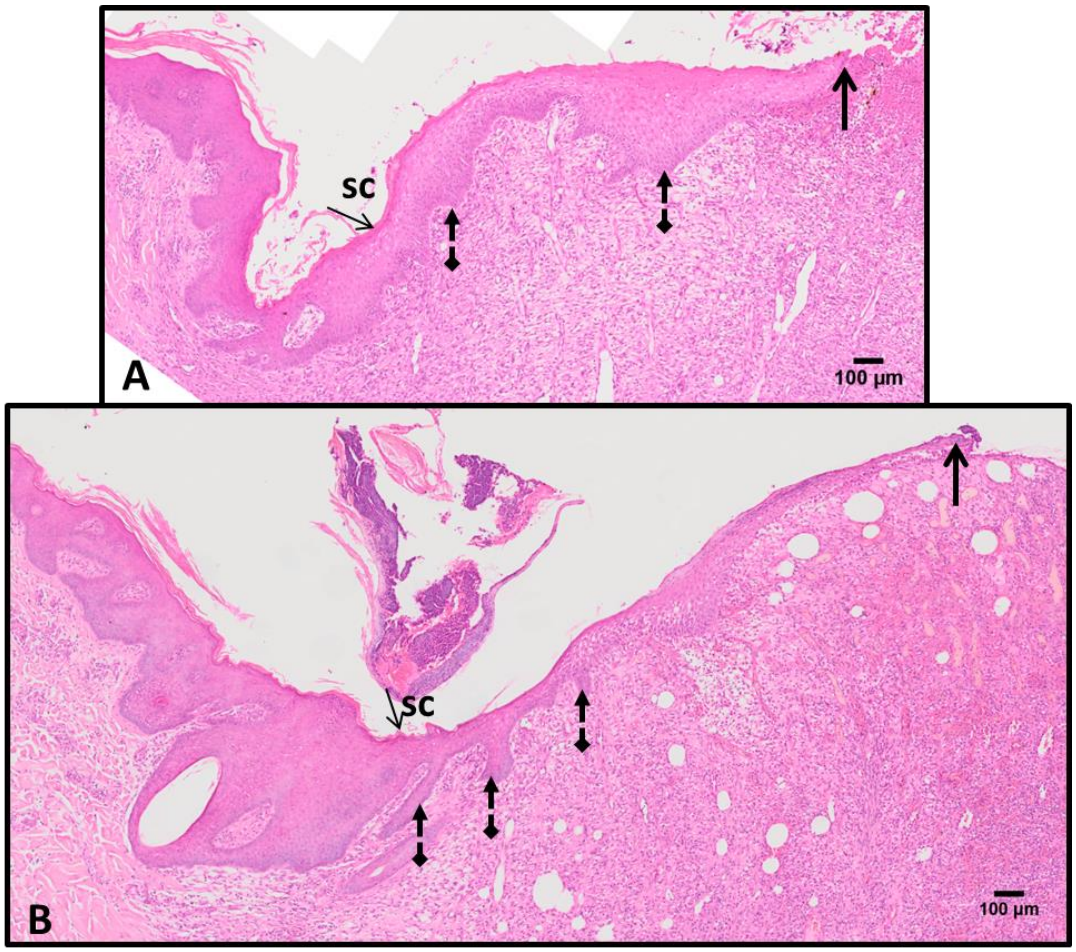

Figure 3.17 Representative photomicrographs of the epithelial tongue in experimental (A) and control (B) wounds which have not re-epithelialised by day 9 post-wounding. Note the stratum corneum (sc) visible on the epithelial tongue at variable distances from the wound edge and the thinner epithelium within the control wounds (B) when compared to experimental wounds (A). Dashed arrows indicate rete ridges. The solid arrows indicate the tip of epithelial tongue. Note: images have been merged to create a composite image. (H&E).

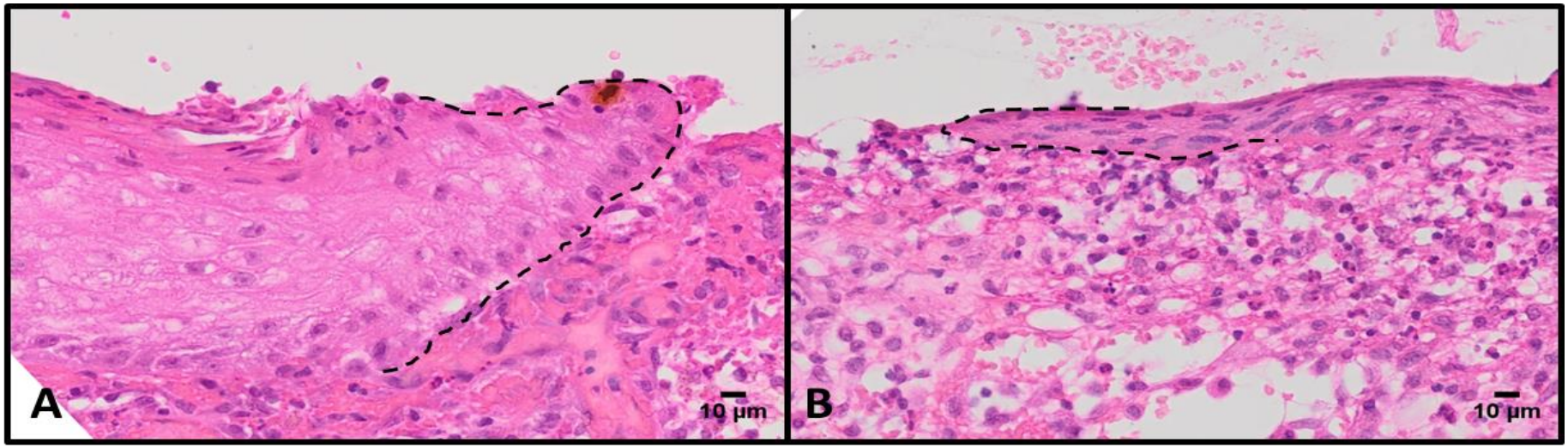

Figure 3.18 Representative photomicrographs of the tip of the epithelial tongue (outlined by the dotted line) in experimental (A) and control (B) wounds which had not re-epithelialised by day 9 post-wounding illustrating the undifferentiated nature of the epithelium.
(H&E, 20X magnification)

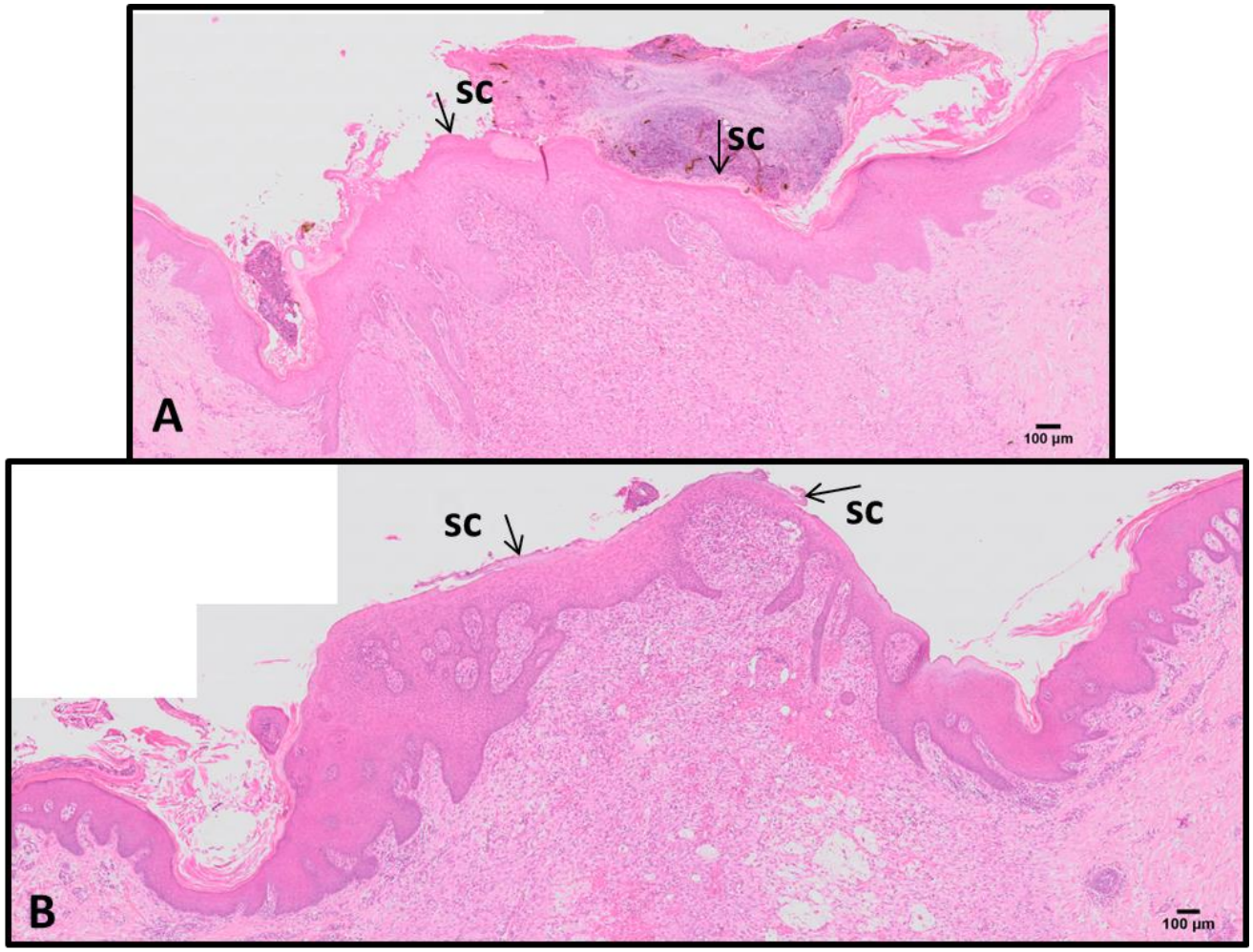

Figure 3.19 Representative photomicrographs of the new epithelium in re-epithelialised experimental (A) and control (B) wounds on day 9 post-wounding. Note the stratum corneum (sc) visible throughout the new epithelium of both wound types. Dashed arrows indicate rete ridges. Note: images have been merged to create a composite image. (H&E)

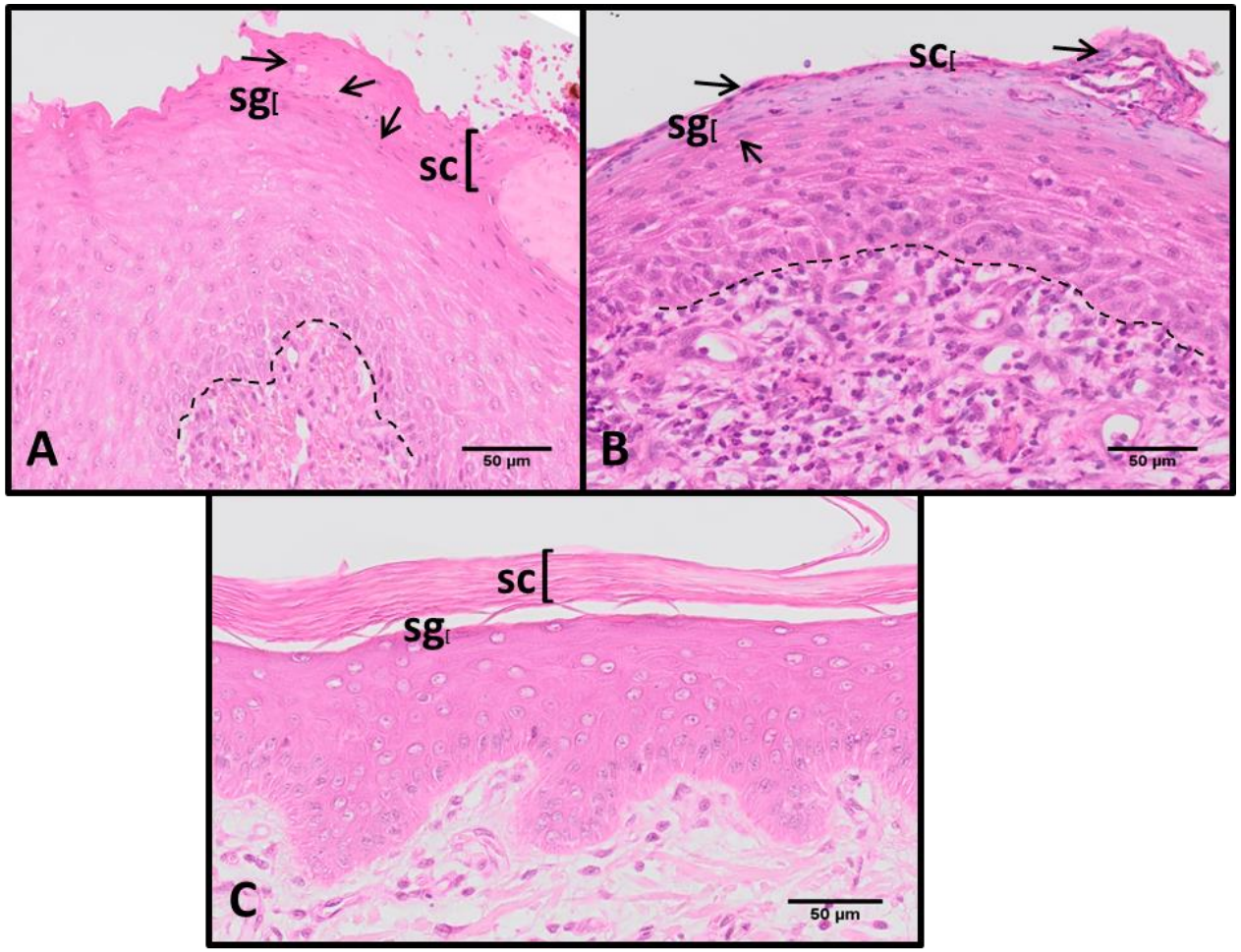

Figure 3.20 Representative photomicrographs of new epithelium from the re-epithelialised experimental (A) and control (B) wounds as well as the epithelium of normal porcine skin (C) on day 9 post-wounding. Note the stratum corneum (sc) and stratum basale (visible above the dotted line) present in both experimental and control wounds. Increased numbers of nuclei (arrows) can be seen in the stratum corneum (sc) and stratum granulosum (sg) of the wounded epidermis (A and B) when compared to normal epidermis (C). (H&E, 20X magnification)

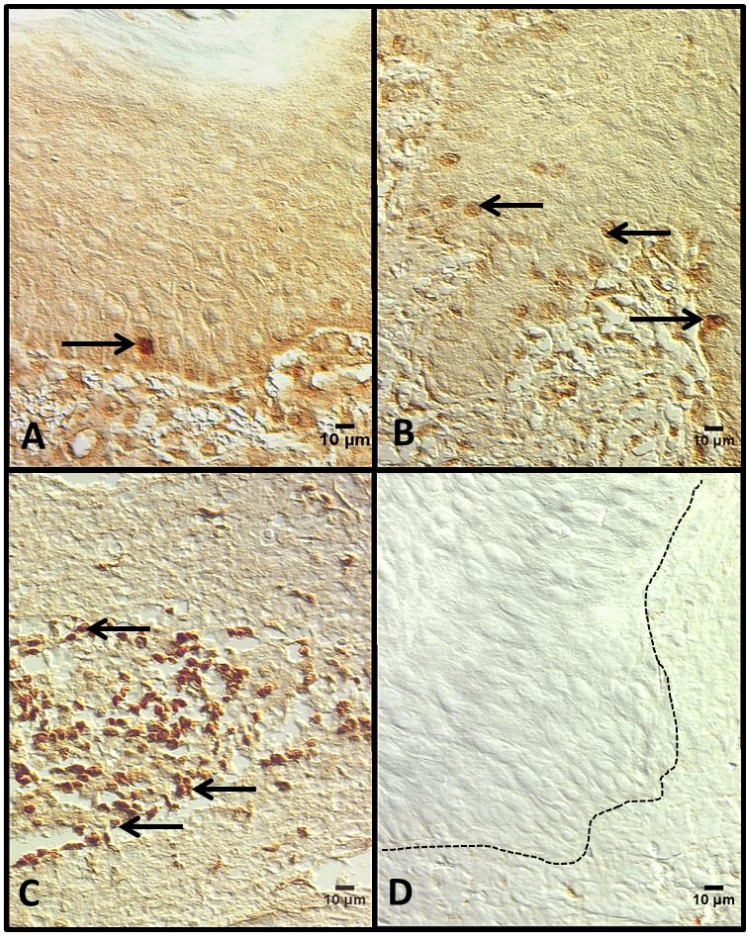

Figure 3.21 Representative photomicrographs of proliferating keratinocytes in the epithelium of experimental (A) and control (B) wounds on day 9 post-wounding. The positive control (C: human tonsil) and negative control (D: an adjacent section to B) are also shown. Arrows indicate examples of the nuclei of proliferating cells immunolabelled for Ki-67. Note the cluster of Ki-67 labelled cells within the control wound (B) compared to the single cells within the experimental wound (A). The dotted line in D indicates the position of the epidermal-dermal junction. Arrows indicate examples of the nuclei of proliferating cells immunolabelled for Ki-67. (Immunocytochemical labelling for Ki-67, DIC microscopy, 25X magnification)

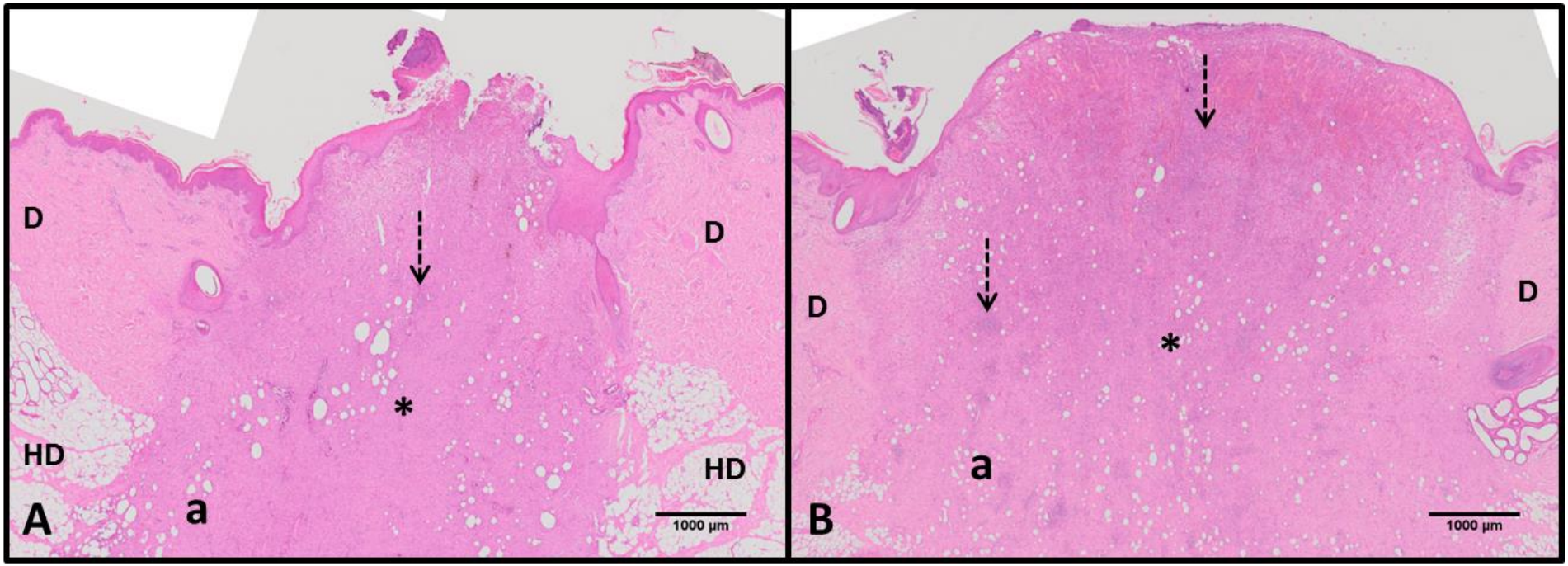

Figure 3.22 Representative photomicrographs of experimental (A) and control (B) wounds which have not re-epithelialised by day 9 post-wounding illustrating granulation tissue (*) within the wound area. The dashed arrows indicate areas of inflammatory cell infiltrates. a: adipocytes D: dermis HD: hypodermis. Note: images have been merged to create a composite image. (H&E)

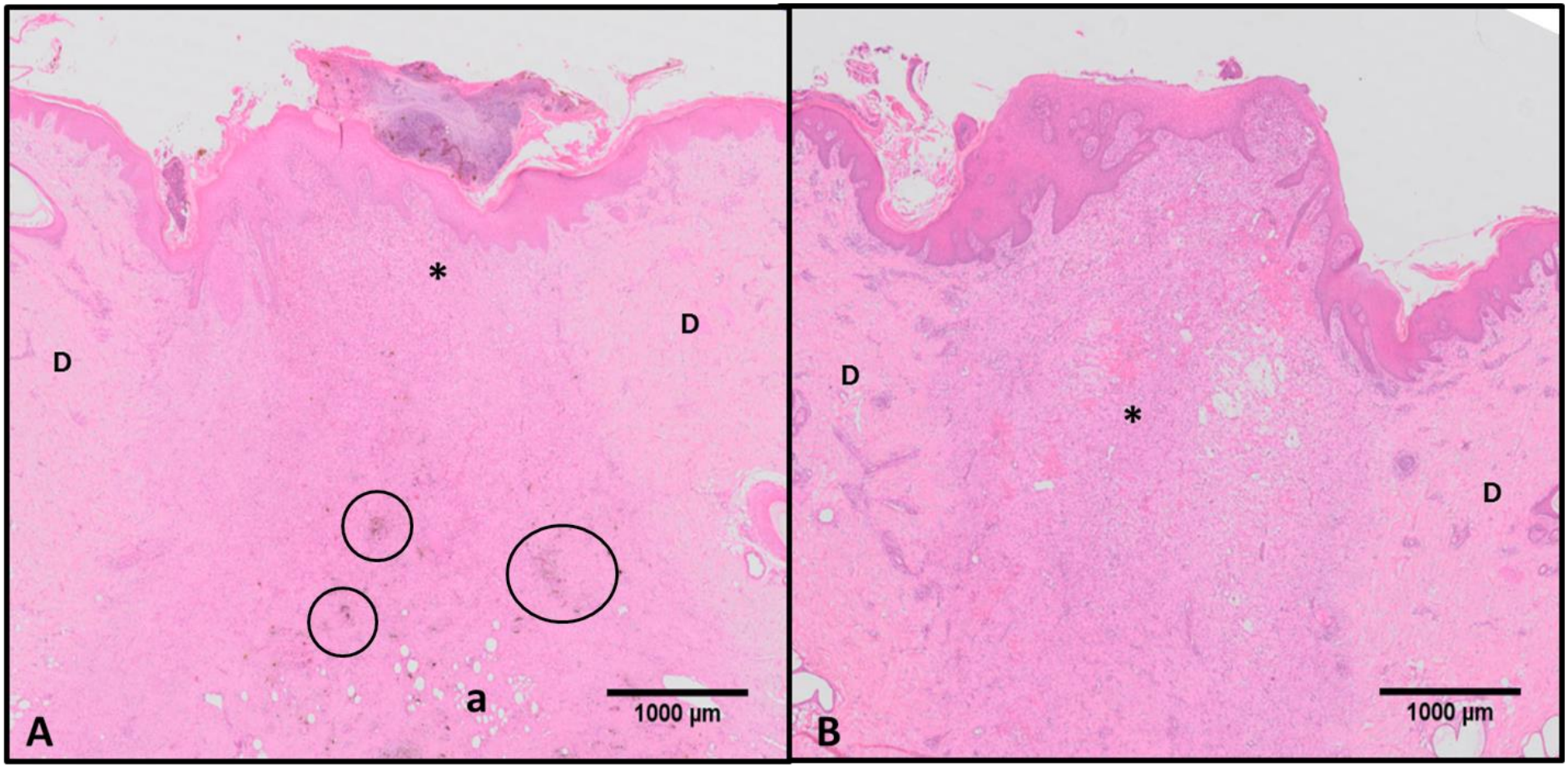

Figure 3.23 Representative photomicrographs of re-epithelialised experimental (A) and control (B) wounds on day 9 post-wounding. The circles indicate areas of inflammatory cell infiltrates associated with silver deposits in the experimental wound (A). a: adipocytes D: dermis HD: hypodermis. Note: images have been merged to create a composite image. (H&E)

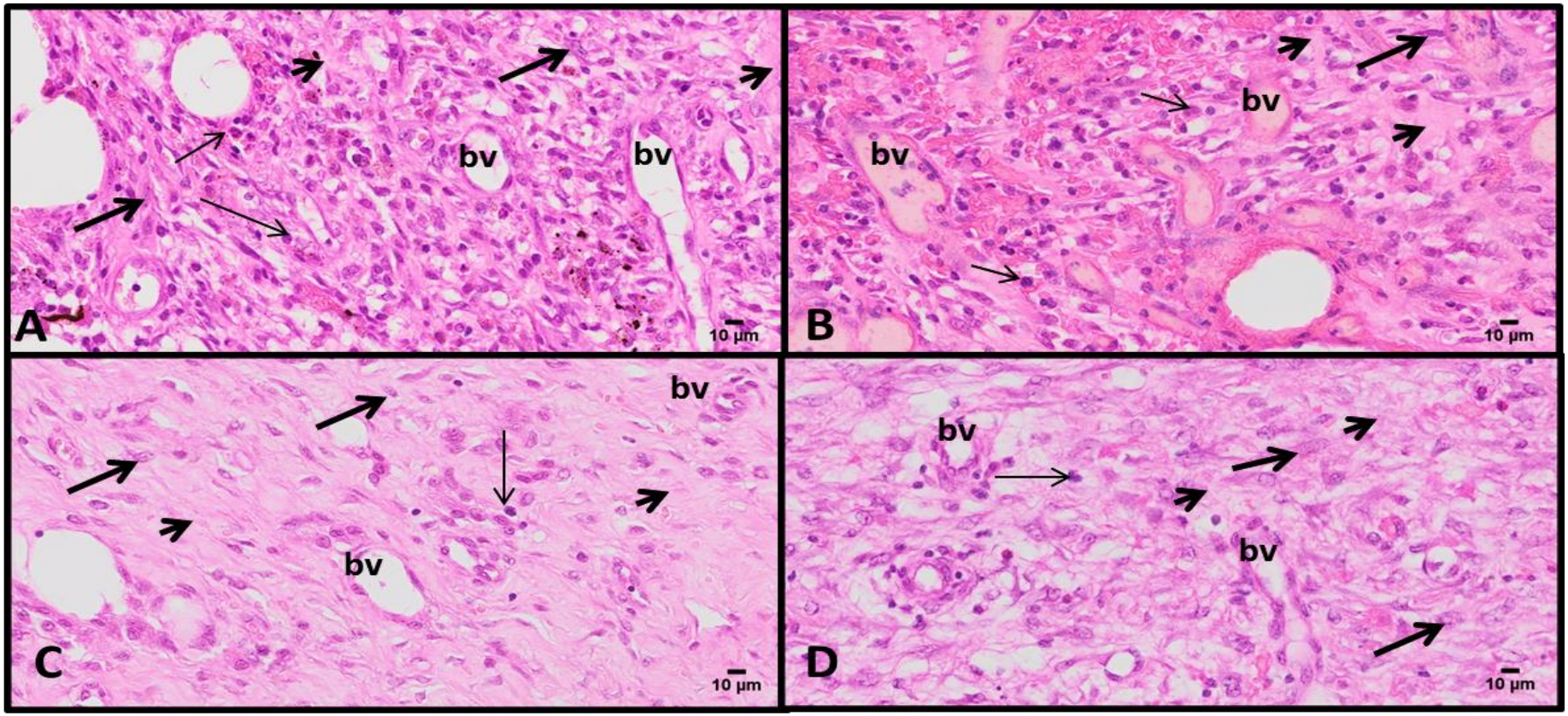

Figure 3.24 Representative photomicrographs of granulation tissue from experimental (A and C) and control (B and D) wounds on day 9 post-wounding. Photomicrographs A and B are from wounds which have not re-epithelialised and illustrate the greater inflammatory response compared to wounds which had re-epithelialised (C and D). Thin arrows indicate inflammatory cell nuclei. Blood vessels (bv) are seen in both wound types. Fibroblasts (thick arrows) and areas of collagen (short arrows) are also visible. (H&E, 20X magnification)

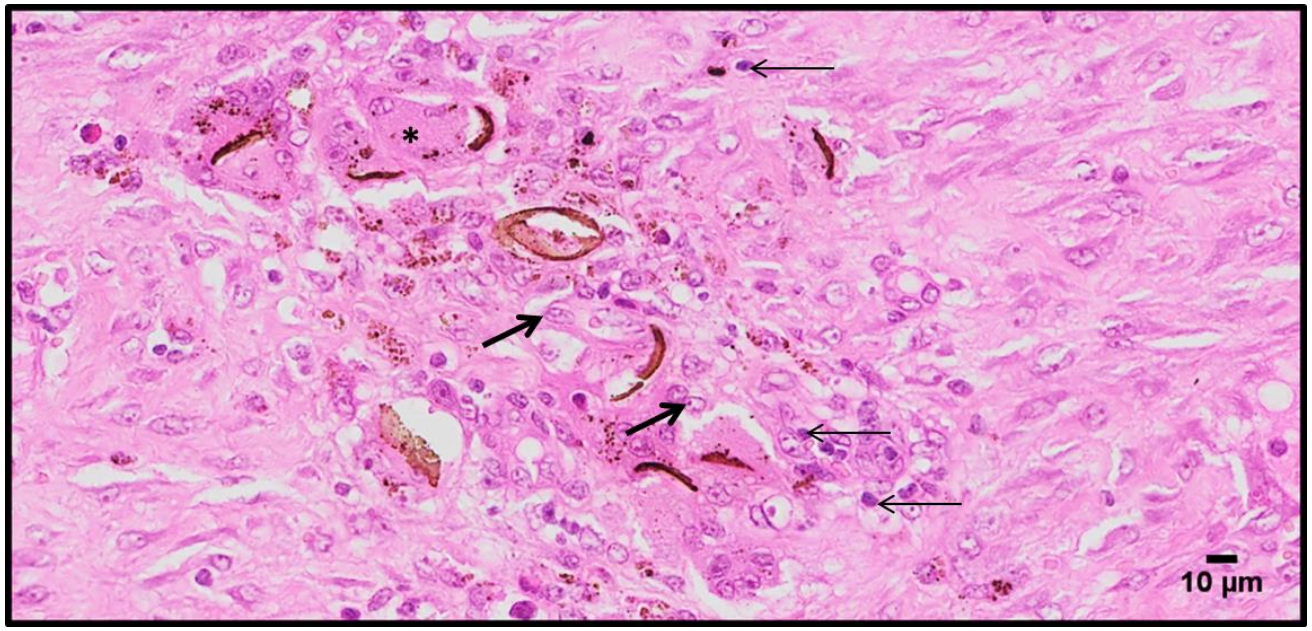

Figure 3.25 Representative photomicrograph of a granuloma in an experimental wound on day 9 post-wounding. * indicates a giant cell; thin arrows indicate inflammatory cell nuclei and thick arrows indicate epithelioid cells. (H&E, 20X magnification)

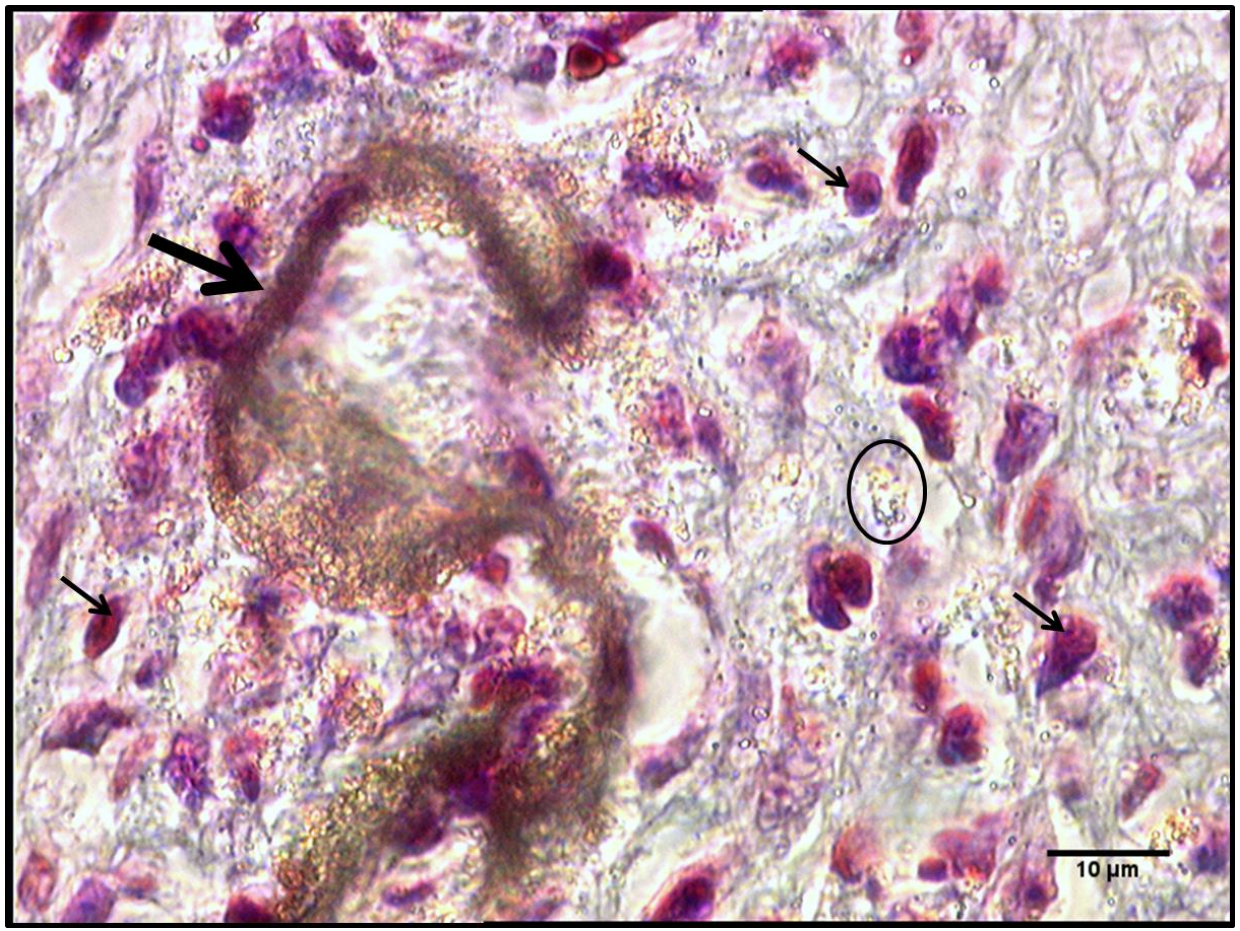

Figure 3.26 Representative photomicrograph of a granuloma in an experimental wound on day 9 post-wounding illustrating the absence of bacteria. Small arrows indicate examples of inflammatory cell nuclei. The large arrow indicates a piece of silver. An example of smaller pieces of silver is circled. (Gram stain, 63X magnification)

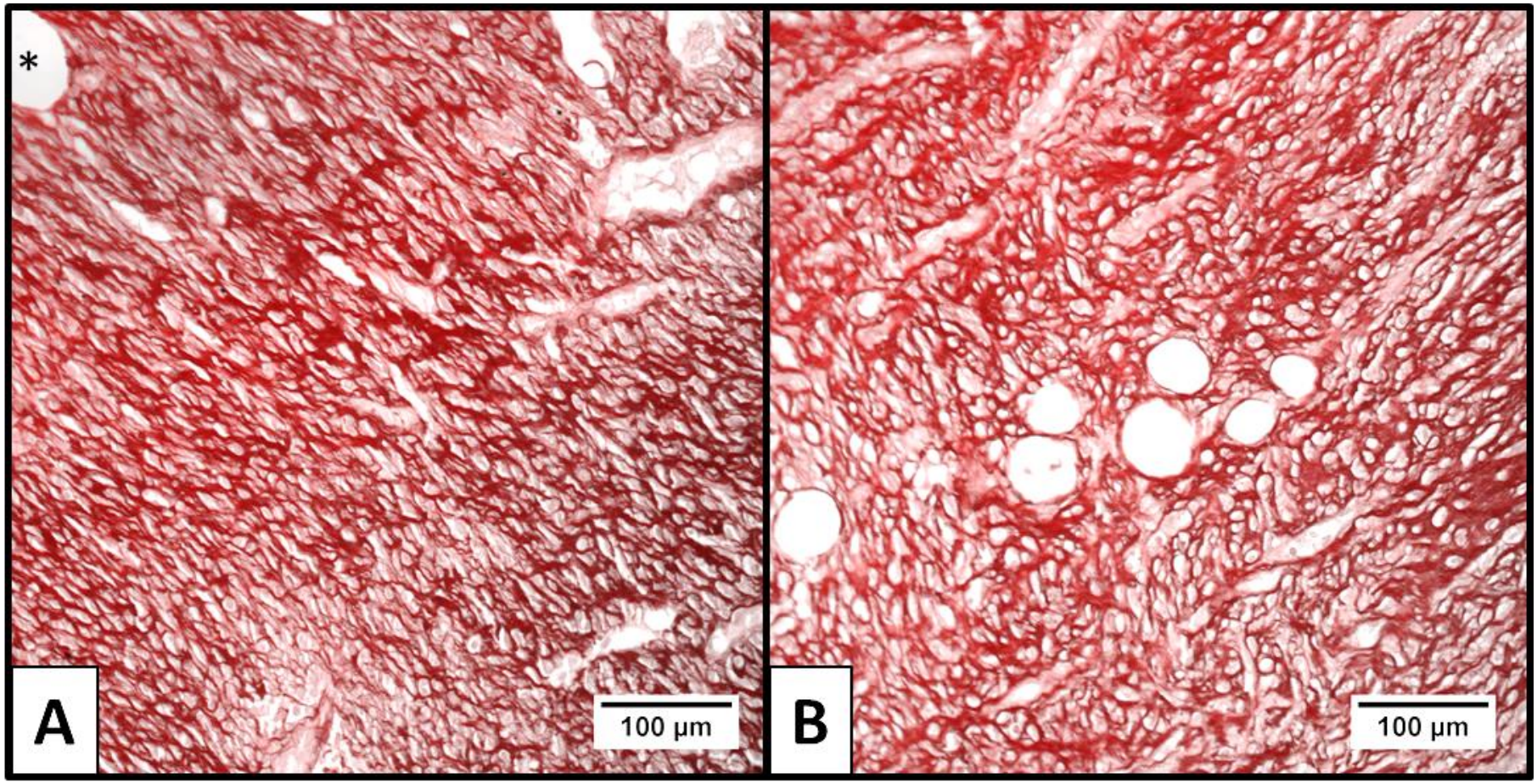

Figure 3.27 Representative photomicrographs of collagen within the wound area of experimental (A) and control (B) wounds on day 9 post-wounding illustrating medium sized collagen bundles. Note in the experimental wound (A) the collagen bundles are arranged in parallel whereas the collagen is less organised in the control wound (B). (Picrosirius red stain, confocal microscopy, 25X magnification).

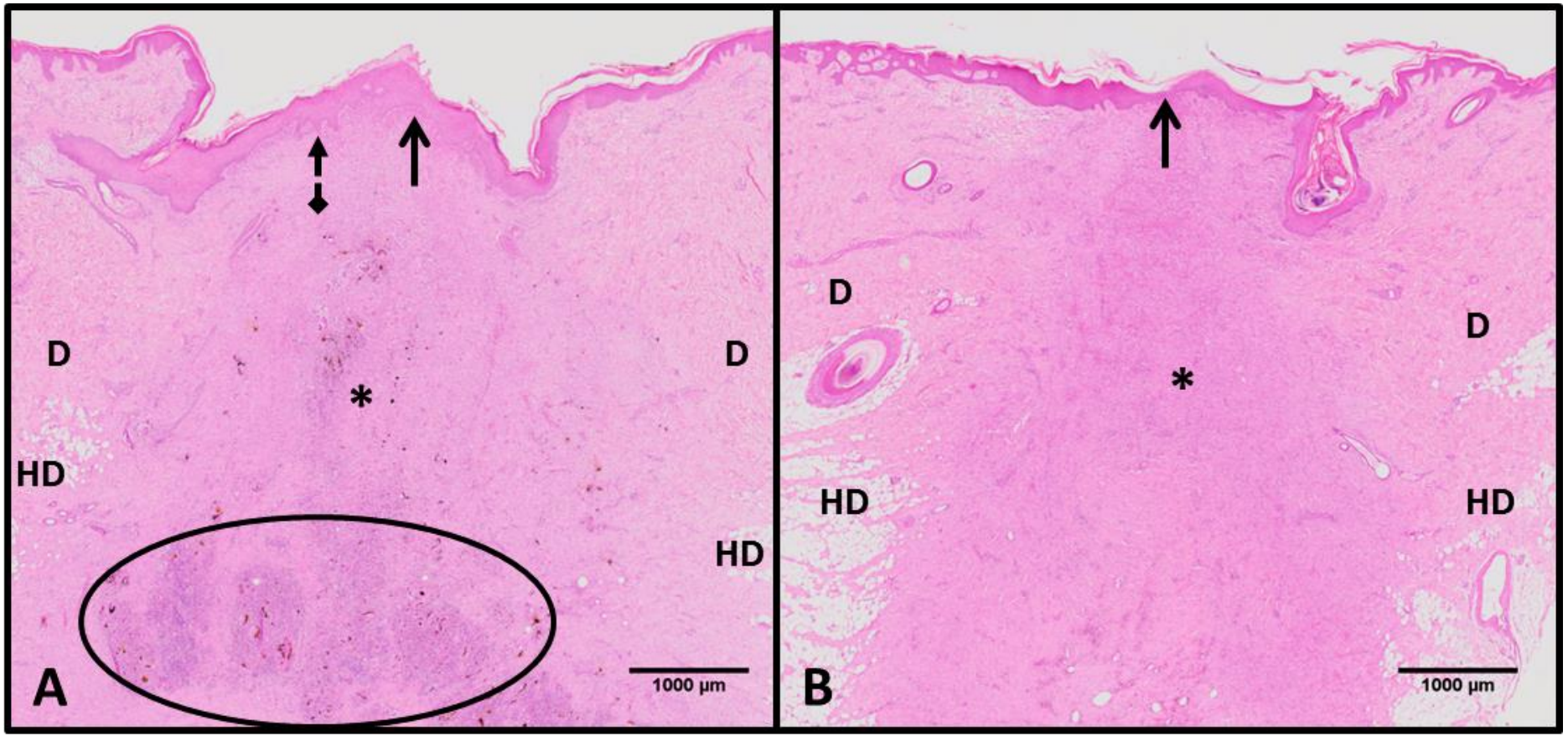

Figure 3.28 Representative photomicrographs of re-epithelialised experimental (A) and control (B) wounds on day 15 post-wounding. Note the thicker new epithelium (solid arrow) and larger rete ridges (dashed arrow) within the experimental wound (A). Within the granulation tissue (*) of the experimental wound (A), an inflammatory cell infiltrate associated with silver particles (circled) can be seen at the level of the lower dermis (D) and hypodermis (HD). Note: images have been merged to create a composite image. (H&E).

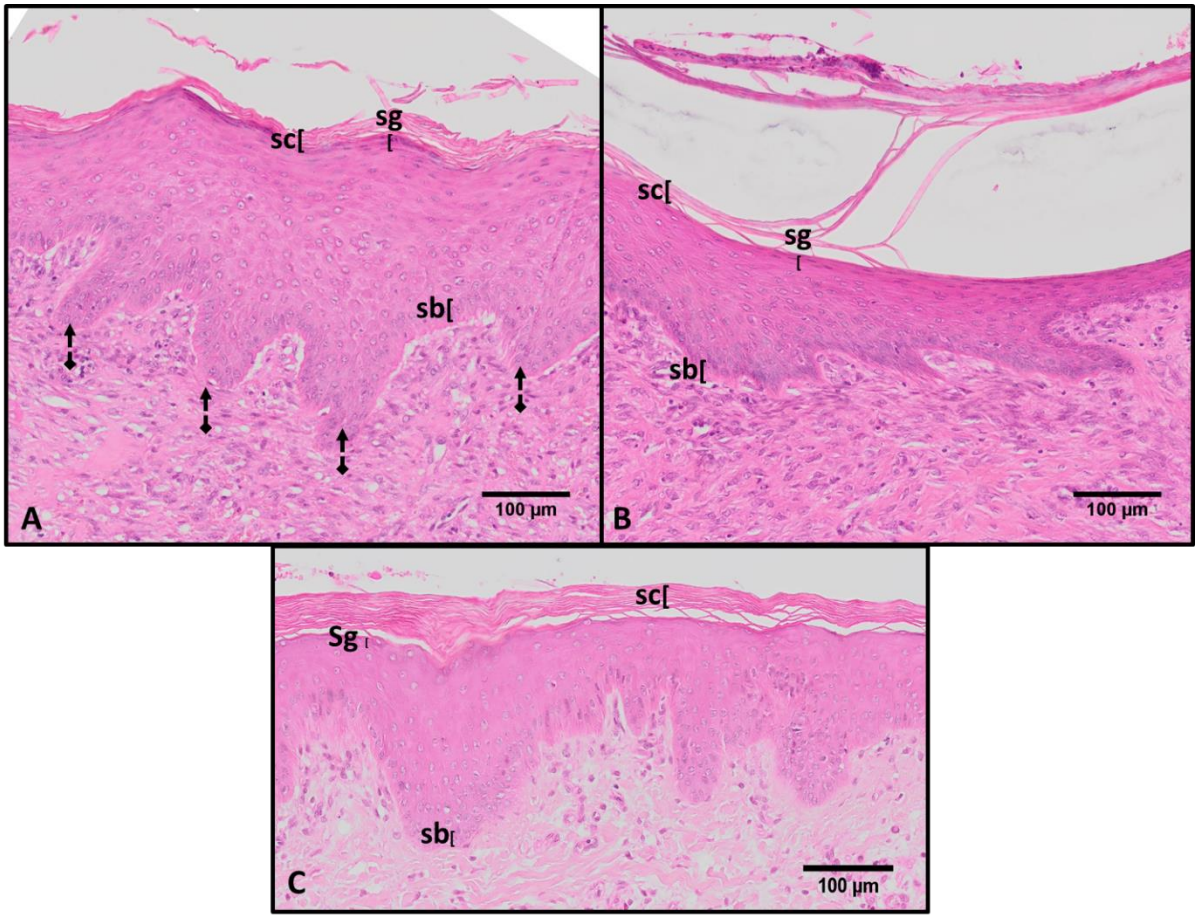

Figure 3.29 Representative photomicrographs of new epithelium at the centre of the wound in re-epithelialised experimental (A) and control (B) wounds on day 15 post-wounding. Image C is a representative photomicrograph of normal skin. Note the thicker epithelium with larger and more numerous rete ridges (dashed arrows) in the experimental wound. In addition, all layers of the epidermis, including the stratum corneum (sc), stratum granulosum (sg) and stratum basale (sb), can be seen in both experimental (A) and control wounds (B). (H&E, 20Xmagnification)

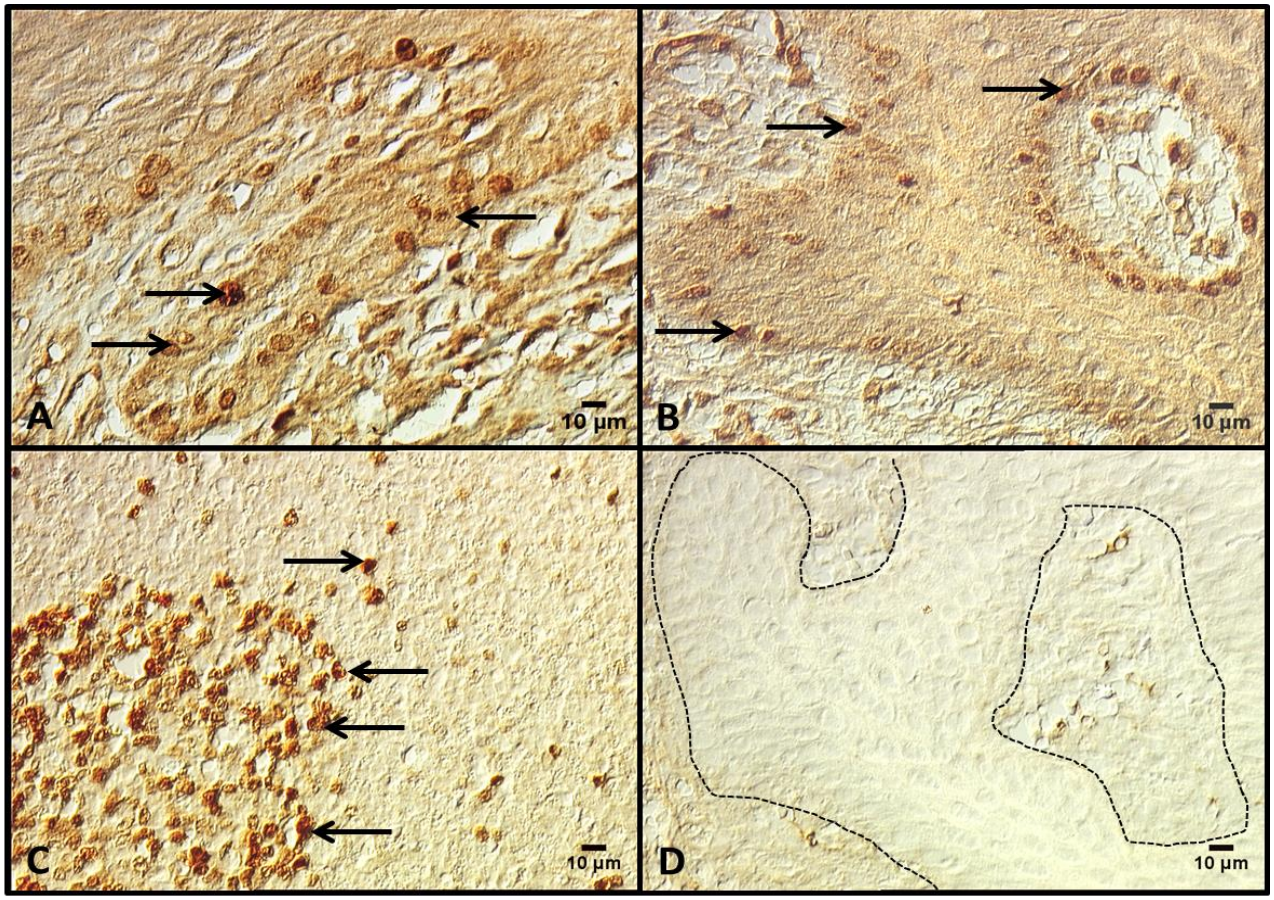

Figure 3.30 Representative photomicrographs of proliferating keratinocytes in the epithelium of experimental (A) and control (B) wounds on day 15 post-wounding. The positive control (C: human tonsil) and negative control (D: an adjacent section to B) are also shown. Arrows indicate examples of the nuclei of proliferating cells immunolabelled for Ki-67. The dotted line in D indicates the position of the epidermal-dermal junction. (Immunocytochemical labelling for Ki-67, DIC microscopy, 25X magnification)

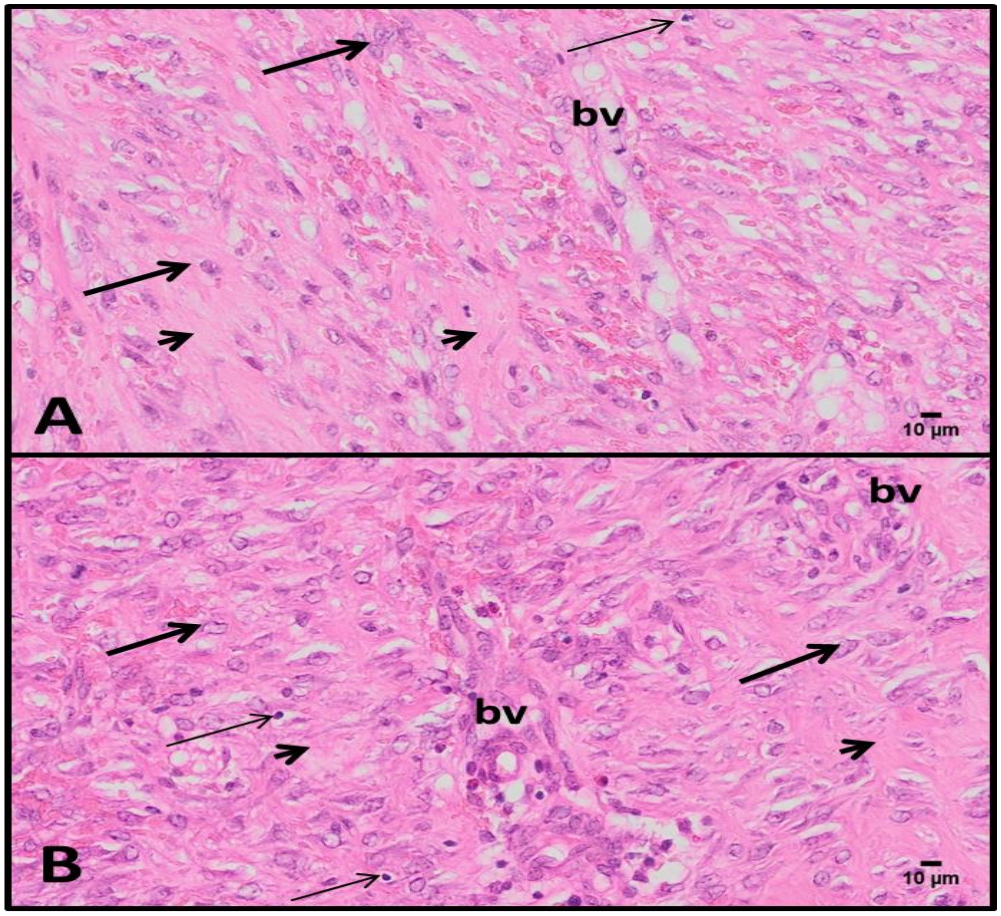

Figure 3.31 Representative photomicrographs of granulation tissue from experimental (A) and control (B) wounds on day 15 post-wounding. Blood vessels (bv) with two layers of tissue within the vessel wall are seen in both wound types, although blood vessels of all types are more numerous in control (B) wounds. Fibroblasts (thick arrows) and areas of collagen (short arrows) are also visible. (H&E, 20X magnification)

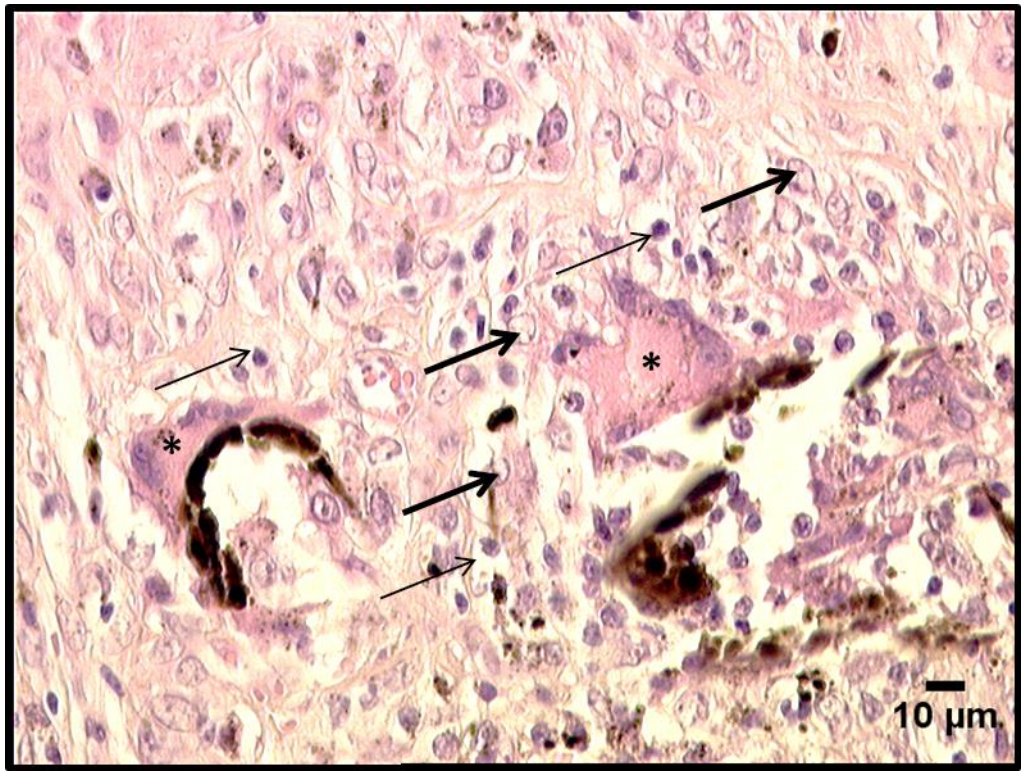

Figure 3.32 Representative photomicrograph of a granuloma in an experimental wound on day 15 post-wounding. * indicates a giant cell; thin arrows indicate inflammatory cell nuclei and thick arrows indicate epithelioid cells. (H&E, 25X magnification).

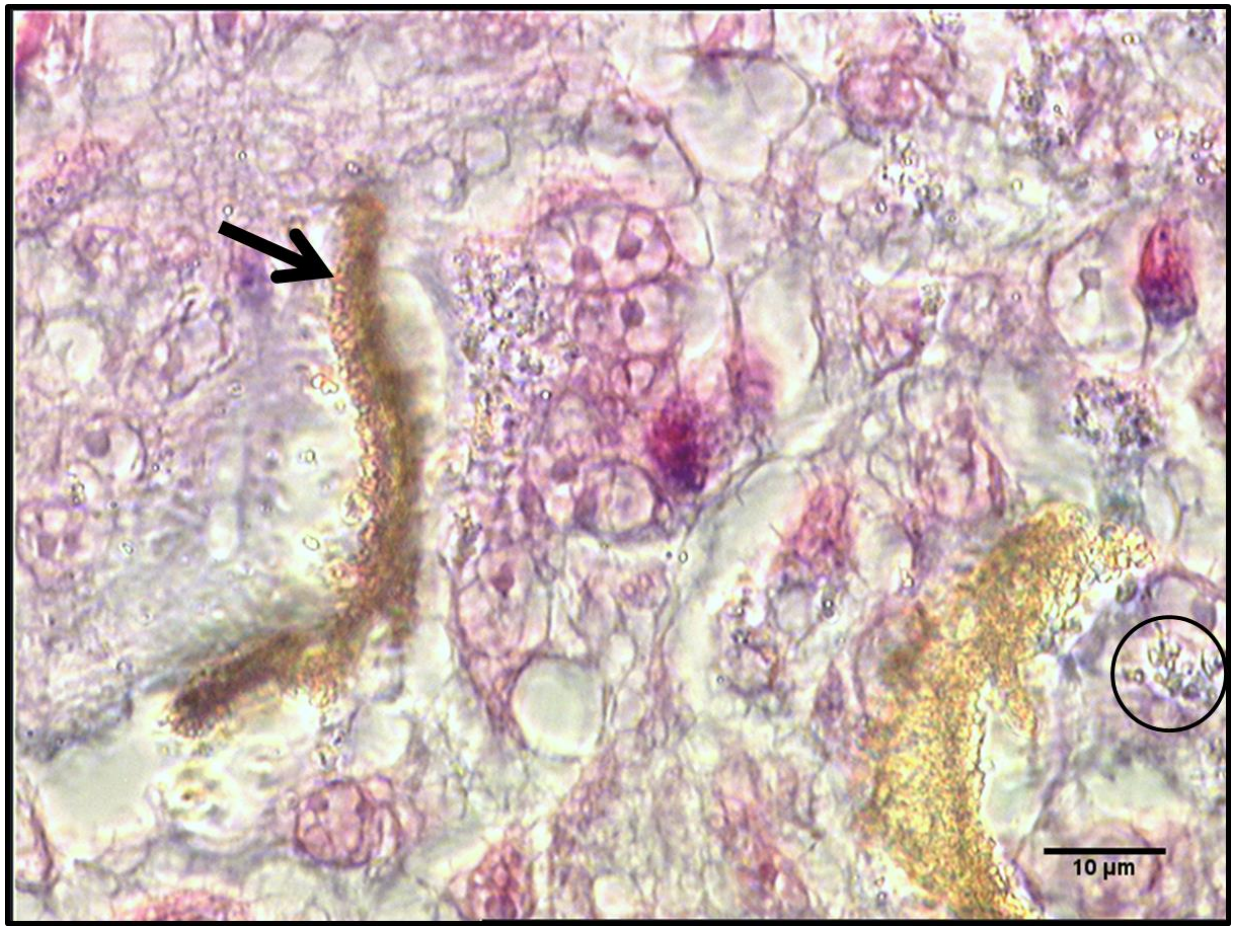

Figure 3.33 Representative photomicrograph of a granuloma in an experimental wound on day 15 post-wounding illustrating the absence of bacteria. The large arrow indicates a piece of silver. Examples of smaller pieces of silver are circled. (Gram stain, 63X magnification)

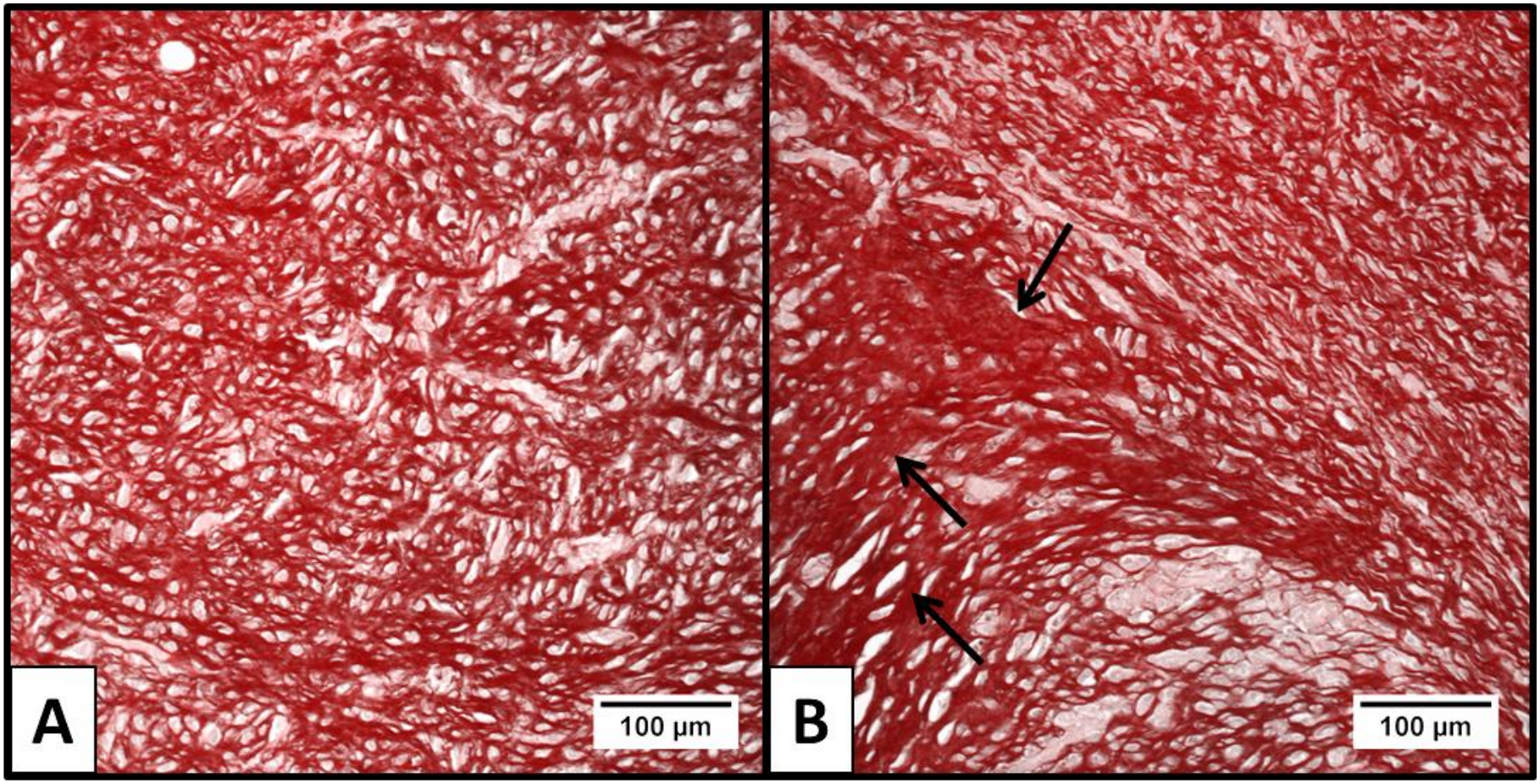

Figure 3.34 Representative photomicrographs of collagen within the wound area of experimental (A) and control (B) wounds on day 15 post-wounding illustrating larger collagen bundles in control wounds (arrows). (Picrosirius red stain, confocal microscopy, 25X magnification).

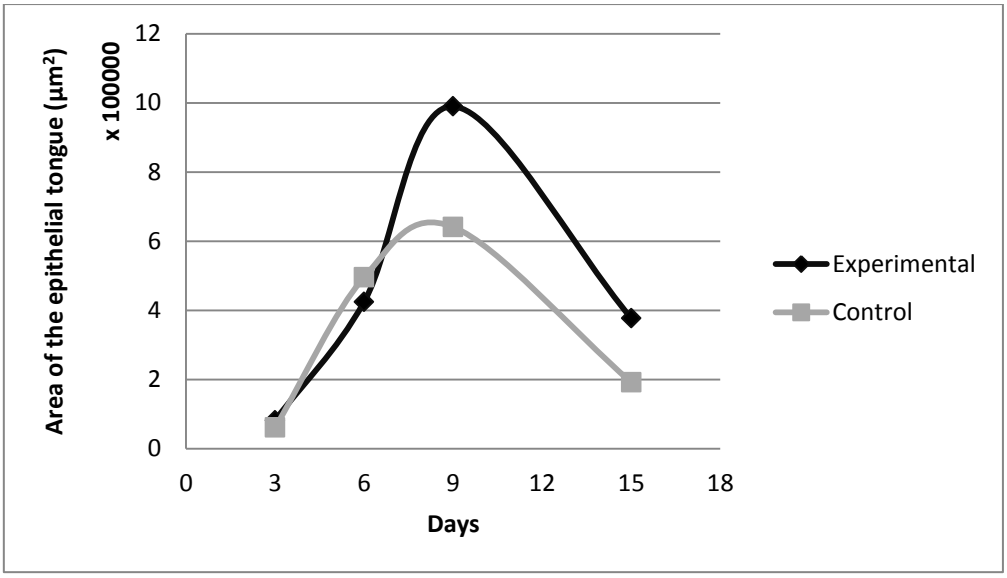

Figure 3.35 Graph of the median values of the area of the epithelial tongue for each day post-wounding. Note the greater increase in the area of the epithelial tongue in experimental wounds (seen in the slope of the graph) from day 6 to day 9 post-wounding.

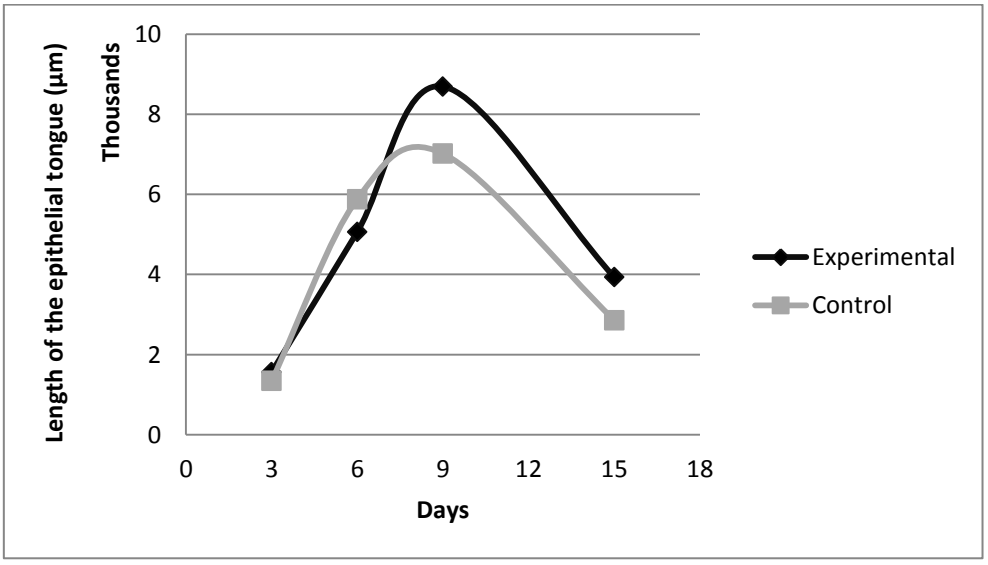

Figure 3.36 Graph of the median values of the length of the epithelial tongue for each day post-wounding. Note the greater increase in the length of the epithelial tongue in experimental wounds (seen in the slope of the graph) from day 6 to day 9 post-wounding.

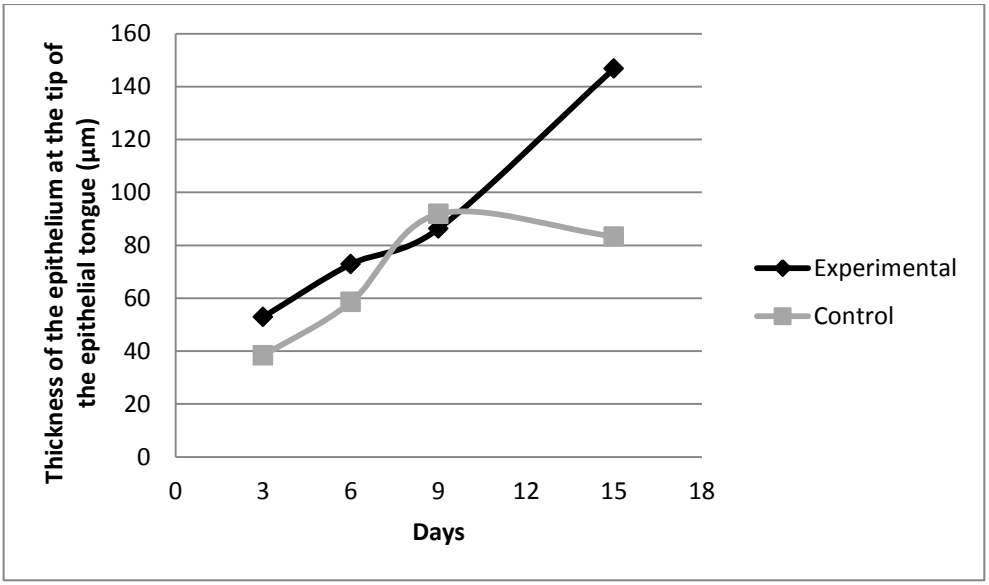

Figure 3.37 Graph of the median values of the thickness of the tip of the epithelial tongue for each day post-wounding. Note the greater increase in the thickness of the tip of the epithelial tongue in experimental wounds (seen in the slope of the graph) from day 9 to day 15 post-wounding.

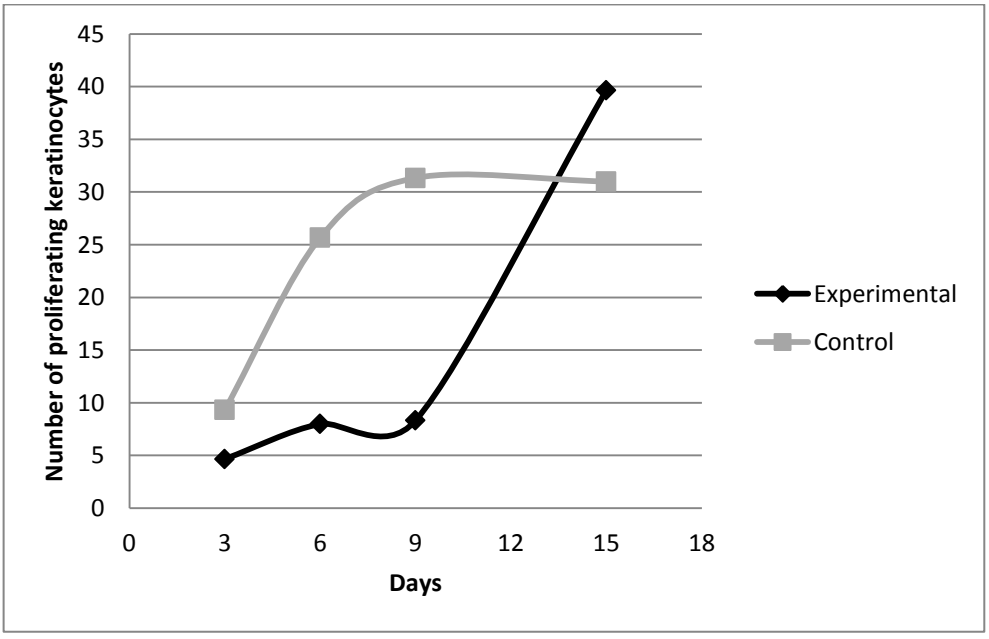

Figure 3.38 Graph of the median values for the number of proliferating keratinocytes for each day post-wounding. Note the greater increase in the number of proliferating keratinocytes in control wounds (seen in the slope of the graph) from day 3 to day 9 post-wounding.

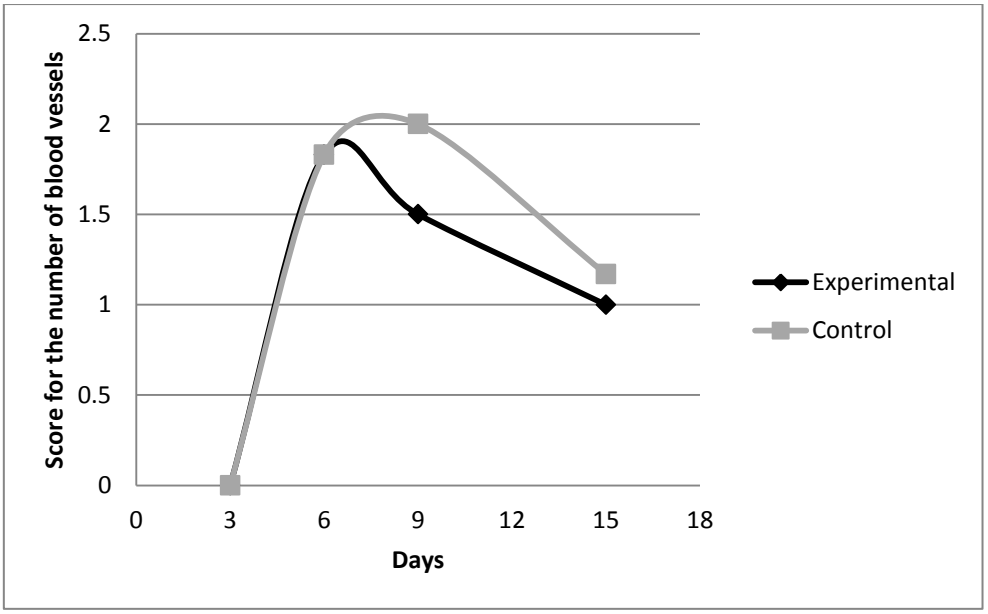

Figure 3.39 Graph of the median values for the score for the number of blood vessels for each day post-wounding.

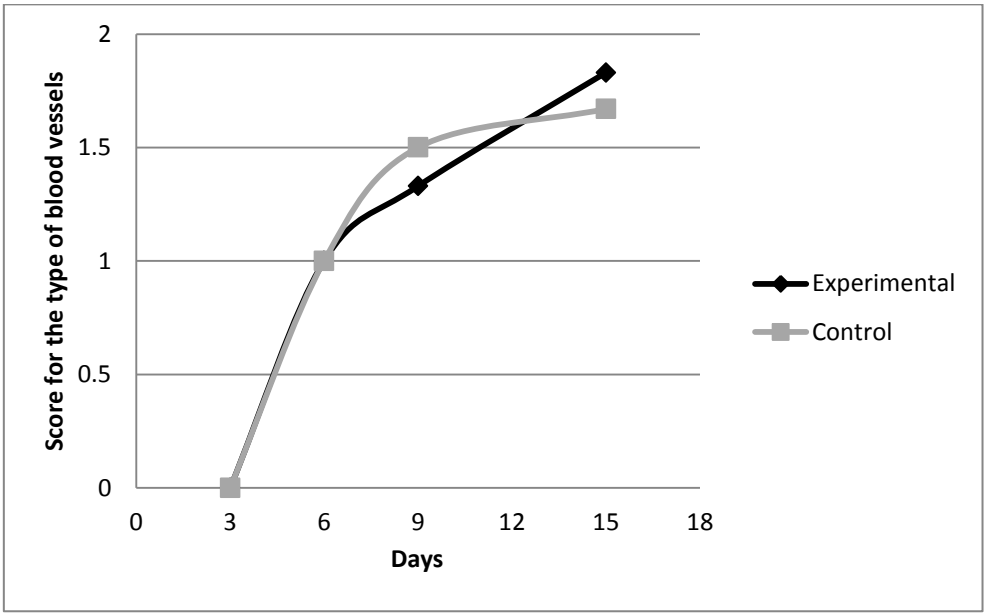

Figure 3.40 Graph of the median values for the score for the type of blood vessels for each day post-wounding.

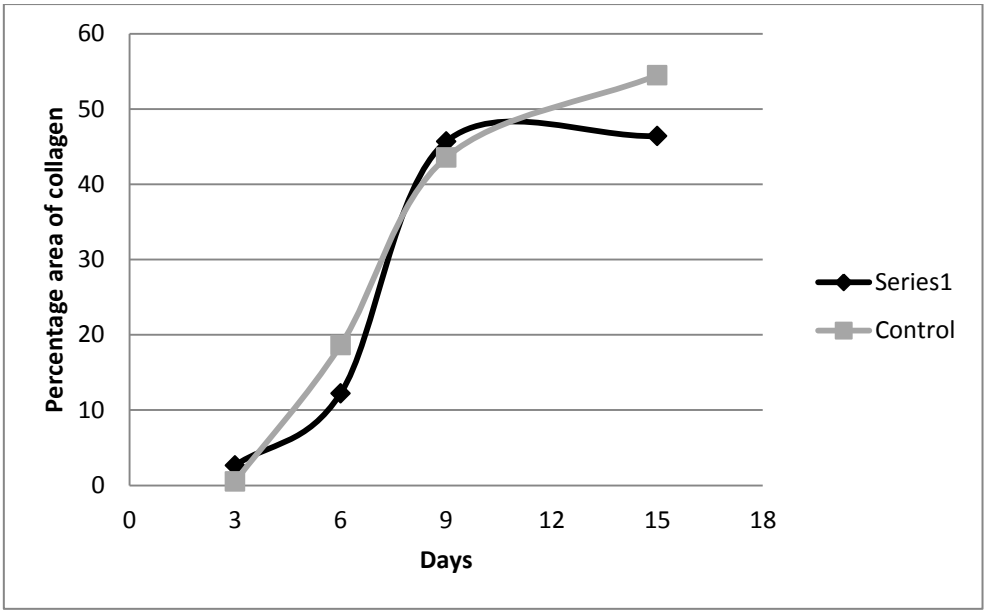

Figure 3.41 Graph of the median values of the percentage area of collagen for each day post-wounding. Note the decrease in experimental wounds from day 9 to day 15 post-wounding.

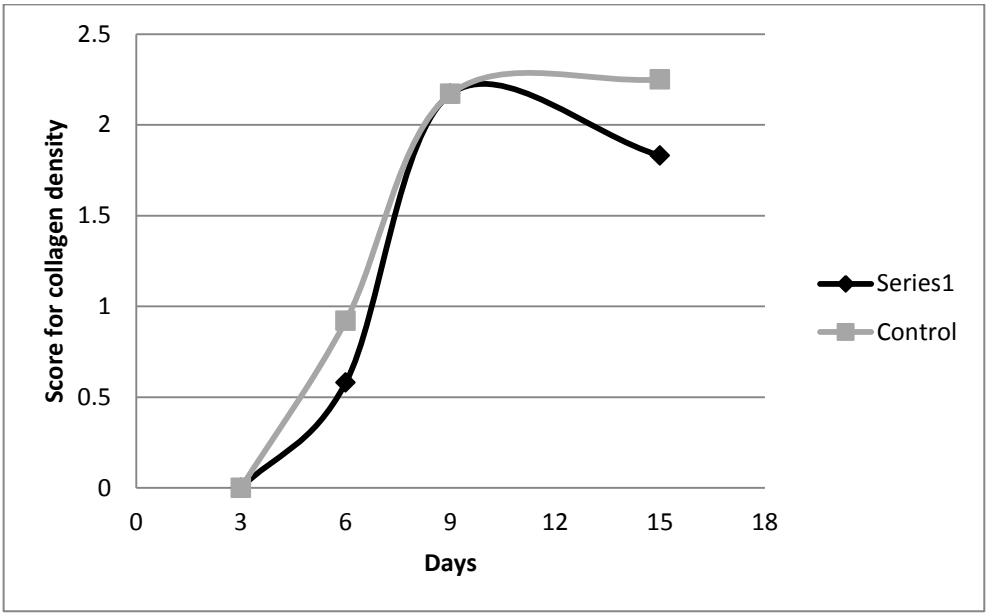

Figure 3.42 Graph of the median values of the score for the density of collagen for each day post-wounding. Note the decrease in experimental wounds from day 9 to day 15 post-wounding.

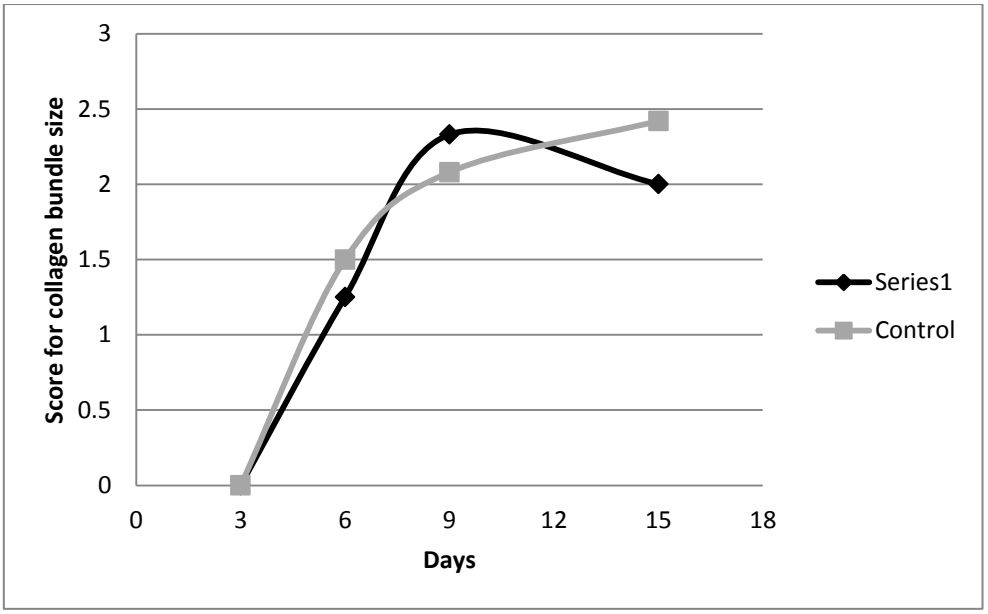

Figure 3.43 Graph of the median values of the score for the size of collagen bundles for each day post-wounding. Note the decrease in experimental wounds from day 9 to day 15 post-wounding.

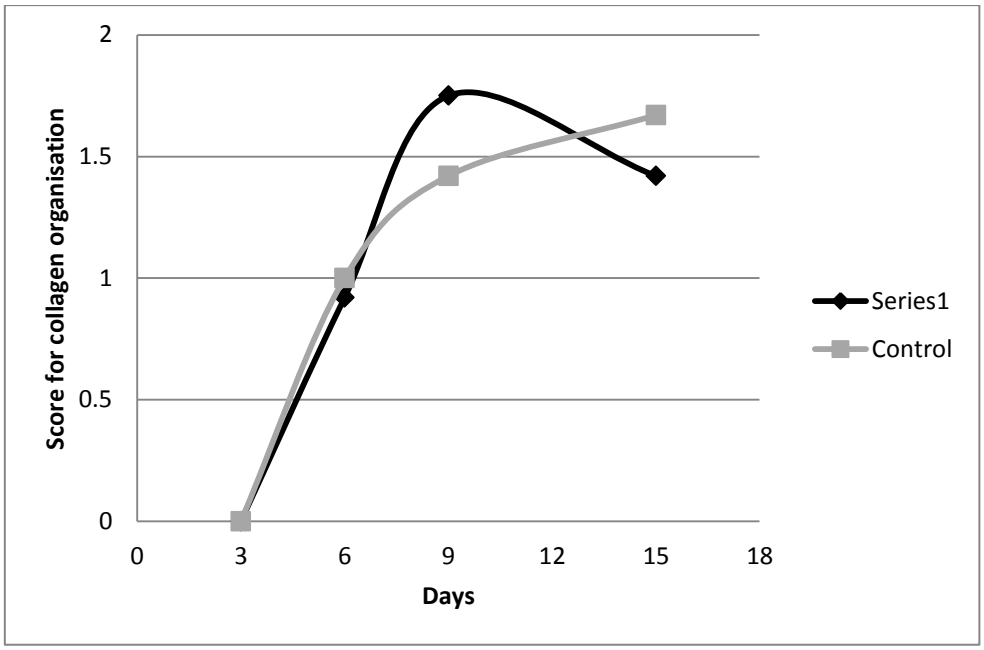

Figure 3.44 Graph of the median values of the score for the organisation of collagen bundles for each day post-wounding. Note the decrease in experimental wounds from day 9 to day 15 post-wounding.

4. DISCUSSION

No clinically relevant difference in the rate of wound closure was found in the present study between acute excisional wounds treated with nanocrystalline silver (Acticoat^{TM}) and those treated with polyurethane film dressings (Opsite^{TM}). However, the results suggest that nanocrystalline silver may improve epithelial restoration resulting in new epithelium which more closely resembles normal epidermis. In addition, nanocrystalline silver stimulates the formation of more mature blood vessels and modulates the deposition of the extracellular matrix, effects which have an impact on the functional and aesthetic properties of scars (Reinke and Sorg, 2012; DiPietro, 2013).

In the current study, there was no significant difference in the percentage change in wound area between experimental and control wounds from day 12 post-wounding. However, all four of the experimental wounds and two of the three control wounds in which complete re-epithelialisation was not observed on day 15 post-wounding, were covered by adherent scabs. The area of the scab could falsely decrease the value of the percentage change in area and the wounds could be re-epithelialised beneath the scabs. Indeed, histological assessment on day 15 post-wounding revealed that re-epithelialisation was complete in all of the regions sampled from the experimental wounds. In comparison, a single control wound had one region which was not completely re-epithelialised on day 15 post-wounding. As no significant differences were found in the macroscopic and histological assessments of wound closure on day 15 post-wounding or on observation, there was no clinically relevant difference in the rate of wound closure between acute excisional wounds treated with nanocrystalline silver and those treated with polyurethane film dressings.

This contrasts with previous studies investigating the effect of silver nanoparticles on healing in acute, uncontaminated full-thickness wounds, which mostly report increased rates of healing (Burd *et al*., 2007; Liu *et al*., 2010; Arican *et al*., 2012; Prestes *et al*., 2012). The investigated dressings included Acticoat™ which was applied every three (Burd *et al*., 2007) or seven days (Arican *et al*., 2012; Prestes *et al*., 2012) as well as a dressing containing 0.04mg/cm2 of silver nanoparticles that was applied daily (Liu *et al*., 2010). Therefore, differences in the silver concentration or the time for which the dressings were applied are unlikely to account for the different results. However, in contrast to the current study, these previous studies were all undertaken in rodent models (Burd *et al*., 2007; Liu *et al*., 2010; Arican *et al*., 2012; Prestes *et al*., 2012). Wound contraction plays a greater role in healing in rodents than in pigs (Sullivan *et al*., 2001). As silver nanoparticles increase the differentiation of myofibroblasts (Liu *et al*., 2010) they may affect the rate of wound contraction. Thus, variations in healing between rodents and pigs may account for the observed differences in the rate of healing.

In the current study, a significantly greater inflammatory response was found on day 3 post-wounding in experimental wounds as compared to control wounds. As no bacteria were visible in the experimental or control wounds, infection was unlikely in either type of wound (Edwards and Harding, 2004). This suggests that the silver nanoparticles or silver ions released from Acitcoat™ were responsible for the increased inflammatory response in experimental wounds. This finding of the present study contrasts strongly with the literature which reports anti-inflammatory effects of silver nanoparticles in pig and mouse models of contact dermatitis (Bhol and Schechter, 2005; Nadworny *et al*., 2008; Nadworny *et al*., 2010), in a mouse burn wound model (Tian *et al*., 2007) and in contaminated full-thickness wounds in pigs (Wright *et al*., 2002). Acticoat™ (Wright *et al*., 2002; Nadworny *et al*., 2008)

as well as other silver nanoparticle formulations (creams and solutions) and concentrations (Bhol and Schechter, 2005; Tian *et al*., 2007; Nadworny *et al*., 2010) were investigated in these studies. Therefore, the decreased inflammatory response, reported in the latter studies as compared to the present study, are unlikely to be due to differences in the delivery vehicle or silver nanoparticle concentration alone. However, in the latter studies the dressings were changed daily. This contrasts with the current study, in which the dressings were changed every three days, and may account for the different inflammatory response seen.

In addition, differences in healing between wound models (Davidson, 1998) as well as differences in inflammatory cell activation may explain the disparate inflammatory response noted in the current analysis. In acute wounds, macrophage activation is not dependent on T-cell interaction (Gordon, 2002). On the contrary, in contact dermatitis T_H1 and CD_8^+ T cells are vital for the initiation of the inflammatory response and stimulation of macrophages (Kimber and Dearman, 2002). *In vitro* studies have shown that macrophages in different states of activation respond differently to silver nanoparticles. Human macrophages cultured with silver nanoparticles showed decreased cell viability at concentrations of 10ppm when stimulated with phytohaemagglutinin (PHA) compared to 15ppm when not stimulated by PHA (Shin *et al*., 2007). In addition, the secretion of IL6 by mouse macrophages in response to toll-like receptor ligands differs if cells are pre-treated with or simply cultured with tiopronin-protected silver nanoparticles (Castillo *et al*., 2008).

However, *in vivo* studies on silver nanoparticle-treated acute, uncontaminated, full-thickness excisional wounds in rodent models, either do not comment on the level of inflammation in the wound (Burd *et al*., 2007; Liu *et al*., 2010) or do not investigate the early phase of healing (Arican *et al*., 2012; Prestes *et al*., 2012). Similar to the results of the present study, no

difference was found in the inflammatory response of Acticoat™-treated uncontaminated full-thickness wounds compared to control wounds (distilled water) from day 7 to day 21 post-wounding in a rat model (Prestes *et al*., 2012). In contrast, Arican *et al* (2012) described sterile abscesses in Acticoat™-treated uncontaminated full-thickness wounds in a rabbit model on day 7 and 14 post-wounding. When considered with the results of Arican *et al* (2012), the results of the current study suggest that Acticoat™ may induce inflammation in acute wounds. In addition, Arican *et al* (2012) and Prestes *et al* (2012) describe the presence of giant cells in the Acticoat™-treated wounds on day 14 and 21 post-wounding. This is similar to the giant cells associated with silver deposits on day 9 and 15 post-wounding observed in the current study. Silver deposits have been described previously at the level of the lower dermis in skin wounds treated with silver (Fredriksson *et al*., 2009; Wang *et al*., 2009). However, the only additional report of granulomatous lesions was in the lungs of rats exposed to silver nanoparticles (18-19nm) via inhalation for 13 weeks (Sung *et al*., 2009). Thus, the findings of this study along with those of Arican *et al* (2012) and Prestes *et al* (2012) suggest that prolonged exposure to silver can induce a foreign body chronic inflammatory reaction, an important consideration as chronic inflammation stimulates scarring (Reinke and Sorg, 2012).

The increased inflammatory response on day 3 post-wounding may also account for the significantly greater increase in the percentage change in wound area in experimental wounds as compared to control wounds on the same day. Increased vascular permeability, due to the inflammatory response, causes oedema (DiPietro, 2013). This swelling results in wound expansion (McGrath and Kersey, 2009) causing an apparent increase in the wound area unrelated to wound closure. Similarly, residual oedema from the increased inflammatory

response in experimental wounds on day 3 post-wounding may be a contributing factor to the slower decrease in the wound area of experimental wounds on day 6 and 9 post-wounding.

Differences in ECM remodelling and wound contraction are an additional consideration. Fibrin clot stimulates fibroblast migration and proliferation (Greaves *et al*., 2013). Therefore, the greater amount of fibrin clot in control wounds on day 3 post-wounding may initiate earlier remodelling of the ECM, decreasing the wound area. Furthermore, no significant differences were found in the measures of epithelial restoration between experimental and control wounds on day 3, 6 or 9 post-wounding. This suggests that the differences in the percentage change in wound area were not due to differences in re-epithelialisation, but rather the inflammatory response or differences in wound contraction.

However, the current study does show that Acticoat^{TM} influenced re-epithelialisation by affecting the proliferation of keratinocytes. The decreased number of proliferating keratinocytes in experimental wounds on day 3, 6 and 9 post-wounding could be due to silver nanoparticle-induced cell cycle arrest, similar to *in vitro* findings (Zanette *et al*., 2011). A cell arrested in the G2/M or S phase of the cell cycle would be positively labelled for Ki-67 (Gerdes *et al*., 1984). Thus, the presence of single positively labelled cells in the epithelium of experimental wounds on day 3, 6 and 9 post-wounding is consistent with keratinocytes that have entered but not completed the cell cycle. Moreover, the clusters of positively labelled cells noted in the epithelium of control wounds on the same days post-wounding would be consistent with cells that have recently completed cell division.

Of note, a considerable increase in the number of proliferating keratinocytes was observed from day 9 to day 15 post-wounding in experimental wounds. This increase was accompanied

by a change in the arrangement of positively-labelled cells in the epithelium of experimental wounds from single cells to clusters indicative of cells completing cell division. The different proliferation response of keratinocytes to silver nanoparticles on day 3 and day 15 post-wounding may be due to a decrease in the concentration of silver nanoparticles as healing progresses. In larger wounds, such as those on day 3 post-wounding, cells are exposed to a greater amount of silver (Lansdown and Williams, 2004; Larese *et al*., 2009). As the wound area decreases, as occurs from day 9 to day 15 post-wounding in the current study, cells in the healed regions of the wound are exposed to less silver, which must diffuse through intact epithelium to reach the cells (Larese *et al*., 2009). The effects of silver nanoparticles on keratinocytes and fibroblasts are concentration dependent (AshaRani *et al*., 2009; Greulich *et al*., 2009; Samberg *et al*., 2010; Hackenberg *et al*., 2011; Zanette *et al*., 2011). As fibroblasts affect keratinocyte proliferation and migration (Werner *et al*., 2007), lower concentrations of silver nanoparticles would not only directly decrease the inhibition of keratinocyte proliferation but also have indirect effects through fibroblast-keratinocyte interactions. Liu *et al* (2010) also reported increased immunolabelling for proliferating cell nuclear antigen in keratinocytes of silver nanoparticle-treated excisional wounds compared to untreated control wounds in mice on day 15 post-wounding. Unfortunately, results before day 15 post-wounding were not clearly reported. Therefore the effect of silver nanoparticles on keratinocyte proliferation in earlier wounds cannot be compared.

However, despite the decreased keratinocyte proliferation noted in experimental wounds in the present study, no significant differences were observed in the measures of epithelial restoration between experimental and control wounds on the same days. This suggests that silver nanoparticles did not substantively affect keratinocyte migration. Indeed, the only significant difference in the epithelium was in the thicker epithelium in the center of

experimental wounds, which more closely resembled normal epithelium, on day 15 post-wounding. The similarity of normal epidermis and new epithelium in wounds treated with silver nanoparticle containing dressings is noted in a number of studies investigating different types of wounds (Wright *et al*., 2002; Bhol and Schechter, 2004; Tian *et al*., 2007; Liu *et al*., 2010). Unfortunately, Burd *et al* (2007), who reported decreased rates of re-epithelialisation in Acticoat^{TM}-treated acute, full thickness wounds in pigs, did not comment on the character of the epithelium. However, Liu *et al* (2010) and the current study both suggest that silver nanoparticles have a beneficial effect on healing of the epidermis in acute full thickness wounds.

The mechanisms by which silver nanoparticles affect re-epithelialisation *in vivo* are not well described. To the author's knowledge, no reports describe the effect of silver nanoparticles on keratinocyte migration *in vivo* or *in vitro*. Furthermore, only the current study and Liu *et al* (2010) report the effects of silver nanoparticles on keratinocyte proliferation *in vivo,* in any wound model. Increased expression of keratinocyte growth factor and epidermal growth factor and decreased expression of interleukin-1, TNF-α and transforming growth factor (TGF)-β, which affect keratinocyte proliferation and/ or migration (Sivamani *et al*., 2007; Werner *et al*., 2007), were associated with increased re-epithelialisation of silver nanoparticle-treated wounds in a porcine model of contact dermatitis (Nadworny *et al*., 2010). However, the effect of silver nanoparticles on other cytokines and growth factors important in regulating re-epithelialisation is unknown. Furthermore, the mechanisms by which silver nanoparticles affect re-epithelialisation in acute wounds, such as those investigated in this study, have not yet been reported. In addition to the effect of silver nanoparticles on fibroblast- keratinocyte and keratinocyte- immune interactions, the effect of silver nanoparticles on melanocytes and keratinocyte-melanocyte interactions may be of

interest. Melanocytes are resident in the epidermis and are important in normal keratinocyte homeostasis (Nordlund, 2007; MacLeod and Havran, 2011). The scope of this study did not include the identification of melanocytes using co-localisation of melanocyte specific antibodies with the Ki-67 antibody. Therefore, it is not known if the decrease in proliferating cells in the epidermis seen in experimental wounds included a decrease in the proliferation of melanocytes in addition to the decrease in the proliferation of keratinocytes. It would be worthwhile to investigate in future studies if keratinocyte-melanocyte interactions are in part responsible for the beneficial effects of silver nanoparticles on epithelial restoration.

Silver nanoparticles may also have a beneficial effect on angiogenesis. While fewer blood vessels were noted in experimental wounds on day 15 post-wounding in the current study, a greater number of these blood vessels were more mature. Wright *et al* (2002) and Prestes *et al* (2012) also noted increased angiogenesis in Acticoat^{TM}-treated wounds. Similarly, Kang *et al* (2011) observed functional blood vessels in silver nanoparticle-impregnated matrigel plug assays in mice. These observations suggest that the effects of silver nanoparticles on angiogenesis in *vivo* are not limited to decreasing endothelial cell viability. However, the mechanisms by which silver nanoparticles affect angiogenesis are also unknown. Complex interactions of different VEGF isoforms, angiopoeitins, platelet derived growth factor, TGF-β and other angiogenic factors occur during angiogenesis (Carmeliet and Jain, 2011). Thus, it is difficult to predict the effect of increased VEGF expression (Tian *et al*., 2007) and decreased TGF-B expression (Tian *et al*., 2007; Nadworny *et al*., 2010) caused by silver nanoparticles. However, as vessel maturation may affect scar formation (DiPietro, 2013), the observation that silver nanoparticles improve vessel maturation warrants further investigation.

In the present study, the effect of silver nanoparticles on scarring could not be assessed as too few wounds were re-epithelialised by day 15 post-wounding. In addition, attempts to quantify collagen deposition using the dye binding method described by Lopez-De Leon and Rojkind (1985) were unsuccessful. The large standard deviations observed in the concentrations of total protein and hydroxyproline suggest that the difficulty lies in the homogenization of the normal pig skin for these assays. However, significant differences were noted between experimental and control wounds in the scores for collagen organisation and bundle size. In addition, the values of all of the parameters assessing collagen decreased in experimental wounds from day 9 to 15 post-wounding. This suggests that silver nanoparticles affect collagen deposition in acute wounds *in vivo*.

The hypothesis that silver nanoparticles influence collagen deposition in acute wounds is supported by Kwan *et al* (2011). Murine full-thickness excisional wounds treated with silver nanoparticles (5-15nm, 0.04mg/cm^2) contained more collagen which was better organized and aligned than in control wounds (Kwan *et al*., 2011). Furthermore, the tensile strength and mechanical properties of silver nanoparticle-treated wounds were significantly better than control wounds and not different from normal skin (Kwan *et al*., 2011). Similarly, increased collagen deposition was noted in mouse incisional wounds treated with chondroitin- and acharan-sulfate silver nanoparticles compared to Vaseline treated controls (Im *et al*., 2013). However, fibrosis was similar in Acticoat^{TM}-treated wounds and wounds treated with distilled water in a rat model of excisional wounds (Prestes *et al*., 2012).

In vitro studies (Arora *et al*., 2008; Hsin *et al*., 2008; AshaRani *et al*., 2009; Wei *et al*., 2010; Park *et al*., 2011; Rigo *et al*., 2013) and an *in vivo* investigation of full-thickness wounds in a mouse model (Liu *et al*., 2010) demonstrate that silver nanoparticles are toxic to fibroblasts.

Thus, decreased fibroblast viability is one mechanism through which silver nanoparticles may affect collagen deposition. In the present study, Ki-67 immunolabelled sections were not suitable to evaluate the proliferation of fibroblasts due to the extent of disruption of the dermis by the antigen retrieval process. Therefore, it is unknown if differences in fibroblast proliferation are responsible for the differences in collagen deposition between experimental and control wounds.

Silver nanoparticles may also influence ECM remodelling by increasing the number of myofibroblasts (Liu *et al*., 2010; Kwan *et al*., 2011) or by affecting the function of matrix metalloproteinases (Wright *et al*., 2002; Nadworny *et al*., 2008; Nadworny *et al*., 2010). However, studies which report decreased MMP function in silver nanoparticle-treated wounds do not comment on the formation of collagen, granulation tissue or scars (Wright *et al*., 2002; Nadworny *et al*., 2008; Nadworny *et al*., 2010). While Tian *et al* (2007) noted improved scarring in mouse burn wounds, clinical studies which describe the quality of scars note increased scarring in silver nanoparticle-treated wounds (Innes *et al*., 2001; Argirova *et al*., 2007).

The findings of this study suggest that Acticoat^{TM} has beneficial effects on epithelial restoration, angiogenesis and collagen deposition in acute excisional wounds. These processes are important in accelerating healing and minimising scar formation (Reinke and Sorg, 2012; DiPietro, 2013). As healing of porcine skin is similar to human skin (Sullivan *et al*., 2001), these results are applicable to the clinical situation. Thus, scar prevention in acute wounds may be a novel indication for the use of Acticoat^{TM}, in addition to the current uses of treating infection and decreasing inflammation in chronic wounds or deep partial thickness burns (Gravante and Montone, 2010; Widgerow, 2010).

However, further investigation is needed into the mechanisms by which silver nanoparticles affect healing in different types of wounds. In particular, the role of silver nanoparticles in inducing chronic inflammation in acute wounds should be examined more closely. Of interest may be the effect of silver nanoparticles on resident immune cells in the skin, including Langerhans cells and dendritic epidermal T cells, which modulate the immune response and keratinocyte and melanocyte function during normal homeostasis as well as healing (Nordlund, 2007; MacLeod and Havran, 2011). In addition to the importance of keratinocyte-melanocyte interactions in normal homeostasis (Nordlund, 2007), a recent report has highlighted the potential role of melanocytes in stimulating the fibroblastic response leading to pathological scarring (Gao *et al.*, 2013). Thus, *in vitro* and *in vivo* studies investigating the effect of silver nanoparticles on the migration, proliferation and differentiation of melanocytes, keratinocytes and fibroblasts and the interactions of these cells would be valuable. The processes of myofibroblast and pericyte differentiation share similarities (Carmeliet and Jain, 2011; Greaves *et al*., 2013). Therefore, the ability of silver nanoparticles to stimulate myofibroblast differentiation (Liu *et* al., 2010) may be of particular interest, as this mechanism may also influence pericyte differentiation, and thereby angiogenesis (Carmeliet and Jain, 2011) and scarring (DiPietro, 2013).

Furthermore, the role of silver nanoparticles in influencing the levels of growth factors, cytokines, TIMPs and MMPs within the wound *in vivo* should be scrutinized. As silver nanoparticles have a particular affinity for cysteine rich proteins such as metallothioneins (Lansdown, 2010), their effect on proteins such as cysteine-rich 61 (cyr61), which is important in collagen deposition (Lau, 2011), should be explored. Such research may elucidate novel mechanisms, apart from the direct influence on fibroblast function (Liu *et al*.,

2010), by which silver nanoparticles modulate collagen deposition and may have implications in scar prevention.

Moreover, large, randomized controlled trials are needed to ensure any beneficial effects of silver nanoparticles reported in animal and *in vitro* studies also occur in the clinical setting. Such clinical studies are of importance in clarifying the role of silver nanoparticles in the treatment of acute and chronic wounds as well as burns, particularly in light of the paucity of studies which compare silver dressings to other treatment modalities (Storm-Versloot *et al*., 2010; Aziz *et al*., 2012; O'Meara *et al*., 2013; Wasiak *et al*., 2013; Vloemans *et al*., 2014).

Thus, silver nanoparticles may have beneficial effects on the healing of acute wounds. However, well-designed, methodologically sound studies are needed to determine the mechanisms by which silver nanoparticles affect healing and their role in the treatment of different types of wounds.

Limitations

Due to difficulties in the protocol for immunolabelling for Ki-67, only one section per wound was assessed to determine the number of proliferating keratinocytes. Thus, these results should be interpreted with caution. However, the clear differences noted between experimental and control wounds suggest that this is an area worthy of discussion and further investigation.

Furthermore, in the current study five experimental and five control wounds were analysed for each day post-wounding. This sample size may prevent significant differences between experimental and control wounds from being apparent. Therefore, observation was used to

assess and verify the quantitative data. In addition, the sample size did not allow analysis of the effect of the pig, weight of the pig or region in which the wound was placed as compared to the effect of the dressing group on the variables studied. As experimental and control wounds were matched on each day post-wounding, the effect of the pig, weight and region was limited in the comparison of experimental and control wounds on the respective day post-wounding. However, the sample size restricted the analysis of the effect of Acticoat^{TM} on healing across the days post-wounding as effect of the pig, weight and region could not be analysed.

5. CONCLUSION

This study has shown that acute full-thickness excisional wounds treated with Acticoat™ heal at a rate comparable to those dressed with a polyurethane film dressing. This is in spite of an increased inflammatory response and decreased keratinocyte proliferation on day 3 post-wounding. In addition, there is evidence that Acticoat™-treated wounds have more mature blood vessels, different collagen deposition and epithelium which more closely resembles normal epithelium compared to the wounds dressed with polyurethane film dressings.

The potent antimicrobial action combined with the low risk of resistance makes silver nanoparticle dressings valuable in the treatment of infected wounds. However, the findings of this study suggest that silver nanoparticle dressings may also have a role in improving scarring. Considering the complex and potentially beneficial effects of silver nanoparticles on healing, further investigation is warranted into the effects and mechanisms of action of silver nanoparticles in different types of wounds. This will clarify the role of dressings such as Acticoat™ in the management burns and chronic wounds and elucidate new uses of these dressings in other wound types.

6. REFERENCES

Ågren, M.S. 1999. Matrix metalloproteinases (MMPs) are required for re-epithelialization of cutaneous wounds. *Archives of Dermatological Research* 291: 583-590.

Ahamed, M., Karns, M., Goodson, M., Rowe, J., Hussain, S.M., Schlager, J.J., Hong, Y. 2008. DNA damage response to different surface chemistry of silver nanoparticles in mammalian cells. *Toxicology and Applied Pharmacology* 233: 404-410.

Ahmed, M.C. 1982. Op-Site for Decubitus Care. *American Journal of Nursing* 82 (1): 61-64.

Allan, J.C. 1982. Learning about statistics. Johannesburg: Macmillan South Africa.

Ansell, D.M., Holden, K.A., Hardman, M.J. 2012. Animal models of wound repair: Are they cutting it? *Experimental Dermatology* 21: 581-585.

Argirova, M., Hadjiski, O., Victorova, A. 2007. Acticoat versus Allevyn as a Split-Thickness Skin Graft Donor-Site Dressing. *Annals of Plastic Surgery* 59 (4): 415-422.

Arican, M., Hatipoglu, F., Uyaroglu, A., Ozdemir, O., Ozkan, K. 2012. Effect of Acticoat® and Cutinova Hydro® on wound healing. *International Wound Journal* 10: 549-554.

Arora, S., Jain, J., Rajwade, J.M., Paknikar, K.M. 2008. Cellular responses induced by silver nanoparticles: *In vitro* studies. *Toxicology Letters* 179: 193-100.

AshaRani, P.V., Mun, G.L.K., Hande, M.P., Valiyaveettil, S. 2009. Cytotoxicity and Genotoxicity of Silver Nanoparticles in Human Cells. *ACS Nano* 3 (2): 279-290.

Atiyeh, B.S., Costagliola, M., Hayek, S.N., Dibo, S.A. 2007. Effect of silver on burn wound infection control and healing: Review of the literature. *Burns* 33: 139-148.

Aziz, Z., Abu, S.F., Chong, N.J. 2012. A systematic review of silver-containing dressings and topical silver agents (used with dressings) for burn wounds. *Burns* 38: 307-318.

Bancroft, J.D., Gamble, M. 2002. Theory and practice of histological techniques. 5th ed. London: Churchill Livingstone.

Baum, C.L., Arpey, C.J. 2005. Normal Cutaneous Wound Healing: Clinical Correlation with Cellular and Molecular Events. *Dermatologic Surgery* 31: 674-686.

Beausang, E., Floyd, H., Dunn, K.W., Orton, C.I., Ferguson, M.W.J. 1998. A New Quantitative Scale for Clinical Scar Assessment.
Plastic and Reconstructive Surgery 102: 1954-1961.

Beer, C., Foldbjerg, R., Hayashi, Y., Sutherland, D.S., Autrup, H. 2012. Toxicity of silver nanoparticles- Nanoparticle or silver ion? *Toxicology Letters* 208: 286-292.

Bhol, K.C., Schechter, P.J. 2004. Anti-inflammatory effect of topical nanocrystalline silver cream on allergic contact dermatitis in a guinea pig model.
Experimental Dermatology 29: 282-287.

Bhol, K.C., Schechter, P. 2005. Topical nanocrystalline silver cream suppresses inflammatory cytokines and induces apoptosis of inflammatory cells in a murine model of allergic contact dermatitis. *British Journal of Dermatology* 152: 1235-1242.

Blackman, N.J., Koval, J.J. 2000. Interval estimation for Cohen's kappa as a measure of agreement. *Statistics in Medicine* 19: 723-741.

Bradford, M.M. 1976. A rapid and sensitive method for the quantitation of microgram quantities of protein utilizing the principle of protein-dye binding.
Analytical Biochemistry 72: 248-254.

Braiman-Wilksman, L., Solomonik, R.S., Tennenbaum, T. 2007. Novel Insights into Wound Healing Sequence of Events. *Toxicologic Pathology* 35: 767-779.

Branski, L.K., Mittermayr, R., Herndon, D.N., Norbury, W.B., Masters, O.E., Hofmann, M., Traber, D.L., Redl, H., Jeschke, M.G. 2008. A porcine model of full-thickness burn, excision and skin auto-grafting. *Burns* 34: 1119-1127.

Bressan, E., Ferroni, L., Gardin, C., Rigo, C., Stocchero, M., Vindigni, V., Cairns, W., Zavan, B. 2013. Silver Nanoparticles and Mitochondrial Interaction.
International Journal of Dentistry 2013: 312747. doi: 10.1155/2013/312747

Broughton, G., Janis, J. E., Attinger, C.E. 2006. The Basic Science of Wound Healing.
Plastic and Reconstructive Surgery 117 (Suppl): 12S-34S.

Burd, A., Kwok, C.H., Hung, S.C., Chan, H.S., Gu, H., Lam., W.K., Huang, L. 2007. A comparative study of the cytotoxicity of silver-based dressings in monolayer cell, tissue explants, and animal models. *Wound Repair and Regeneration* 15: 94-104.

Carlson, C., Hussain, S.M., Schrand, A.M., Braydich-Stolle, L.K., Hess, K.L., Jones, R.L., Schlager, J.J. 2008. Unique Cellular Interaction of Silver Nanoparticles: Size-Dependent Generation of Reactive Oxygen Species. *Journal of Physical Chemistry B* 112: 13608-13619.

Carmeliet, P., Jain, R.K. 2011. Molecular mechanisms and clinical applications of angiogenesis. *Nature* 473 (19): 298-307.

Castellano, J.J., Shafii, S.M., Ko, F., Donate, G., Wright, T.E., Mannari, R.J., Payne, W.G., Smith, D.J., Robson, M.C. 2007. Comparative evaluation of silver-containing antimicrobial dressings and drugs. *International Wound Journal* 4: 114-122.

Castelo-Branco, C., Pons, F., Gratacós, E., Fortuny, A., Vanrell, J.A., González-Merlo, J. 1994. Relationship between skin collagen and bone changes during aging.
Maturitas 18 (3): 199-206.

Castillo, P.M., Herrera, J.L., Fernandez- Montesinos, R., Caro, C., Zaderenko, A.P., Mejías, J.A., Pozo, D. 2008. Tiopronin monolayer-protected silver nanoparticles modulate IL-6 secretion mediated by Toll-like receptor ligands. *Nanomedicine* 3 (5): 627-635.

Chambers, J.L., Christoph, G.G., Krieger, M., Kay, L., Stroud, R.M. 1974. Silver ion inhibition of serine proteases: crystallographic study of silver-trypsin.
Biochemical and Biophysical Research Communications 59 (1): 70-74.

Cohen, J. 1960. A Coefficient of agreement for Nominal Scales.
Educational and Psychological Measurement 20 (1): 37-46.

Cox, S.G., Cullingworth, L., Rode, H. 2011. Treatment of paediatric burns with a nanocrystalline silver dressing compared with standard wound care in a burns unit: A cost analysis. *South African Medical Journal* 101: 728-731.

Cuttle, L., Kempf, M., Phillips, G.E., Mill, J., Hayes, M.T., Fraser, J.F., Wang, X., Kimble, R.M. 2006. A porcine deep dermal partial thickness burn model with hypertrophic scarring.
Burns 32: 806-820.

Cuttle, L., Naidu, S., Mill, J., Hoskins, W., Das, K., Kimble, R.M. 2007. A retrospective cohort study of Acticoat™ versus Silvazine™ in a paediatric population. *Burns* 33: 701-707.

Davidson, J.M. 1998. Animal models for wound repair.
Archives of Dermatological Research 290 (Suppl): S1-S11.

de Lima, R., Seabra, A.B., Durán, N. 2012. Silver nanoparticles: A brief review of cytotoxicity and genotoxicity of chemically and biologically synthesized nanoparticles.
Journal of Applied Toxicology 32 (11): 867- 879.

Demling, R.H., DeSanti, L. 2002. The rate of re-epithelialization across meshed skin grafts is increased with exposure to silver. *Burns* 28: 264-266.

DiPietro, L.A. 2013. Angiogenesis and scar formation in healing wounds.
Current Opinions in Rheumatology 25 (1): 87-91.

Dolber, P.C., Spach, M.S. 1993. Conventional and confocal fluorescence microscopy of collagen fibers in the heart. *Journal of Histochemistry and Cytochemistry* 41 (3): 465-469.

Dokter, J., Boxma, H., Oen, I.M.M.H., van Baar, M.E., van der Vlies, C.H. 2013. Reduction in skin grafting after introduction of hydrofiber dressings in partial thickness burns: A comparison between a hydrofiber and silver sulfadiazine. *Burns* 39: 130-135.

Dunn, K., Edwards-Jones, V. 2004. The role of Acticoat™ with nanocrystalline silver in the management of burns. *Burns* 30 (Suppl): S1-S9.

Edwards, R., Harding, K.G. 2004. Bacteria and wound healing.
Current Opinion in Infectious Diseases 17: 91-95.

Edwards-Jones, V. 2006. Antimicrobial and barrier effects of silver against methicillin-resistant *Staphylococcus aureus*. *Journal of Wound Care* 15 (7): 285-290.

Ehrlich, H.P., Krummel, T.M. 1996. Regulation of wound healing from a connective tissue perspective. *Wound Repair and Regeneration* 4: 203-2010.

Ehrlich, H.P., Hunt, T.K. 2012. Collagen Organization Critical Role in Wound Contraction. *Advances in Wound Care* 1 (1): 3-9.

Foldbjerg, R., Olesen, P., Hougaard, M., Dang, D.A., Hoffmann, H.J., Autrup, H. 2009. PVP-coated silver nanoparticles and silver ions induce reactive oxygen species, apoptosis and necrosis in THP-1 monocytes. *Toxicology Letters* 190: 156-162.

Fong, J., Wood, F., Fowler, B. 2005. A silver coated dressing reduces the incidence of early burn wound cellulitis and associated costs of inpatient treatment: Comparative patient care audits. *Burns* 31: 562-567.

Fraser, J.F., Cuttle, L., Kempf, M., Kimble, R.M. 2004. Cytotoxicity of topical antimicrobial agents used in burn wounds in Australasia.
Australian and New Zealand Journal of Surgery 74: 139-142.

Fredriksson, C., Kratz, G., Huss, F. 2009. Accumulation of Silver and Delayed Re-epithelialization in Normal Human Skin: An *ex-vivo* Study of Different Silver Dressings. *Wounds* 21 (5): 116-123.

Gao, F., Jin, R., Zhang, L., Zhang, Y. 2013. The contribution of melanocytes to pathological scar formation during wound healing.
International Journal of Experimental Medicine 6 (7): 609-613.

Gerdes, J., Lemke, H., Baisch, H., Wacker, H., Schwab, U., Stein, H. 1984. Cell cycle analysis of a cell proliferation-associated human nuclear antigen defined by the monoclonal antibody Ki-67. *The Journal of Immunology* 133 (4): 1710-1715.

Gordon, S. 2002. Alternative activation of macrophages.
Nature Reviews Immunology 3: 23-35.

Gravante, G., Montone, A. 2010. A retrospective analysis of ambulatory burn patients: focus on wound dressings and healing times.
Annals of the Royal College of Surgeons of England 92: 118-123.

Greaves, N.S., Ashcroft, K.J., Baguneid, M., Bayat, A. 2013. Current understanding of the molecular and cellular mechanisms in fibroplasia and angiogenesis during acute wound healing. *Journal of Dermatological Science* 72: 206-217.

Greulich, C., Kittler, S., Epple, M., Muhr, G., Köller, M. 2009. Studies on the biocompatibility and the interaction of silver nanoparticles with human mesenchymal stem cells (hMSCs). *Langenbecks Archives of Surgery* 394: 495-502.

Greulich, C., Diendorf, J., Geßmann, J., Simon, T., Habijan, T., Eggeler, G., Schildhauer, T.A., Epple, M., Köller, M. 2011a. Cell type-specific responses of peripheral blood mononuclear cells to silver nanoparticles. *Acta Biomaterialia* 7: 3505-3514.

Greulich, C., Diendorf, J., Simon, T., Eggeler, G., Epple, M., Köller, M. 2011b. Uptake and intracellular distribution of silver nanoparticles in human mesenchymal stem cells. *Acta Biomaterialia* 7: 347-354.

Guo, S., DiPietro, L.A. 2010. Factors affecting wound healing. *Journal of Dental Research* 89 (3): 219-229.

Gurunathan, S., Lee, K., Kalishwaralal, K., Sheikpranbabu, S., Vaidyanathan, R., Eom, S.H. 2009. Antiangiogenic properties of silver nanoparticles. *Biomaterials* 30: 6341-6350.

Haase, A., Tentschert, J., Jungnickel, H., Graf, P., Mantion, A., Draude, F., Plendl, J., Goetz, M.E., Galla, S., Mašić, A., Thuenemann, A.F., Taubert, A. Arlinghaus, H.F., Luch, A. 2011. Toxicity of silver nanoparticles in human macrophages: uptake, intracellular distribution and cellular responses. *Journal of Physics: Conference Series* 304: 012030. doi: 10.1088/1742-6596/304/1/012030

Hackenberg, S., Scherzed, A., Kessler, M., Hummel, S., Technau, A., Froelich, K., Ginzkey, C., Koehler, C., Hagen, R., Kleinsasser, N. 2011. Silver nanoparticles: Evaluation of DNA damage, toxicity and functional impairment in human mesenchymal stem cells. *Toxicology Letters* 201: 27-33.

Heggers, J., Goodheart, R.E., Washington, J., McCoy, L., Carino, E., Dang, T., Edgar, P., Maness, C., Chinkes, D. 2005. Therapeutic Efficacy of Three Silver Dressings in an Infected Animal Model. *Journal of Burn Care and Rehabilitation* 26: 53-56.

Hidalgo, E., Domínguez, C. 1998. Study of cytotoxicity mechanisms of silver nitrate in human dermal fibroblasts. *Toxicology Letters* 98: 169-179.

Ho, J.K., Hantash, B.M. 2013. The principles of wound healing. *Expert Reviews in Dermatology* 8 (6): 639-658.

Hoeksema, H., Vandekerckhove, D., Verbelen, J., Heyneman, A., Monstrey, S. 2013. A comparative study of 1% silver sulphadiazine (Flammazine®) versus an enzyme alginogel (Flaminal®) in the treatment of partial thickness burns. *Burns* 39: 1234-1241.

Hsin, Y., Chen, C., Huang, S., Shih, T., Lai, P., Chueh, P.J. 2008. The apoptotic effect of nanosilver is mediated by a ROS- and JNK- dependent mechanism involving the mitochondrial pathway in NIH3T3 cells. *Toxicology Letters* 179: 130-139.

Huang, Y., Li, X., Liao, Z., Zhang, G., Liu, Q., Tang, J., Peng, Y., Liu, X., Luo, Q. 2007. A randomized comparative trial between Acticoat and SD-Ag in the treatment of residual burn wounds, including safety analysis. *Burns* 33: 161-166.

Im, A., Kim, J.Y., Kim, H., Cho, S., Park, Y., Kim, Y.S. 2013. Wound healing and antibacterial activities of chondroitin sulfate- and acharan sulfate-reduced silver nanoparticles. *Nanotechnology* 24: 395102. doi: 10.1088/0957-4484/24/39/395102

Innes, M.E., Umraw, N., Fish, J.S., Gomez, M., Cartotto, R.C. 2001. The use of silver coated dressings on donor site wounds: a prospective, controlled matched pair study. *Burns* 27: 621-627.

Ip, M., Lui, S.L., Poon, V.K.M., Lung, I., Burd, A. 2006. Antimicrobial activities of silver dressings: an *in vitro* comparison. *Journal of Medical Microbiology* 55: 59-63.

James, J., Bosch, K.S., Aronson, D.C., Houtkooper, J.M. 1990. Sirius red histophotometry and spectrophotometry of sections in the assessment of the collagen content of liver tissue and its application in the growing rat liver. *Liver* 10 (1): 1-5.

Javerzat, S., Auguste, P., Bikfalvi, A. 2002. The role of fibroblast growth factors in vascular development. *Trends in Molecular Medicine* 8 (10): 483-489.

Jia, S., Zhao, Y., Law, M., Galiano, R.D., Mustoe, T.A. 2011. The Effect of Collegenase on Ischaemic Wound Healing: Results of an *In Vivo* Study.
Ostomy Wound Management 57 (8): 20-26.

Jørgenson, B., Price, P., Andersen, K.E., Gottrup, F., Bech-Thomsen, N., Scanlon, E., Kirsner, R., Rheinen, H., Roed-Petersen, J., Romanelli, M., Jemec, G., Leaper, D.J., Neumann, M.H., Veraart, J., Coerper, S., Agerslev, R.H., Bendz, S.H., Larsen, J.R., Sibbald, R.G. 2005. The silver-releasing foam dresssing, Contreet Foam, promotes faster healing of critically colonised venous leg ulcers: a randomised, controlled trial.
International Wound Journal 2 (1): 64-73.

Jovanovic, A., Ermis, R., Mewaldt, R., Shi, L., Carson, D. 2012. The Influence of Metal Salts, Surfactants, and Wound Care Products on Enzymatic Activity of Collegenase, the Wound Debriding Enzyme. *Wounds* 24 (9): 242-253.

Kalishwaralal, K., Banumathi, E., Pandian, S.R.K., Deepak, V., Muniyandi, J., Eom, S.H., Gurunathan, S. 2009. Silver nanoparticles inhibit VEGF induced cell proliferation and migration in bovine retinal endothelial cells.
Colloids and Surfaces B: Biointerfaces 73: 51-57.

Kang, K., Lim, D., Choi, I., Kang, T., Lee, K., Moon, E., Yang, Y., Lee, M., Lim, J. 2011. Vascular tube formation and angiogenesis induced by polyvinylpyrrolidone-coated silver nanoparticles. *Toxicology Letters* 205: 227-234.

Kaufman, T., Hirshowitz, B.1983. Treatment of Chronic Leg Ulcers with Op-site.
Chirurgia Plastica 7: 211-215.

Kempf, M., Kimble, R.M., Cuttle, L. 2011. Cytotoxicity testing of burn wound dressings, ointments and creams: A method using polycarbonate cell culture inserts on a cell culture system. *Burns* 37: 994-1000.

Khundkar, R., Malic, C., Burge, T. 2010. Use of Acticoat™ dressings in burns: What is the evidence? *Burns* 36: 751-758.

Kimber, I., Dearman, R.J. 2002. Allergic contact dermatitis: the cellular effectors.
Contact Dermatitis 46: 1-5.

Kwan, K.H.L., Liu, X., To, M.K.T., Yeung, K.W.K., Ho, C., Wong, K.K.Y. 2011. Modulation of collagen alignment by silver nanoparticles results in better mechanical properties in wound healing. *Nanomedicine: Nanotechnology, Biology, and Medicine* 7 (4): 497-504.

Lam, P.K., Chan, E.S.Y., Ho, W.S., Liew, C.T. 2004. *In vitro* cytotoxicity testing of a nanocrystalline silver dressing (Acticoat) on cultured keratinocytes. *British Journal of Biomedical Science* 61 (3): 125-127.

Lansdown, A.B.G., Williams, A. 2004. How safe is silver in wound care?
Journal of Wound Care 13 (4): 131-136.

Lansdown, A.B.G. 2010. A Pharmacological and Toxicological Profile of Silver as an Antimicrobial Agent in Medical Devices.
Advances in Pharmacological Sciences 2010: 910686. doi: 10.1155/2010/910686

Larese, F.F., D'Agostin, F., Crosera, M., Adami, G., Renzi, N., Bovenzi, M., Maina, G. 2009. Human skin penetration of silver nanoparticles through intact and damaged skin.
Toxicology 255: 33-37.

Lau, L.F. 2011. CCN1/ CYR61: the very model of a modern matricellular protein. *Cellular and Molecular Life Sciences* 68: 3149–3163.

Lee, A.C., Moon, H.K. 2003. Effect of Topically Applied Silver Sulfadiazine on Fibroblast Cell Proliferation and Biomechanical Properties of the Wound.
Archives of Pharmacal Research 26 (10): 855-860.

Lee, J.H., Kwak, J.J., Shin, H.B., Jung, H.W., Lee, Y.K., Yeo, E.D., Yang, S.S. 2013. Comparative Efficacy of Silver-Containing Dressing Materials for Treating MRSA-Infected Wounds in Rats with Streptozotocin-Induced Diabetes. *Wounds* 25 (12): 345-354.

Levey, V., Lindon, C., Zheng, Y., Harfe, B.D., Morgan, B.A. 2007. Epidermal stem cells arise from the hair follicle after wounding. *FASEB Journal* 21: 1358-1366.

Li, J., Chen, J., Kirsner, R. 2007. Pathophysiology of acute wound healing.
Clinics in Dermatology 25: 9-18.

Lin, L.I. 1989. A concordance correlation coefficient to evaluate reproducibility.
Biometrics 45 (1): 255-268.

Liu, X., Lee, P., Ho, C., Lui, V.C.H., Chen, Y., Che, C., Tam, P.K.H., Wong, K.K.Y. 2010. Silver nanoparticles Mediate Differential Responses in Keratinocytes and Fibroblasts during Skin Wound Healing. *ChemMedChem* 5: 468-475.

Lopez-De Leon, A., Rojkind, M. 1985. A Simple Micromethod for Collagen and Total Protein Determination in Formalin-fixed Paraffin-embedded sections.
Journal of Histochemistry and Cytochemistry 33 (8): 737-743.

MacLeod, A.S., Havran, W.L. 2011. Functions of skin-resident γδ T cells.
Cellular and Molecular Life Sciences 68: 2399-2408.

Malik, K.I., Malik, M.A.N., Aslam, A. 2010. Honey compared with silver sulphadiazine in the treatment of superficial partial-thickness burns.
International Wound Journal 7 (5): 413-417.

McCarty, S.M., Percival, S.L. 2013. Proteases and Delayed Wound Healing.
Advances in Wound Care 2 (8): 438-447.

McCauley, R.L., Linares, H.A., Pelligrini, V., Herndon, D.N., Robson, M.C., Heggers, J.P. 1989. *In Vitro* toxicity of Topical Antimicrobial Agents to Human Fibroblasts.
Journal of Surgical Research 46: 267-274.

McGrath, E.J., Kersey, P. 2009. Quantification of wound oedema after dermatological surgery. *British Journal of Dermatology* 161: 1376-1378.

Meyer, W., Neurand, K., Radke, B. 1981. Elastic fibre arrangement in the skin of the pig.
Archives of Dermatological Research 270: 391-401.

Meyer, W., Neurand, K., Radke, B. 1982. Collagen fibre arrangement in the skin of the pig.
Journal of Anatomy 134 (1): 139-148.

Morris, G., Hopewell, J. 1990. Epidermal cell kinetics of the pig: a review.
Cell Tissue Kinetics 23: 271-282.

Mowafy, M., Cassens, R. 1975. Microscopic structure of pig skin.
Journal of Animal Science 41 (5): 1281-1290.

Muangman, P., Chuntrasakul, C., Silthram, S., Suvanchote, S., Benjathanung, R., Kittidacha, S., Rueksomtawin, S. 2006. Comparison of Efficacy of 1% Silver Sulfadiazine and Acticoat^{TM} for Treatment of Partial-Thickness Burn Wounds.
Journal of the Medical Association of Thailand 89 (7): 953-958.

Münter, K.C., Beele, H., Russell, L., Crespi, A., Basse, P., Alikadic, N., Fraulin, F. 2006. Effect of a sustained silver-releasing dressing on ulcers with delayed healing: the CONTOP study. *Journal of Wound Care* 15 (5): 199-206.

Nadworny, P.L., Wang, J., Tredget, E.E., Burrell, R.E. 2008. Anti-inflammatory activity of nanocrystalline silver in a porcine contact dermatitis model.
Nanomedicine: Nanotechnology, Biology and Medicine 4: 241-251.

Nadworny, P.L., Wang, J., Tredget, E.E., Burrell, R.E. 2010. Anti-inflammatory activity of nanocrystalline silver-derived solutions in porcine contact dermatitis.
Journal of Inflammation 7: 13-32.

Nordlund, J.J. 2007. The Melanocyte and the Epidermal Melanin Unit: An Expanded Concept. *Dermatology Clinics* 25: 271-281.

O'Meara, S., Al-Kurdi, D., Ologun, Y., Ovington, L.G., Martyn-St James, M., Richardson, R. 2013. Antibiotics and antiseptics for venous leg ulcers (Review).
Cochrane Database Systematic Review 1.

Odland, G., Ross, R. 1968. Human wound repair I: Epidermal Regeneration.
The Journal of Cell Biology 39: 135-151.

Olson, M.E., Wright, J.B., Lam, K., Burrell, R.E. 2000. Healing of Porcine Donor Sites Covered with Silver-coated Dressings. *European Journal of Surgery* 166: 486-489.

Pardali, E., Goumans, M., ten Dijke, P. 2010. Signaling by members of the TGF-β family in vascular morphogenesis and disease. *Trends in Cell Biology* 20: 556-567.

Park, E., Yi, J., Kim, Y., Choi, K., Park, K. 2010. Silver nanoparticles induce cytotoxicity by a Trojan-horse type mechanism. *Toxicology in Vitro* 24: 872-878.

Park, M.V.D.Z., Neigh, A.M., Vermeulen, J.P., de la Fonteyne, L.J.J., Verharen, H.W., Briedé, J.J., van Loveren, H., de Jong, W.H. 2011. The effect of particle size on the cytotoxicity, inflammation, developmental toxicity and genotoxicity of silver nanoparticles.
Biomaterials 32: 9810-9817.

Pather, N. 2009. The *in vitro* and *in vivo* effects of *Bulbine frutescens* and *Bulbine natalensis* on cutaneous wound healing [thesis]. Johannesburg: University of the Witwatersrand.

Percival, S.L., Bowler, P.G., Russell, D. 2005. Bacterial resistance to silver in wound care. *Journal of Hospital Infection* 60: 1-7.

Poon, K.M., Burd, A. 2004. *In vitro* cytotoxicity of silver: implication for clinical wound care. *Burns* 30: 140-147.

Prestes, M.A., Ribas, C.A.P.M., Filho, J.M.R., Moreira, L.B., Boldt, A.B.W., Brustolin, E.V., Castanho, L.S., Bernardi, J.A., Dias, F.C. 2012. Wound healing using ionic silver dressing and nanocrystalline silver dressing in rats. *Acta Cirúrgica Brasileira* 27 (11): 761-767.

Reddy, G., Enwemeka, C. 1996. A Simplified Method for the Analysis of Hydroxyproline in Biological Tissues. *Clinical Biochemistry* 29 (3): 225-229.

Reinke, J.M., Sorg, H. 2012. Wound Repair and Regeneration.
European Surgical Research 49: 35-43.

Rigo, C., Roman, M., Munivrana, I., Vindigni, V., Azzena, B., Barbante, C., Cairns, W.R.L. 2012. Characterization and evaluation of silver release from four different dressings used in burns care. *Burns* 38: 1131-1142.

Rigo, C., Ferroni, L., Tocco, I., Roman, M., Munivrana, I., Gardin, C., Cairns, W.R.L., Vindigni, V., Azzena, B., Barbante, C., Zavan, B. 2013. Active Silver Nanoparticles for Wound Healing. *International Journal of Molecular Sciences* 14: 4817-4840.

Bancroft, J.D., Gamble, M. 2002. Theory and practice of histological techniques. 5th ed. London: Churchill Livingstone.

Ross, M.H., Pawlina, W. 2006. Histology. A text and atlas. 5th ed.
Baltimore: Lippincott Williams & Wilkins.

Samberg, M.E., Oldenburg, S.J., Monteiro-Riviere, N.A. 2010. Evaluation of Silver Nanoparticle Toxicity in Skin *in vivo* and Keratinocytes *in vitro*. *Environmental Health Perspectives* 118 (3): 407-413.

Shi, L., Ermis, R., Kiedaisch, B., Carson, D. 2010. The Effect of Various Wound Dressings on the Activity of Debriding Enzymes. *Advances in Skin and Wound Care* 23 (10): 456-462.

Shin, S., Ye, M., Kim, H., Kang, H. 2007. The effects of nano-silver on the proliferation and cytokine expression by peripheral blood mononuclear cells. *International Immunopharmacology* 7: 1813-1818.

Silver, G.M., Robertson, S.W., Halerz, M.M., Conrad, P., Supple, K.G., Gamelli, R.L. 2007. A Silver-Coated Antimicrobial Barrier Dressing Used Postoperatively on Meshed Autografts: A Dressing Comparison Study. *Journal of Burn Care Research* 28: 715-719.

Sindrilaru, A., Scharffetter-Kochanek, K. 2013. Disclosure of the Culprits: Macrophages-Versatile Regulators of Wound Healing. *Advances in Wound Care* 2 (7): 357-368.

Singer, A.J., McClain, S.A. 2006. Development of a porcine incisional wound model and novel scarring scales. *Wound Repair and Regeneration* 14 (4): 492-497.

Singh, R.P., Ramarao, P. 2012. Cellular uptake, intracellular trafficking and cytotoxicity of silver nanoparticles. *Toxicology Letters* 213: 249-259.

Sivamani, R.K., Garcia, M.S., Isseroff, R.R. 2007. Wound re-epithelialization: modulating keratinocyte migration in wound healing. *Frontiers in Bioscience* 12: 2849-2868.

Storm-Versloot, M.N., Vos, C.G., Ubbink, D.T., Vermeulen, H. 2010. Topical silver for preventing wound infection (Review). *Cochrane Database Systematic Review* 3.

Sullivan, T.P., Eaglstein, W. H., Davis, S.C., Mertz, P. 2001. The pig as a model for human wound healing. *Wound Repair and Regeneration* 9: 66-76.

Sung, J.H., Ji, J.H., Park, J.D., Yoon, J.U., Kim, D.S., Jeon, K.S., Song, M.Y., Jeong, J., Han, B.S., Han, J.H., Chung, Y.H., Chang, H.K., Lee, J.H., Cho, M.H., Kelman, B.J., Yu, I.J. 2009. Subchronic Inhalation Toxicity of Silver Nanoparticles. *Toxicological Sciences* 108 (2): 452-461.

Teodoro, J.S., Simões, A.M., Duarte, F.V., Rolo, A.P., Murdoch, R.C., Hussain, S.M., Palmeira, C.M. 2011. Assessment of the toxicity of silver nanoparticles *in vitro*: A mitochondrial perspective. *Toxicology in Vitro* 25: 664-670.

Therkildsen, P., Hædersdal, M., Lock-Andersen, J., de Fine Olivarius, F., Poulsen, T., Wulf, H.C. 1998. Epidermal thickness measured by light microscopy: a methodological study. *Skin Research and Technology* 4: 174-179.

Theunissen, D. 2001. Measurements in wound healing: effects of topical agents on full thickness dermal incised wounds in an animal model [dissertation]. Cape Town: University of Cape Town.

Thomas, S., McCubbin, P. 2003. A comparison of the antimicrobial effects of four silver-containing dressings on three organisms. *Journal of Wound Care* 12 (3): 101-107.

Tian, J., Wong, K.K.Y., Ho, C., Lok, C., Yu, W., Che, C., Chiu, J., Tam, P.K.H. 2007. Topical Delivery of Silver Nanoparticles Promotes Wound Healing. *ChemMedChem* 2: 129-136.

Tredget, E.E., Shankowsky, H.A., Groeneveld, A., Burrell, R. 1998. A Matched-Pair, Randomized Study Evaluating the Efficacy and Safety of Acticoat Silver-Coated Dressing for the Treatment of Burn Wounds. *Journal of Burn Care and Rehabilitation* 19: 531-537.

Tredget, E.B., Demare, J., Chandran, G., Tredget, E.E., Yang, L., Ghahary, A. 2005. Transforming growth factor-β and its effect on Reepithelialization of partial-thickness ear wounds in transgenic mice. *Wound Repair and Regeneration* 13: 61-67.

Uygur, F., Öncül, O., Evinç, R., Diktas, H., Acar, A., Ülkür, E. 2009. Effects of three different topical antibacterial dressings on *Acinetobacter baumanii*-contaminated full-thickness burns in rats. *Burns* 35: 270-273.

Van Den Plas, D., De Smet, K., Lens, D., Sollie, P. 2008. Differential cell death programmes induced by silver dressings *in vitro. European Journal of Dermatology* 18 (4): 416-421.

Varas, R.P., O'Keeffe, T., Namias, N., Pizano, L.R., Quintana, O.D., Tellachea, M.H., Rashid, Q., Ward, C.G. 2005. A Prospective, Randomized Trial of Acticoat Versus Silver Sulfadiazine in the Treatment of Partial-Thickness Burns: Which Method Is Less Painful? *Journal of Burn Care and Rehabilitation* 26: 344-347.

Vardaxis, N.J.V., Brans, T.A., Boon, M.E., Kreis, R.W., Marres, L.M. 1997. Confocal laser scanning microscopy of porcine skin: implications for human wound healing studies. *Journal of Anatomy* 190: 601-611.

Vloemans, A.F.P.M., Hermans, M.H.E., van der Wal, M.B.A., Liebregts, J., Middelkoop, E. 2014. Optimal treatment of partial thickness burns in children: A systematic review. *Burns* 40: 177-190.

Walker, M., Bowler, P.G., Cochrane, C.A. 2007. *In Vitro* Studies to Show Sequestration of Matrix Metalloproteinases by Silver-Containing Wound Care Products. *Ostomy Wound Management* 53 (9): 18-25.

Wang, X., Chang, H., Francis, R., Olszowy, H., Liu, P., Kempf, M., Cuttle, L., Kravchuk, O., Phillips, G.E., Kimble, R.M. 2009. Silver deposits in cutaneous burn scar tissue is a common phenomenon following application of a silver dressing. *Journal of Cutaneous Pathology* 36: 788-792.

Wang, X., Kravchuk, O., Kimble, R.M. 2010. A retrospective review of burn dressings on a porcine burn model. *Burns* 36: 680-687.

Wasiak, J., Cleland, H., Campbell, F., Spinks, A. 2013. Dressings for superficial and partial thickness burns (Review). *Cochrane Database Systematic Review* 3.

Wei, L., Tang, J., Zhang, Z., Chen, Y., Zhou, G., Xi, T. 2010. Investigation of the cytotoxicity mechanism of silver nanoparticles *in vitro*.
Biomedical Materials 5 (4): 044103. doi: 10.1088/1748-6041/5/4/044103

Weibel, E., Gomez, D. 1962. A principle for counting tissue structures on random sections. *Journal of Applied Physiology* 17 (2): 343-348.

Werner, S., Smola, H. 2001. Paracrine regulation of keratinocyte proliferation and differentiation. *Trends in Cell Biology* 11 (4): 143-146.

Werner, S., Krieg, T., Smola, H. 2007. Keratinocyte-Fibroblast interactions in Wound Healing. *Journal of Investigative Dermatology* 127: 998-1008.

Whitley, E., Ball, J. 2002. Statistics review 1: Presenting and summarizing data.
Critical Care 6 (1): 66-71.
Widgerow, A.D. 2010. Nanocrystalline silver, gelatinases and the clinical implications.
Burns 36: 965-974.

Widgerow, A.D. 2011. Chronic wound fluid- thinking outside the box.
Wound Repair and Regeneration 19: 287-291.

Widgerow, A.D. 2012. Deconstructing the Stalled Wound. *Wounds* 24 (3): 58-66.

Wilgus, T. 2012. Growth Factor- Extracellular Matrix Interactions Regulate Wound Repair.
Advances in Wound Care 1 (6): 249-254.

Wilgus, T.A., Roy, S., McDaniel, J.C. 2013. Neutrophils and Wound Repair: Positive Actions and Negative Reactions. *Advances in Wound Care* 2 (7): 379-387.

Woessner, J. 1961. The Determination of Hydroxyproline in Tissue and Protein Samples Containing Small Proportions of this Imino Acid.
Archives of Biochemistry and Biophysics 93: 440-447.

Wollina, U., Berger, U., Mahrle, G. 1991. Immunohistochemistry of porcine skin.
Acta Histochemica 90 (1): 87-91.

Wright, J.B., Lam, K., Hansen, D., Burrell, R.E. 1999. Efficacy of topical silver against fungal burn wound pathogens. *American Journal of Infection Control* 27: 344-350.

Wright, J.B., Lam, K., Buret, A. G., Olson, M.E., Burrell, R.E. 2002. Early healing events in a porcine model of contaminated wounds: effect of nanocrystalline silver on matrix metalloproteinases, cell apoptosis, and healing.
Wound Repair and Regeneration 10: 141-151.

Yin, H.Q., Langford, R., Burrell, R.E. 1999. Comparative Evaluation of Antimicrobial Activity of Acticoat Antimicrobial Barrier Dressing.
Journal of Burn Care and Rehabilitation 20: 195-200.

Zanette, C., Pelin, M., Crosera, M., Adami, G., Bovenzi, M., Larese, F.F., Florio, C. 2011. Silver nanoparticles exert a long-lasting antiproliferative effect on human keratinocyte HaCaT cell line. *Toxicology in Vitro* 25: 1053-1060.

7. APPENDICES

A. Ethical clearance certificate from the Animal Ethics Screening Committee of the University of the Witwatersrand

AESC 3

UNIVERSITY OF THE WITWATERSRAND, JOHANNESBURG

STRICTLY CONFIDENTIAL

ANIMAL ETHICS SCREENING COMMITTEE (AESC)

CLEARANCE CERTIFICATE NO. 2009/26/04

APPLICANT: Dr C Mann

SCHOOL: Anatomical Sciences
DEPARTMENT:
LOCATION:

PROJECT TITLE: **The biochemical and histological effects of ano-crystalline silver dressings (Acticoal) on wound healing in full thickness excisional dermal wounds in a porcine model**

Number and Species

8 30-40kg M/F Large White Pigs

Approval was given for the use of animals for the project described above at an AESC meeting held on 30.06.2009. This approval remains valid until 30.06.2011

The use of these animals is subject to AESC guidelines for the use and care of animals, is limited to the procedures described in the application form and to the following additional conditions:

Signed: _____ Date: 17/07/2009
(Chairperson, AESC)

I am satisfied that the persons listed in this application are competent to perform the procedures therein, in terms of Section 23 (1) (c) of the Veterinary and Para-Veterinary Professions Act (19 of 1982)

Signed: _____ Date: 17/07/2009
(Registered Veterinarian)

cc: Supervisor:
Director: CAS

Works 2000/lain0015/AESCCert.wps

PLEASE NOTE: Carol Mann became Carol Hartmann in 2010.

REAGENTS AND BUFFERS USED FOR HISTOLOGY

B1. 10% buffered (neutral) formalin

100ml	40% formaldehyde
900ml	Distilled water
4g	sodium dihydrogen phosphate monoxide
6,5g	di-sodium hydrogen orthophosphate anhydrous

B2. Mayer's Haematoxylin and Eosin stain

Haematoxylin: Haematoxylin 4g

Distilled water 1000ml

Sodium iodate 0,3g

Potassium Alum 50g

Citric acid 1,5g

Chloral hydrate 75g

Eosin: 1% Eosin 500ml

1% Phloxine 250ml

Distilled water 750ml

1. Incubate sections in two changes of xylene, two changes of 100% alcohol and one change of 95% alcohol (5 minutes each).
2. Wash in running tap water for 5 min.
3. Stain in haematoxylin for 5 minutes.
4. Wash in tap water until excess stain removed.
5. Dip in 1% Acid alcohol.
6. Wash in running tap water for 5 minutes.
7. Counter stain in Eosin for 30 seconds to 1 minute.
8. Wash briefly in running tap water.
9. Pass sections through one change of 95% alcohol, two changes of 100% alcohol and two changes of xylene before mounting the coverslip with entellan.

C. Ethical clearance certificate from the Human Research Ethics Committee of the University of the Witwatersrand

UNIVERSITY OF THE WITWATERSRAND, JOHANNESBURG
Division of the Deputy Registrar (Research)

HUMAN RESEARCH ETHICS COMMITTEE (MEDICAL)
R14/49 Dr Carol Hartmann

CLEARANCE CERTIFICATE	M110801
PROJECT	The Effect of a Nano-Crystalline Silver Dressing (Acticoat TM) on Wound Healing in Full Thickness Excisional Dermal Wounds in a Porcine Model
	Approved unconditionally
INVESTIGATORS	Dr Carol Hartmann
DEPARTMENT	School of Anatomical Sciences
DATE CONSIDERED	26/08/2011
DECISION OF THE COMMITTEE*	
	26/08/2011

Unless otherwise specified this ethical clearance is valid for 5 years and may be renewed upon application.

DATE **CHAIRPERSON** .....
(Professor PE Cleaton-Jones)

*Guidelines for written 'informed consent' attached where applicable
cc: Supervisor : Professor B Kramer

DECLARATION OF INVESTIGATOR(S)

To be completed in duplicate and **ONE COPY** returned to the Secretary at Room 10004, 10th Floor, Senate House, University.
I/We fully understand the conditions under which I am/we are authorized to carry out the abovementioned research and I/we guarantee to ensure compliance with these conditions. Should any departure to be contemplated from the research procedure as approved I/we undertake to resubmit the protocol to the Committee. **I agree to a completion of a yearly progress report.**
PLEASE QUOTE THE PROTOCOL NUMBER IN ALL ENQUIRIES...

REAGENTS AND BUFFERS FOR IMMUNOCYTOCHEMISTRY

C1. Tris EDTA buffer pH 9.0:

1.21g Tris

0.37g ethylenediaminetetraacetic acid (EDTA)

1000ml distilled water

Adjust pH using 1M HCl

0.5ml Tween 20

C2. Initial immunocytochemistry protocol

1. Incubate sections in two changes of xylene (10 minutes) before passing through two changes of 100% alcohol and one change of 95% alcohol.
2. Wash in running tap water for 5 minutes.
3. Incubate sections in EDTA (pH 9.0) in a microwave (900W) for 10 minutes.
4. Cool at room temperature for 10 minutes.
5. Incubate sections with 3% Hydrogen peroxide for 15 minutes at room temperature.
6. Wash in running tap water for 5 minutes.
7. Wash twice in TBS 1% BSA (Appendix C5) containing 0.025% triton for 10 minutes:
8. Incubate each section with 75µl of 10% Normal Goat Serum in TBS 1% BSA for 45 minutes at room temperature.
9. Incubate each section with 100 µl of primary antibody (polyclonal rabbit anti-Ki-67 antibody) diluted 1:1000 in TBS 1% BSA overnight at 4^{o}C in a humidified chamber.
10. Wash twice in TBS 1% BSA for 10 minutes.
11. Incubate each section with 100µl of secondary antibody (goat anti-rabbit antibody) diluted 1:300 in TBS 1% BSA for 30 minutes at room temperature.
12. Wash twice in TBS 1% BSA for 10 minutes.
13. Incubate each section with 100µl of solution, obtained by mixing reagents A and B (ABC kit) with TBS 1% BSA as per the manufacturer's instructions, for 30 minutes at room temperature.
14. Wash twice in TBS 1% BSA for 10 minutes.
15. Incubate each section with 100µl diaminobenzidine (DAB) (Appendix C6) for 5 minutes at room temperature.
16. Wash in running tap water for 5 minutes.
17. Pass sections through one change of 95% alcohol, two changes of 100% alcohol and two changes of xylene before mounting the coverslip with entellan.

C3. Citrate buffer pH 6.0 or pH 8.0:

2.94g trisodium citrate

1000ml distilled water

Adjust pH using 1M HCl.

C4. 5% Tris Urea buffer pH 9.5:

24.24g Tris

100g urea crystals

2000ml distilled water

Adjust pH using 1M HCl

C5. Tris Buffered Saline pH 7.6:

17,54g sodium chloride
12,12g Tris base
2000ml distilled water
Adjust pH to 7.6 with 5M HCl.

To make TBS 1% BSA: Add 1g bovine serum albumin (BSA) (Sigma-Aldrich, USA) to 100ml TBS.

C6. DAB

0.001g diaminobenzidine

2ml Tris buffered saline

To this solution add 20µl of a solution composed of 1µl 30% hydrogen peroxide in 29µl iced, distilled water. Vortex and filter before use.

REAGENTS AND BUFFERS FOR PICROSIRIUS RED STAINING AND HYDROXYPROLINE AND TOTAL PROTEIN DETERMINATION

D1. Picrosirius red stain

0.5g Sirius Red F3B

500ml Saturated aqueous solution of picric acid

Let solution stand for 24 hours before use.

1. Incubate sections in two changes of xylene, two changes of 100% alcohol and one change of 95% alcohol (5 minutes each).
2. Wash in running tap water for 5 minutes.
3. Stain in haematoxylin for 8 minutes.
4. Wash in running tap water for 10 minutes.
5. Stain in picrosirius red for one hour.
6. Wash in two changes of acidified water (2 minutes per change).
7. Pass sections through one change of 95% alcohol, two changes of 100% alcohol and two changes of xylene before mounting the coverslip with entellan.

D2. Chloramine T reagent:

0.32g Chloramine T

5.2ml distilled water

6.5ml N-propanol

13.3ml stock buffer (Appendix D5)

D3. Erhlichs reagent solution:

3.73g Dimethylaminobenzaldehyde

15ml N-Propanol

6.5ml Perchloric acid

Distilled water to final volume 25ml

D4. Assay buffer:

1 part stock buffer (Appendix D5) to 10 parts distilled water

---

D5. Stock buffer:

50g Citric acid monohydrate

12ml glacial acetic acid

120g Sodium acetate trihydrate

34g Sodium hydroxide

1000ml distilled water

Adjust to pH 6.5 using 1M HCl

D6. Homogenising buffer:

50mM Tris HCl (pH 7.5)

5mM acetate

0.2mM EDTA

10% glycerol

1% Triton X-100

Add 500µl of 0.5M Dithiothreitol (Sigma-Aldrich, USA) and 50µl of protease inhibitor cocktail for general use (Sigma-Aldrich, USA) to 10ml homogenizing buffer just before protein extraction.

D7. Mean absorbance of serial dilutions of 0.01% Fast Green at 540nm and 620nm

% Fast Green	Mean A_{620} (n=12)	Mean A_{540} (n=12)	A_{540}/A_{620} (%)
0.01	9.99 ($\pm$1.86 x 10^{-5})	0.37 ($\pm$0.005)	-
0.005	2.21 ($\pm$0.072)	0.22 ($\pm$0.006)	9.76
0.0025	1.20 ($\pm$0.055)	0.13($\pm$0.005)	11.18
0.00125	0.65 ($\pm$0.027)	0.09 ($\pm$0.003)	13.90
0.000625	0.35 ($\pm$0.015)	0.07 ($\pm$0.003)	18.98
0.000313	0.20 ($\pm$0.008)	0.05 ($\pm$0.001)	26.58
0.000156	0.12 ($\pm$0.003)	0.05 ($\pm$0.001)	38.98
7.81 x10^{-5}	0.08 ($\pm$0.005)	0.05 ($\pm$0.001)	53.73
3.91 x10^{-5}	0.06 ($\pm$0.002)	0.04 ($\pm$0.001)	68.21
1.95 x10^{-5}	0.06 ($\pm$0.001)	0.04 ($\pm$0.002)	81.02

A_{620}: Absorbance at 620nm; A_{540}: Absorbance at 540nm; A_{540}/A_{620}: Absorbance at 540nm expressed as a percentage of the absorbance at 620nm.

Relationship defined by the equation: $A_{540}= 0.08(A_{620}) + 0.039$ (r=0.99)

D8. Calculation of the colour equivalences (CE) for total protein (TP) and collagen.

Area of skin	Collagen (mg/ml)	TP (mg/ml)	A_{620}	Corrected A_{540}	Collagen CE	TP CE
Pig 1 dorsum	0.08 ± 0.01	0.87 ± 0.11	0.20	0.99	13.00	0.25
Pig 2 dorsum	0.09 ± 0.01	0.65 ± 0.26	0.32	1.68	18.86	0.57
Pig 3 dorsum	0.10 ± 0.02	0.67 ± 0.17	0.21	1.20	12.57	0.37
Pig 4 abdomen	0.15 ± 0.02	0.67 ± 0.10	0.20	1.07	7.06	0.38
Pig 4 dorsum	0.08 ± 0.003	0.87 ± 0.50	0.36	1.62	20.75	0.45
Pig 5 abdomen	0.10 ± 0.02	0.95 ± 0.25	0.19	0.74	7.25	0.22
Pig 5 dorsum	0.09 ± 0.31	0.75 ± 0.17	0.44	2.21	24.37	0.67
Pig 6 dorsum	0.10 ± 0.25	0.70 ± 0.09	0.68	2.39	24.98	1.12
Pig 7 abdomen	0.10 ± 0.50	0.83 ± 0.14	0.33	1.30	13.24	0.45
Pig 7 dorsum	0.10 ± 0.86	0.59 ± 0.29	0.32	1.86	19.28	0.66

A_{620}: Absorbance at 620nm; Corrected A_{540}: Absorbance at 540nm excluding contribution of Fast Green (Calculated using the equation in Appendix D7)

Colour equivalences calculated using the following formulae (Lopez-De Leon and Rojkind, 1985): Colour equivalence of collagen = $\frac{\text{Corrected } A_{540}}{\text{Mean collagen value}}$

Colour equivalence of total protein = $\frac{A_{620}}{\text{Mean total protein value- mean collagen value}}$

REAGENTS AND BUFFERS FOR GRAM STAINING

E. Gram method for paraffin sections (Bancroft and Gamble, 2002)

Crystal Violet Solution

0.5% Crystal Violet in 25% alcohol. Filter before use.

Lugol's Iodine solution

Iodine 1.0g

Potassium iodide 2.0g

Distilled water 300ml

Dissolve the potassium iodide in 10ml distilled water.

Add the iodine and mix before adding the remaining distilled water.

Neutral red

Neutral red 1.0g

Acetic acid 2ml

Distilled water 1000ml

Filter before use.

1. Incubate sections in two changes of xylene, two changes of 100% alcohol and one change of 95% alcohol (5 minutes each).
2. Wash in running tap water for 5 minutes and rinse in distilled water.
3. Stain in crystal violet for 2 minutes.
4. Wash in running tap water and drain off excess water.
5. Stain in Lugol's iodine for 2 minutes.
6. Rinse in running tap water.
7. Working with single sections, blot each section dry and differentiate by dipping in 95% alcohol.
8. Wash in running tap water.
9. Stain in neutral red for 3 minutes.
10. Blot and dehydrate rapidly by passing sections through one change of 95% alcohol, two changes of 100% alcohol and two changes of xylene before mounting the coverslip with entellan.

F. Lin's concordance correlation and Cohen's kappa coefficients

	Intra-error (Left/ Right)	Inter-error (Left/ Right)
Percentage change	0.99	0.91
Epithelial gap (μm)	0.99	0.98
% by which the wound has closed	0.99	0.95
Area of the regenerated epithelium (μm^2)	1.00	0.91
Epithelial tongue length (μm)	1.00	0.97
Epithelial thickness at the wound edge (μm)	0.99/ 0.97	0.98/ 0.99
Epithelial thickness at the tip of the epithelial tongue (μm)	0.99/ 0.99	0.88/ 0.96
Average score for hair follicles	0.96/ 0.90	0.83/ 0.87
Number of inflammatory cells	1.00	0.98
Average score for blood vessel type	0.83/ 0.86	0.86/ 0.86
Average score for blood vessel number	0.85/ 0.85	0.86/ 0.81
Number of proliferating keratinocytes	0.99	0.99
% area of collagen (μm^2)	1.00	0.99
Average score for collagen density	0.95	0.95
Average score for collagen bundle size	0.98	0.95
Average score for collagen organisation	0.97	0.89

G. Results of the Shapiro-Wilks test by day post-wounding and treatment group

	Day 3		Day 6		Day 9		Day 12		Day 15	
	E	**C**	**E**	**C**	**E**	**C**	**E**	**C**	**E**	**C**
Percentage change in area over time	**0.001**	0.27	0.70	**0.03**	0.99	0.51	0.28	**0.03**	0.88	**0.04**
Size of the epithelial gap (µm)	N	N	N	N	0.09	0.50	N	N	-	**0.0001**
Percentage by which the wound has closed	N	N	N	N	0.32	0.44	N	N	-	**0.0001**
Width of the wound area (µm)	N	N	N	N	0.93	**0.04**	N	N	0.12	0.14
Area of the epithelial tongue (μm^2)	0.71	0.90	0.23	0.28	0.66	0.93	N	N	0.34	0.67
Length of the epithelial tongue (µm)	0.30	0.43	0.38	0.91	0.13	0.48	N	N	0.48	0.57
Thickness of the epithelium at the wound edge (µm)	0.23	0.16	0.99	0.92	0.72	0.82	N	N	0.76	0.44
Thickness of the epithelium at the tip of the epithelial tongue (µm)	0.64	0.40	0.28	0.53	0.75	0.95	N	N	0.16	0.07
Score for epidermal appendages	**0.02**	**0.02**	0.42	0.31	0.45	0.05	N	N	0.15	0.20
Number of proliferating keratinocytes	0.76	**0.03**	0.28	**0.03**	0.43	0.47	N	N	0.83	0.91
Number of inflammatory cells	0.89	0.31	**0.02**	0.16	0.49	0.44	N	N	0.84	0.10
Score for blood vessel type	-	-	-	0.05	0.27	0.38	N	N	**0.01**	0.15
Score for blood vessel number	-	-	0.31	0.68	**0.0001**	0.66	N	N	**0.01**	0.42
Percentage area of collagen (μm^2)	0.85	0.16	0.49	0.76	0.39	0.87	N	N	0.94	0.71
Score for collagen density	-	-	0.65	0.86	0.70	0.07	N	N	0.95	0.42
Score for collagen bundle size	-	-	0.46	0.69	**0.03**	0.97	N	N	**0.0001**	0.49
Score for collagen organisation	-	-	0.74	0.95	0.35	0.78	N	N	0.35	0.42

E: experimental wound, C: control wound; N: parameter not measured on that day post-wounding.

Please note: - indicates parameters which could not be tested as all results equaled a single value, bold values indicate data that are not normally distributed ($p<0.05$)